Contents

Preface

Preface

After the very positive response to the first report on our activities in Soft Condensed Matter research at the Physics Department of the University of Konstanz, this is now the second volume assembled in the same spirit. The report is intended to be informative for experts in this area but also to attract the attention of researchers of other disciplines. In addition, we hope it may help to stimulate discussions and possibly new cooperations.

The main purpose of this report is to give a representative survey of our experimental and theoretical work and to point out the numerous fruitful collaborations between different projects. We decided to describe only well advanced or finished projects while those still in progress will be included in the next report. In order to allow a rapid overview, we have adopted again a rather compact form and referred to the original publications where necessary.

We want to thank all our scientific collaborators - in house and abroad -, the technical and administrative staff and the central facilities of the University of Konstanz for their support. We address special thanks also to the students whose engagement and motivation has significantly contributed to the successful development of the research on Soft Condensed Matter in Konstanz.

Konstanz, June 2001

Wolfgang Dietrich
Rudolf Klein
Paul Leiderer
Georg Maret
Peter Nielaba

A Liquids

A1   Melting of hard disks in two dimensions

S. Sengupta, K. Binder, P. Nielaba

One of the first continuous systems to be studied by computer simulations [1] is the system of hard disks of diameter σ (=1) interacting with the two body potential,

$$V(r) = \begin{cases} \infty & r \le \sigma \\ 0 & r > \sigma \end{cases} \qquad (1)$$

Despite its simplicity, this system was shown to undergo a phase transition from solid to liquid as the density ρ was decreased. The nature of this phase transition, however, is still being debated. Early simulations [1] always found strong first order transitions. As computational power increased the observed strength of the first order transition progressively decreased! Using sophisticated techniques Lee and Strandburg [2] and Zollweg and Chester [3] found evidence for, at best, a weak first order transition. A first order transition has also been predicted by theoretical approaches based on density functional theory [4]. On the other hand, recent simulations of hard disks [5] find evidence for a Kosterlitz -Thouless -Halperin -Nelson -Young (KTHNY) transition [6] from liquid to a hexatic phase, with orientational but no translational order, at $\rho = 0.899$. Nothing could be ascertained, however, about the expected hexatic to the crystalline solid transition at higher densities because the computations became prohibitively expensive. The solid to hexatic melting transition was estimated to occur at a density $\rho_c \ge .91$. A priori, it is difficult to assess why various simulations give contradicting results concerning the order of the transition. In Ref. [7] we took an approach, complementary to Jaster's, and investigated the melting transition of the solid phase. We showed that the hard disk solid is unstable to perturbations which attempt to produce free dislocations leading to a solid $\rightarrow$ hexatic transition in accordance with KTHNY theory [6] and recent experiments in colloidal systems [8]. Though this has been attempted in the past [9,10], numerical difficulties, especially with regard to equilibration of defect degrees of freedom, makes this task highly challenging.

The elastic Hamiltonian for hard disks is given by,

$$F = -P\epsilon_+ + B/2\epsilon_+^2 + (\mu + P)(\epsilon_-/2 + 2\epsilon_{xy}), \quad (2)$$

where B is the bulk modulus. The quantity $\mu_{eff} = \mu + P$ is the "effective" shear modulus (the slope of the shear stress vs shear strain curve) and P is the pressure. The Lagrangian elastic strains are defined as,

$$\epsilon_{ij} = \frac{1}{2}\left(\frac{\partial u_i}{\partial R_j} + \frac{\partial u_j}{\partial R_i} + \frac{\partial u_i}{\partial R_k}\frac{\partial u_k}{\partial R_j}\right), \qquad (3)$$

where the indices i, j go over x and y and finally, $\epsilon_+ = \epsilon_{xx} + \epsilon_{yy}$, and $\epsilon_- = \epsilon_{xx} - \epsilon_{yy}$. The displacement vector $\mathbf{u}$ is the deviation of an atom from the nearest perfect lattice point $\mathbf{R}$.

The KTHNY- theory [6] is presented usually for a 2-d triangular solid under *zero external stress*. It is shown that the dimensionless Young's modulus of a two-dimensional solid, $K = (8/\sqrt{3}\rho)(\mu/\{1 + \mu/(\lambda + \mu)\})$, where μ and λ are the Lamé constants, depends on the fugacity of dislocation pairs, $y = \exp(-E_c)$, where E_c is the core energy of the dislocation, and the "coarse -graining" length scale l. This dependence is expressed in the form of the following coupled recursion relations for the renormalization of K and y:

$$\frac{\partial K^{-1}}{\partial l} = 3\pi y^2 e^{\frac{K}{8\pi}}[\frac{1}{2}I_0(\frac{K}{8\pi}) - \frac{1}{4}I_1(\frac{K}{8\pi})], \quad (4)$$
$$\frac{\partial y}{\partial l} = (2 - \frac{K}{8\pi})y + 2\pi y^2 e^{\frac{K}{16\pi}}I_0(\frac{K}{8\pi}).$$

where I_0 and I_1 are Bessel functions. The thermodynamic value is recovered by taking the limit $l \rightarrow \infty$.

We see in Fig. (1) that the trajectories in y-K plane can be classified in two classes, namely those for which $y \rightarrow 0$ as $l \rightarrow \infty$ (ordered phase) and those $y \rightarrow \infty$ as $l \rightarrow \infty$ (disordered phase). These two classes of flows are separated by lines called the separatrix. The transition temperature T_c (or ρ_c) is given by the intersection of the separatrix with the line of initial conditions $K(\rho, T)$ and $y = \exp(-E_c(K))$ where $E_c \sim cK/16\pi$. The disordered phase is a phase where free dislocations proliferate. Proliferation of dislocations however *does not* produce a liquid, rather a liquid crystalline phase called a "hexatic" with quasi- long ranged (QLR) orientational order but short ranged positional order. A *second* K-T transition destroys QLR orientational order and takes the hexatic to the liquid phase by the proliferation of "disclinations" (scalar charges). Apart from T_c there are several universal predictions from KTHNY- theory, for example, the order parameter correlation length and susceptibility has essential singularities ($\sim e^{bt^{-\nu}}, t \equiv T/T_c - 1$) near T_c. All these predictions can, in principle, be checked in simulations [5].

One way to circumvent the problem of large finite size effects and slow relaxation due to diverging correlation lengths is to simulate a system which is constrained to remain defect (dislocation) free and, as it turns out, without a phase transition. Surprisingly, using this data it is possible to predict the expected equilibrium behaviour of the unconstrained system. The simulation [7] is always started from a perfect triangular lattice which fits into our box – the size of the box determining the density. Once a regular MC move is about to be accepted, we perform a *local* Delaunay triangulation involving the moved disk and its nearest and next nearest neighbors. We compare

the connectivity of this Delaunay triangulation with that of the reference lattice (a copy of the initial state) around the same particle. If any old bond is broken and a new bond formed (Fig. 2) we reject the move since one can show that this is equivalent to a dislocation - antidislocation pair separated by one lattice constant involving dislocations of the smallest Burger's vector.
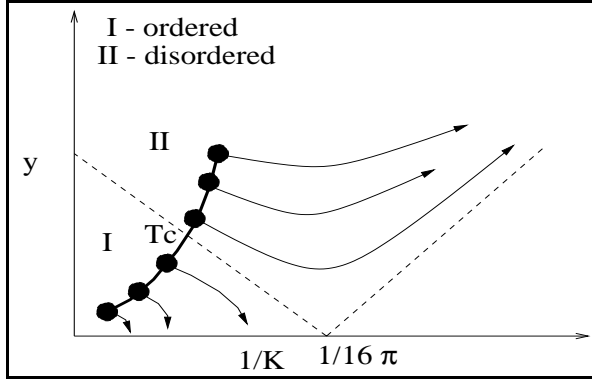

Figure 1: Schematic flows of the coupling constant K and the defect fugacity y under the action of the KTHNY recursion relations. The dashed line is the separatrix whose intersection with the line of initial state (solid line connecting filled circles, $y(T, l = 0)$, $K^{-1}(T, l = 0)$) determines the transition point T_c
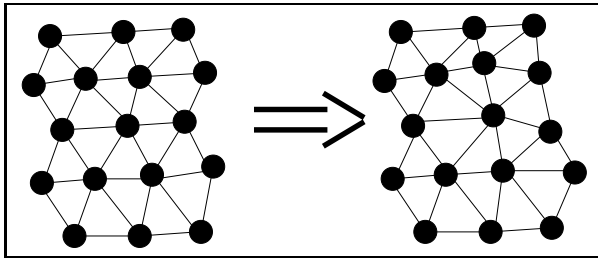

Figure 2: Typical move which attempts to change the coordination number and therefore the local connectivity around the central particle. Such moves were rejected in our simulation.

Microscopic strains $\epsilon_{ij}(\mathbf{R})$ can be calculated now for every reference lattice point $\mathbf{R}$. Next, we coarse grain (average) the microscopic strains within a sub-box of size L_b, $\bar{\epsilon}_{ij} = L_b^{-d} \int^{L_b} d^d r \epsilon_{ij}(\mathbf{r})$ and calculate the (L_b dependent) quantities [11],

$$S_{++}^{L_b} = <\bar{\epsilon}_+\bar{\epsilon}_+>, \; S_{--}^{L_b} =<\bar{\epsilon}_-\bar{\epsilon}_->, \quad (5)$$
$$S_{33}^{L_b} = 4<\bar{\epsilon}_{xy}\bar{\epsilon}_{xy}>$$

The elastic constants in the thermodynamic limit are obtained from, the set: $B = 1/2S_{++}^{\infty}$ and $\mu_{eff} = 1/2S_{--}^{\infty} = 1/2S_{33}^{\infty}$. We obtain highly accurate values of the unrenormalized coupling constant K and the defect fugacity y which can be used as inputs to the KTHNY recursion relations. Numerical solution of these recursion relations then yields the renormalized coupling K_R and hence the density and pressure of the solid to hexatic melting transition.

We can draw a few very precise conclusions from our results. Firstly, a solid without dislocations is stable against fluctuations of the amplitude of the solid order parameter and against long wavelength phonons. So any melting transition mediated by phonon or amplitude fluctuation is ruled out in our system. Secondly, the core energy $E_c > 2.7$ at the transition so KTHNY perturbation theory is valid though numerical values of nonuniversal quantities may depend on the order of the perturbation analysis. Thirdly, solution of the recursion relations shows that a KTHNY transition at $P_c = 9.39$ *preempts* the first order transition at $P_1 = 9.2$. Since these transitions, as well as the hexatic -liquid KTHNY transition lies so close to each other, the effect of, as yet unknown, higher order corrections to the recursion relations may need to be examined in the future. Due to this caveat, our conclusion that a hexatic phase exists over some region of density exceeding $\rho = .899$ still must be taken as preliminary. Also, in actual simulations, cross over effects near the bicritical point, where two critical lines corresponding to the liquid -hexatic and hexatic -solid transitions meet a first order liquid -solid line (see for e.g. Ref. [12] for a corresponding lattice model where such a situation is discussed) may complicate the analysis of the data, which may, in part, explain the confusion which persists in the literature on this subject.

[1] B.J. Alder, T.E. Wainwright, Phys.Rev.**127**, 359 (1962).

[2] J. Lee and K. Strandburg, Phys. Rev. **B46**, 11190 (1992).

[3] J.A.Zollweg, G.V.Chester, Phys.Rev.**B46**,11186 (1992).

[4] T. V. Ramakrishnan, Phys. Rev. Lett. **42**, 795 (1979); X. C. Zeng and D. W. Oxtoby, J. Chem. Phys. **93**, 2692 (1990); Y. Rosenfeld, Phys. Rev. **A42**, 5978 (1990). V. N. Ryzhov and E. E. Tareyeva, Phys. Rev. **B51**, 8789 (1995).

[5] A. Jaster, Phys. Rev. E **59**, 2594 (1999).

[6] J. M. Kosterlitz, D. J. Thouless, J. Phys. **C 6**, 1181 (1973); B.I. Halperin and D.R. Nelson, Phys. Rev. Lett. **41**, 121 (1978); D. R. Nelson and B. I. Halperin, Phys. Rev. B **19**, 2457 (1979); A.P. Young, Phys. Rev. B **19**, 1855 (1979).

[7] S. Sengupta, P. Nielaba, K. Binder, Phys. Rev. **E 61**, 6294 (2000).

[8] K. Zahn, R. Lenke and G. Maret, Phys. Rev. Lett. **82**, 2721, (1999)

[9] K. W. Wojciechowski and A. C. Brańka, Phys. Lett. **134A**, 314 (1988).

[10] M. Bates and D. Frenkel, preprint.

[11] S.Sengupta, P.Nielaba, M.Rao, K.Binder, Phys.Rev.**E 61**, 1072 (2000).

[12] W.Janke, H.Kleinert, Phys.Rev.Lett.**61**,2344 (1988).

A2   Phase transitions in pore condensates

J. Hoffmann, P. Nielaba

Phase transitions of pore condensates in nano-pores (i.e. Vycor) have been investigated by experimental methods recently [1,2]. Besides spinodal decomposition, phase transition temperature reductions have been studied for cylindrical nano-pores with small diameters.

With computer simulations (CRAY-T3E) we have analyzed [3,4] many interesting properties of Ar- and Ne-pore condensates recently (modelled as Lennard-Jones systems with particle diameter σ and interaction energy ϵ). These systems have - like the "bulk"- systems a gas-liquid phase transition at low temperatures, the precise shape of the phase diagram is strongly influenced by the system geometry (pore radius). In turns out that with increasing attractive wall interaction the critical density increases, the adsorbate density increases strongly, and the condensate density increases weakly. A meniscus is formed with increasing curvature, the configurations become less stable and the critical temperature decreases.

The critical temperature is reduced with decreasing pore diameter. Beginning from the wall a formation of layered shell structures is found which may allow or permit the occupancy of sites at the pore axis due to packing effects. In Figure 1 we present the density profiles (cylindrical average) as well as the radial density distribution in the condensate (center part of the system in the left picture). We note the layering structure and an oscillatory behav-

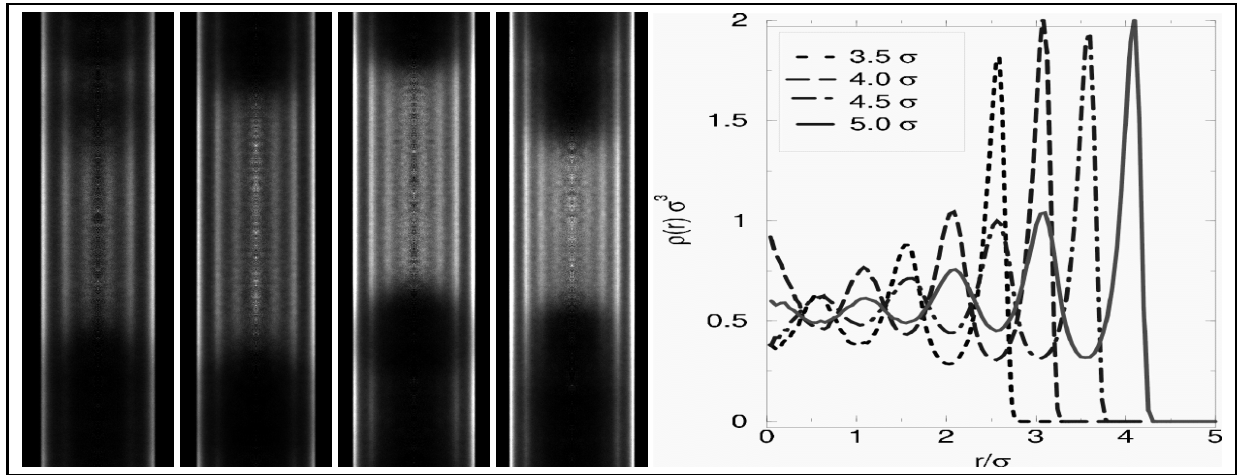**Figure 1:** Density distributions (cylindrical average) for Ar in a cylindrical pore at $T^* = 0.86$. Left: density profile for pores with radii 3.5 σ, 4 σ, 4.5 σ, 5 σ (from left to right). Right: radial density distribution in the condensate (center part left).
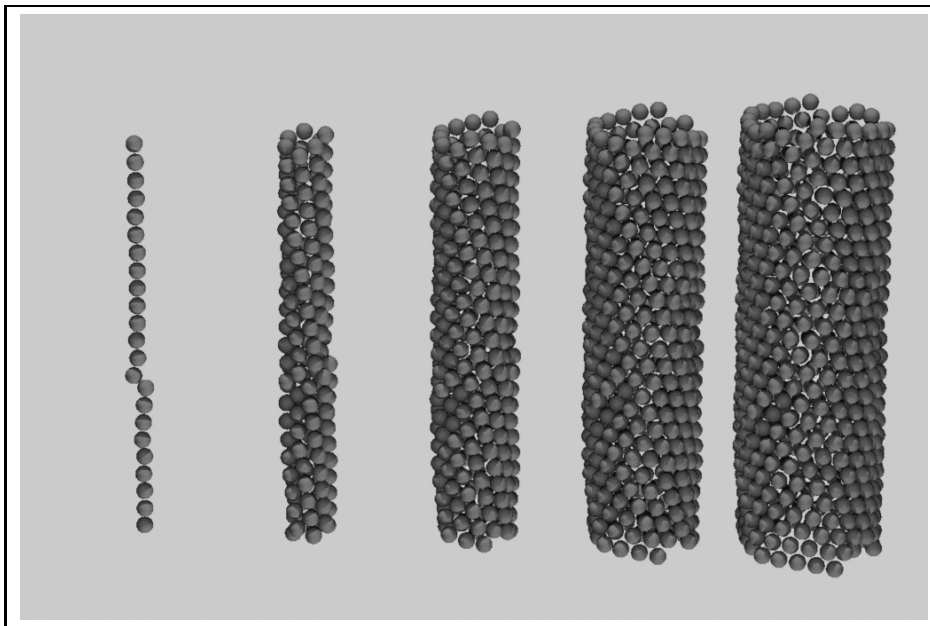

Figure 2: Radial- layers- resolved pore Ar- condensate in cylindrical pore with diameter 5 σ.

ior of the density at the pore axis (r=0) as a function of pore radius with density maxima for pore radii of $n\sigma$ and minima for pore radii of $(n + 1/2)\sigma$.

For large pore diameters the density oscillations decay from the wall towards the pore axis and the system approaches the "bulk".

At higher densities we obtain [3,4] a phase transition into a solid phase with long ranged positional order. In this solid phase radial layering structures are formed with triangular lattice structures in azimuthal direction. In Fig. 2 we show such layers for a pore with radius 5σ in a NVT-ensemble simulation indicating a meniscus shaped interface in the solid phase. The meniscus curvature decreases with the temperature in the solid as well as in the fluid phase. The triple point temperature is influenced by the geometrical finite size effects (pore radius) as well as by the wall- particle interaction. Increasing interaction strength results in an increasing freezing temperature. Only a small radius effect on the triple point temperature was detected. The geometrical finite size effect of the pore radius results in a packing effect with preferential occupancy of sites at the pore axis for pores with diameters 3.75 σ and 4.75 σ, whereas for diameters of 3.25 σ and 4.25 σ the density at the axis is reduced. Beyond these results a two step phase transition from the fluid to the solid phase was found in agreement with results obtained in experimental studies of specific heat capacities at the freezing of Ar in Vycor [5].

By path integral Monte Carlo (PIMC) simulations [6,7,8,9] the effect of the quantum mechanics on the potential energy as a function of the temperature has been quantified [3,4]. In contrast to classical simulations we obtain by PIMC simulations for Ar- and Ne-condensates an horizontal temperature dependency of the energy resulting in a decrease of the specific heat to zero at small temperatures in agreement with the third law of thermodynamics. The resulting phase diagram for Ar- and Ne- condensates and a comparison with classical computations is shown in Figure 3. In the Ne- system (containing the lighter particles) a significant reduction (by about 5%) of the critical temperature is found due to quantum delocalizations as well as a strong reduction of the solid density and a crystal structure modification in comparison with the classical case.
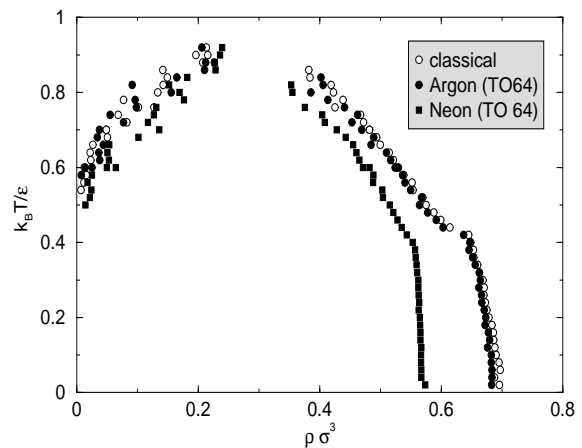
Figure 3: Phase diagrams of Ar and Ne in cylindrical pores (radius 3.25 σ, lenght 37.7 σ). Comparison of PIMC simulations (Trotter-order: 64) with classical simulations.

[1] Z. Zhang, A. Chakrabarti, Phys. Rev. **E 50**, R4290 (1994); J.C. Lee, Phys. Rev. Lett. **70**, 3599 (1993); A. Chakrabarti, Phys. Rev. Lett. **69**, 1548 (1992); A.J. Liu, G.S. Grest, Phys. Rev. **A 44**, R7894 (1991); A.J. Liu, D.J. Durian, E. Herbolzheimer, S.A. Safran, Phys. Rev. Lett. **65**, 1897 (1990); L. Monette, A.J. Liu, G.S. Grest, Phys. Rev. **A 46**, 7664 (1992); Z. Zhang, A. Chakrabarti, Phys. Rev. **E 52**, 2736 (1995).

[2] M.W. Maddox, K.E. Gubbins, M. Sliwinska- Bartkowiak, Soong- hyuck Suh, Mol. Simulat. **17**, 333 (1997); M.W. Maddox, K.E. Gubbins, J. Chem. Phys. **107**, 9659 (1997); R. Radhakrishnan, K.E. Gubbins, Phys. Rev. Lett. **79**, 2847 (1997); L.D. Gelb, K.E. Gubbins, Phys. Rev. **E 56**, 3185 (1997); P. Huber, K. Knorr, Phys. Rev.**B 60**, 12657 (1999).

[3] J. Hoffmann, Ph.D.-thesis, University of Konstanz (in preparation).

[4] J. Hoffmann, P. Nielaba, in preparation.

[5] D. Wallacher, K. Knorr, private note (2000).

[6] P. Nielaba, in: *Computational Methods in Surface and Colloid Science*, M. Borowko (Ed.), Marcel Dekker Inc., New York (2000), pp.77-134.

[7] M. Presber, D. Löding, R. Martonak, P. Nielaba, Phys. Rev. **B 58**, 11937 (1998).

[8] M. Reber, D. Löding, M. Presber, Chr. Rickward, P. Nielaba, Comp. Phys. Commun. **121-122**, 524 (1999).

[9] C. Rickwardt, P. Nielaba, M.H. Müser, K. Binder, Phys. Rev. **B63**, 045204 (2001).

A3   Elastic constants from microscopic strain fluctuations

S. Sengupta, M. Rao, K. Binder, P. Nielaba

One is often interested in long length scale and long time scale phenomena in solids (eg. late stage kinetics of solid state phase transformations; motion of domain walls interfaces; fracture; friction etc.). Such phenomena are usually described by continuum theories. Microscopic simulations [1] of finite systems, on the other hand, like molecular dynamics, lattice Boltzmann or Monte Carlo, deal with microscopic variables like the positions and velocities of constituent particles and together with detailed knowledge of interatomic potentials, hope to build up a description of the macro system from a knowledge of these micro variables. How does one recover continuum physics from simulating the dynamics of N particles? This requires a "coarse-graining" procedure in space (for equilibrium) or both space and time for non-equilibrium continuum theories. Over what coarse graining length and time scale does one recover results consistent with continuum theories? We attempted to answer these questions [2] for the simplest nontrivial case, namely, a crystalline solid, (without any point, line or surface defects [3]) in equilibrium, at a non zero temperature far away from phase transitions. Fluctuations of the instantaneous local Lagrangian strain $\epsilon_{ij}(\mathbf{r}, \mathbf{t})$, measured with respect to a static "reference" lattice, are used to obtain accurate estimates of the elastic constants of model solids from atomistic computer simulations. The measured strains are systematically coarse - grained by averaging them within subsystems (of size L_b) of a system (of total size L) in the canonical ensemble. Using a simple finite size scaling theory we predict the behaviour of the fluctuations $< \epsilon_{ij}\epsilon_{kl} >$ as a function of L_b/L and extract elastic constants of the system *in the thermodynamic limit* at nonzero temperature. Our method is simple to implement, efficient and general enough to be able to handle a wide class of model systems including those with singular potentials without any essential modification.

Imagine a system in the constant NVT (canonical) ensemble at a fixed density $\rho = N/V$ evolving in time t. For any "snapshot" of this system taken from this ensemble, the local instantaneous displacement field $\mathbf{u_R}(t)$ defined over the set of lattice vectors $\{\mathbf{R}\}$ of a reference lattice (at the same density ρ) is: $\mathbf{u_R}(t) = \mathbf{R}(t) - \mathbf{R}$, where $\mathbf{R}(t)$ is the instantaneous position of the particle tagged by the reference lattice point $\mathbf{R}$. Let us concentrate only on perfect crystalline lattices; if topological defects such as dislocations are present the analysis below needs to be modified. The instantaneous Lagrangian strain tensor ϵ_{ij} defined at $\mathbf{R}$ is then given by [3],

$$\epsilon_{ij} = \frac{1}{2}\left(\frac{\partial u_i}{\partial R_j} + \frac{\partial u_j}{\partial R_i} + \frac{\partial u_i}{\partial R_k}\frac{\partial u_k}{\partial R_j}\right) \qquad (1)$$

The strains considered here are always small and so we, hereafter, neglect the non -linear terms in the definition given above for simplicity. The derivatives are required at the reference lattice points $\mathbf{R}$ and can be calculated by any suitable finite difference scheme once $\mathbf{u_R}(t)$ is known. We are now in a position to define coarse grained variables $\epsilon_{ij}^{L_b}$ which are simply averages of the strain over a sub-block of size L_b. The fluctuation of this variable then defines the size dependent compliance matrices $S_{ijkl} = < \epsilon_{ij}\epsilon_{kl} >$. Before proceeding further, we introduce a compact Voigt notation (which replaces a pair of indices ij with one α) appropriate for two dimensional strains - the only case considered here. Using $1 \equiv x$ and $2 \equiv y$ we have,

$$
\begin{array}{rcccc}
ij & = & 11 & 22 & 12 \\
\alpha & = & 1 & 2 & 3
\end{array}
\qquad (2)
$$

The nonzero components of the compliance matrix are

$$
\begin{aligned}
S_{11} &= < \epsilon_{xx}\epsilon_{xx} > = S_{22} \qquad (3) \\
S_{12} &= < \epsilon_{xx}\epsilon_{yy} > = S_{21} \\
S_{33} &= 4 < \epsilon_{xy}\epsilon_{xy} >
\end{aligned}
$$

It is useful to define the following linear combinations

$$
\begin{aligned}
S_{++} &= < \epsilon_+\epsilon_+ > = 2(S_{11} + S_{12}) \qquad (4) \\
S_{--} &= < \epsilon_-\epsilon_- > = 2(S_{11} - S_{12})
\end{aligned}
$$

where $\epsilon_+ = \epsilon_{xx} + \epsilon_{yy}$ and $\epsilon_- = \epsilon_{xx} - \epsilon_{yy}$. Once the block averaged strains $\epsilon_{ij}^{L_b}$ are obtained, it is straight -forward to calculate these fluctuations (for each value of L_b).

Since we are interested in the elastic properties of the system far away from any phase transition, a quadratic functional for the Helmholtz free energy F suffices. We therefore use the following Landau functional appropriate for a two dimensional solid involving coarse grained strains to quadratic order in strains and its derivatives.

$$
\begin{aligned}
F &= \int d^d r \ \{c_1\epsilon_+^2 + c_2\epsilon_-^2 + c_3\epsilon_3^2 \qquad (5) \\
&+ \ d_1(\nabla\epsilon_+(\mathbf{r}))^2 + d_2(\nabla\epsilon_-(\mathbf{r}))^2 + d_3(\nabla\epsilon_3(\mathbf{r}))^2\}
\end{aligned}
$$

Even in the canonical ensemble with fixed box dimensions, the microscopic strain fluctuations over the whole box are not zero but remains a small number of the order of $(a/L)^2$ where a is the lattice parameter so that,

$$\int^L d^d r < \epsilon_\alpha(\mathbf{r})\epsilon_\beta(0) > = C_{\alpha\beta}\left(\frac{a}{L}\right)^2 . \qquad (6)$$

For $S_{\gamma\gamma}^{L_b}$ we obtain [2]:

$$S_{\gamma\gamma}^{L_b} = S_{\gamma\gamma}^{\infty} \left[\Psi(xL/\xi) - \left(\Psi(L/\xi) - C \left(\frac{a}{L} \right)^2 \right) x^2 \right]$$
$$+ \mathcal{O}(x^4). \tag{7}$$

where the index γ takes the values $+,-$ or 3 and $x = L_b/L$ and we have suppressed subscripts on the correlation length ξ and on C for clarity. The function $\Psi(\alpha)$ is given by [2]:,

$$\Psi(\alpha) = \frac{2}{\pi} \alpha^2 \int_0^1 \int_0^1 dxdy \ K_0(\alpha\sqrt{x^2 + y^2}) , \quad (8)$$

where K_0 is a Bessel function.

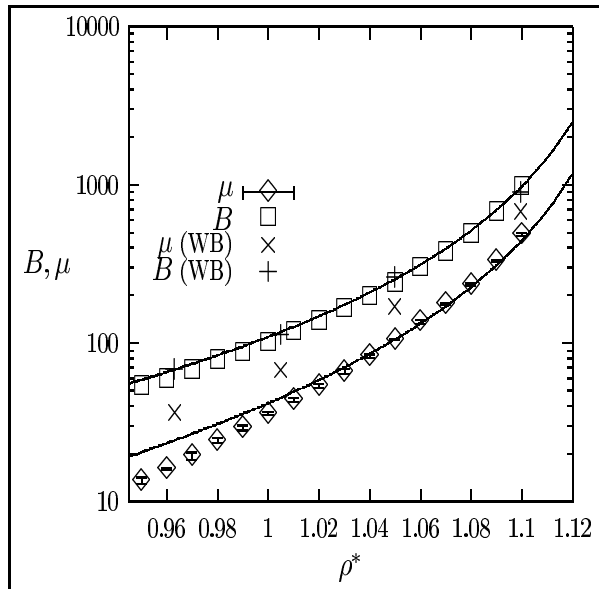The above equation Eq.(7) can now be used to obtain the *system size independent* quantities $S_{\alpha\beta}^{\infty}$, ξ and C.

Figure 1: The bulk (B) and shear (μ) moduli in units of $k_B T/\sigma^2$ for the hard disk solid. Our results for B (μ) are given by squares (diamonds). The values for the corresponding quantities from Ref. [5] are given by $+$ and $\times$. The line through the bulk modulus values is the analytical expression obtained from the free volume prediction for the pressure. The line through our shear modulus values is obtained from the free volume bulk modulus using the Cauchy relation $\mu = B/2 - P$.

Once the finite size scaled compliances are obtained the elastic constants viz. the Bulk modulus $B = \rho\partial P/\partial\rho$ and the shear modulus μ are obtained simply using the formulae [4]

$$\beta B = \frac{1}{2S_{++}} \tag{9}$$

$$\beta\mu = \frac{1}{2S_{--}} - \beta P \tag{10}$$

$$\beta\mu = \frac{1}{2S_{33}} - \beta P \tag{11}$$

where we assume that the system is under an uniform hydrostatic pressure P.

As an example we present our results for elastic constants of the hard disk system in Fig. 1. The two expressions for the shear modulus in Eqs. (10,11) give almost identical results and this gives us confidence about the internal consistency of our method. We have also compared our results to those of Wojciechowski and Brańka [5]. We find that while their values of the pressure and bulk modulus are in good agreement with ours (and with free volume theory) they grossly overestimate the shear modulus. This is probably due to the extreme small size of their systems and/or insufficient averaging. Our results for the sub-block analysis shows that finite size effects are non - trivial for elastic strain fluctuations and they cannot be evaluated by varying the total size of the system from 24 to 90, an interval which is less than half of a decade. One immediate consequence of our results is that the Cauchy relation [5,6] $\mu = B/2 - P^*$ is seen to be valid upto $\pm 15\%$ over the entire density range we studied though there is a systematic deviation which changes sign going from negative for small densities to positive as the density is increased. This is in agreement with the usual situation in a variety of real systems [6] with central potentials and highly symmetric lattices and in disagreement with Ref. [5]. We have also compared our estimates for the elastic constants with the density functional theory (DFT) of Rhysov and Tareyeva [7]. We find that both the bulk and the shear moduli are grossly overestimated - sometimes by as much as 100%.

[1]   D.P. Landau, K. Binder, *A Guide to Monte Carlo Simulations in Statistical Physics*, Cambridge University Press (2000).

[2]   S. Sengupta, P. Nielaba, M. Rao, K. Binder, Phys.Rev.**E 61**, 1072 (2000).

[3]   P.M.Chaikin, T.C.Lubensky, *Principles of condensed matter physics*, (Cambridge University Press, Cambridge, 1995).

[4]   D. C. Wallace, in *Solid state physics*, eds. H. Ehrenreich, F. Seitz and D. Turnbull (Academic Press, New York, 1958); J. H. Weiner, *Statistical mechanics of elasticity* (Wiley, New York, 1983).

[5]   K.W. Wojciechowski, A.C. Brańka, Phys.Lett. **134A**, 314 (1988).

[6]   for general discussions on Cauchy relations see F. Seitz, *Modern Theory of Solids* (McGaraw-Hill, New York, 1940) and M. Born and K. Huang, *Dynamical Theory of Crystal Lattices* (Oxford University Press, Oxford, 1954); For experimental temperature dependent elastic constants of solid argon see, H. Meixner, P. Leiderer, P. Berberich and E. Lüscher, Phys. Lett. **40A**, 257 (1972).

[7]   V.N. Ryzhov, E.E. Tareyeva, Phys.Rev.**B51**, 8789 (1995).

A4   Enrichment of surfaces in contact with stable binary mixtures

H.L. Frisch, S. Puri, P. Nielaba

There has been much interest in the temporal behaviour of homogeneous binary mixtures in contact with a surface which has a preferential attraction for one of the components of the mixture [1,2]. Typically, there are two experimentally relevant situations. Firstly, one can consider the case where the mixture is below the bulk critical temperature T_c, so that the binary mixture undergoes phase separation. In this case, the surface becomes the origin of surface-directed spinodal decomposition waves [3], which propagate into the bulk. The second case corresponds to a situation in which the temperature (T) of the binary mixture is greater than T_c so that the homogeneous bulk is stable. Nevertheless, the surface becomes enriched in the preferred component, resulting in a time-dependent surface enrichment profile, which propagates into the bulk [4].

The first case mentioned above (with $T < T_c$) has been extensively studied, both experimentally [3,2] and numerically [1,5,6,7]. However, because of the dominance of nonlinear effects in the late stages of phase separation, the equations governing surface-directed spinodal decomposition have not proven analytically tractable. One can invoke a linear approximation to study the early stages of phase separation [8,9] but this is valid only for a limited time-range. On the contrary, for the second case mentioned above (i.e., $T > T_c$) with weak surface fields, the linear approximation is valid for almost all times and can be used to solve the dynamical equations exactly [10]. As a matter of fact, it turns out that the linear approximation provides a good description of the time-dependent behaviour even for strong surface fields, where the order parameter values in the vicinity of the surface are sufficiently large that the linear description is no longer valid [11].

We have considered [12] the experimentally relevant situation of a stable binary mixture in contact with a surface which has a preference for one of the components of the mixture. In particular, we focused on the dynamics of surface enrichment resulting from a surface field turned on at zero time. We analytically solved this problem in the linearised approximation and used these solutions to extract the asymptotic behaviours of various characteristics of the enrichment profiles. Our numerical results indicate that some of the important predictions of linearised theory are valid even in the strongly nonlinear regime.

For details of our modelling see [5,1,12]. We merely present our phenomenological model for the dynamics of

a binary mixture near a surface. The bulk dynamics is governed by the usual Cahn-Hilliard (CH) equation

$$\frac{\partial \Phi(\vec{R}, Z, \tau)}{\partial \tau} = -\nabla^2 \left[\text{sgn}(T_c - T)\Phi(\vec{R}, Z, \tau) \right.$$
$$\left. - \Phi(\vec{R}, Z, \tau)^3 + \frac{1}{2}\nabla^2 \Phi(\vec{R}, Z, \tau) - V(Z) \right] \quad (1)$$

($Z > 0$), where all quantities have been rescaled into dimensionless units [5]. In (1), $\Phi(\vec{R}, Z, \tau)$ denotes the order parameter variable, which is proportional to the difference in densities of the two species (A and B) of the binary mixture AB. The order parameter depends on dimensionless time τ and space $(\vec{R}, Z)$, with $\vec{R}$ denoting the coordinates parallel to the surface and Z denoting the coordinate perpendicular to the surface located at $Z = 0$. The surface is the source of a potential of strength $V(Z)(< 0)$, which enriches the surface in A, in our present description. We are typically interested in potentials which are flat within a certain range of the surface and decay in a power-law fashion. The surface is mimicked by two boundary conditions as follows :

$$\frac{\partial \Phi(\vec{R}, Z, \tau)}{\partial \tau} = h_1 + g\Phi(\vec{R}, 0, \tau) + \gamma \frac{\partial \Phi(\vec{R}, Z, \tau)}{\partial Z}\bigg|_{Z=0},$$
$$(2)$$

$$0 = \frac{\partial}{\partial Z} \left[\text{sgn}(T_c - T)\Phi(\vec{R}, Z, \tau) \right. \qquad (3)$$
$$\left. - \Phi(\vec{R}, Z, \tau)^3 + \frac{1}{2}\nabla^2 \Phi(\vec{R}, Z, \tau) \right]\bigg|_{Z=0}.$$

Let us consider the evolution of an initial condition consisting of fluctuations about a uniform background, viz., $\Phi(\vec{R}, Z, \tau) = \phi_0 + \phi(\vec{R}, Z, \tau)$. We linearise Eqs. (1)-(3) in the fluctuation field $\phi(\vec{R}, Z, \tau)$, and for simplicity we restrict our considerations to the case where the order parameter field is homogeneous parallel to the surface ($\phi(\vec{R}, Z, \tau) \equiv \phi(Z, \tau)$). After a Laplace transform of the resulting equations we obtain [12] an analytic solution for $\phi(Z, s) = \int_0^\infty d\tau e^{-s\tau}\phi(Z, \tau)$ and the leading asymptotic time-dependence of the m-th moment of Z as

$$\langle Z^m \rangle = -\frac{\Gamma(m+1)}{\Gamma(\frac{m}{2}+1)} \left(\frac{h_1\sqrt{2} + g(A + h_1\sqrt{2})}{2(\gamma\sqrt{2} - g)} + B \right) \tau^{\frac{m}{2}}$$
$$(4)$$

Therefore, the time-dependence of the profile moments (when defined) is also similar to that in the case where there is a delta-function field at the surface [10,11].

The analytical results are strongly universal as regards the time-dependence of $\phi(0, \tau)$ and $< Z^m >$ for a wide range of physical potentials. Of course, these analytical results have been obtained in the context of a linear theory. However, as our numerical results demonstrate, the same behaviours arise in the nonlinear case also.

We have also solved the 1-dimensional version of our model in Eqs. (1)-(3) (with $T < T_c$) numerically, using a simple Euler discretisation scheme. The mesh sizes for discretisation were $\Delta\tau = 0.01$ and $\Delta Z = 0.6$. The lattice size was $N = 4000$ so that the lattice length $L = N\Delta Z = 2400$. The boundary conditions in Eqs. (2)-(3) were applied at $Z = 0$ and flat boundary conditions were applied at $Z = L$. The initial condition for all the results presented here is $\phi(Z, 0) = 0$, corresponding to a critical composition of the binary mixture AB without any fluctuations. The surface field is turned on at time $\tau = 0$. In our simulations, we used the power-law potential

$$
\begin{aligned}
V(Z) &= -h_1, \quad Z < \epsilon, \\
&= -h_1 \left(\frac{\epsilon}{Z}\right)^n, \quad Z > \epsilon, \quad (5)
\end{aligned}
$$

where the cut-off ϵ is introduced to control the divergence of the potential as $Z \to 0$. In our simulations, we set $\epsilon = \Delta Z$. The decay of the potential is characterised by the exponent n. The cases with $n = 3$ and 4 correspond to the usual cases of nonretarded and retarded Van der Waals' interactions between the surface and the preferred component A.

In the "weak"-field case ($h_1 = 2$ and $n = 2, 3$) the saturation value of order parameter at the surface is sufficiently small ($\phi \simeq 0.4$) that nonlinear effects are negligible. In this case the numerical solution of the linearised model is nearly identical to that described above for the fully nonlinear model. The temporal evolution of profiles is described well by the linearised model for both $n = 2$ and $n = 3$ [13]. It is gratifying to have a regime of fields in which there is no appreciable difference between the results obtained from the nonlinear and linear models. In this regime, the analytical solutions (see above) are valid and we have then obtained a complete solution of the problem of surface enrichment with arbitrary potentials. As the field strength is increased, we expect the validity of the linear theory to breakdown. Though this is definitely true for the time-dependent profiles, it is interesting that the diffusive behaviour of various characteristics of the profile is unaffected, even in the strongly nonlinear regime. This is known for the case with a delta-function potential [11] and turns out to be valid for the case with long-ranged potentials also.

Our analytical results were obtained in the context of a linear model and predict diffusive behaviour for the moments and surface value of the time-dependent enrichment profiles. The analytical results are expected to be valid in the weak-field regime, where the enrichment is sufficiently small at the surface that nonlinear effects are negligible. However, even for strong surface fields, where the enrichment profiles are considerably different from the profiles obtained from a linear model, the behaviour

of various profile characteristics still remains diffusive. This universality over a wide range of potential functions and surface field strengths is the most relevant aspect of [12] and earlier work on delta-function surface fields [11].

[1]   For a review of modelling and numerical simulations of this problem, see S.Puri and H.L.Frisch, J. Phys. Condensed Matter **9**, 2109 (1997).

[2]   For a review of experimental techniques and results for this problem, see G.Krausch, Mat. Science and Engineering Reports **R14**, 1 (1995).

[3]   R.A.L.Jones, L.J.Norton, E.J.Kramer, F.S.Bates and P.Wiltzius, Phys. Rev. Lett. **66**, 1326 (1991).

[4]   R.A.L.Jones, E.J.Kramer, M.H.Rafailovich, J.Sokolov and S.A.Schwarz, Phys. Rev. Lett. **62**, 280 (1989);
R.A.L.Jones and E.J.Kramer, Phil. Mag. B **62**, 129 (1990).

[5]   S.Puri and K.Binder, Phys. Rev. A **46**, R4487 (1992);
S.Puri and K.Binder, Phys. Rev. E **49**, 5359 (1994);
S.Puri and K.Binder, J. Stat. Phys. **77**, 145 (1994);
S.Puri, K.Binder and H.L.Frisch, to appear in Phys. Rev. E.

[6]   G.Brown and A.Chakrabarti, Phys. Rev. A **46**, 4829 (1992).

[7]   J.F.Marko, Phys. Rev. E **48**, 2861 (1993).

[8]   H.L.Frisch, P.Nielaba and K.Binder, Phys. Rev. E **52**, 2848 (1995).

[9]   H.P.Fischer, P.Maass and W.Dieterich, Phys. Rev. Lett. **79**, 893 (1997).

[10]   For the case of a delta-function surface field, this has been done by K.Binder and H.L.Frisch, Z. Phys. B **84**, 403 (1991).

[11]   S.Puri and H.L.Frisch, J. Chem. Phys. **79**, 5560 (1993).

[12]   H.L. Frisch, S. Puri, P. Nielaba, J. Chem. Phys. **110**, 10514 (1999).

[13]   We do not directly compare our numerical and analytical results because a very fine discretisation mesh is required to obtain numerical results which reasonably approximate the continuum limit [9].

A5 Formation of sub-micrometer structures by combination of a sol-gel technique with micro-contact printing

C. Schäfle, P. Leiderer, C. Bechinger

The sol-gel technique is a wide-spread method of synthesizing materials and depositing them in form of thin homogeneous films. Accordingly, it has gained importance with respect to scientific and application purposes. Based on the chemistry of the synthesis, a large variety of materials, e.g. oxidic semiconductors, glasses and even super conducting films can be obtained [1] [2]. In this process an inorganic or organic molecular precursor $M(OR)_n$, a sol, is used as starting material, where M is a metal and (OR) is an organic compound, respectively. A macromolecular oxide network is then obtained in a moist environment through hydrolysis and polycondensation which transforms the precursor into a highly viscous (gel-like) hydrated metal oxide (MO_x). In a final heat treatment at typically $100° – 300°$ C the coating is then dried in an oven to complete hydrolysis and condensation. In principle the sol-gel reaction can be written as [1]

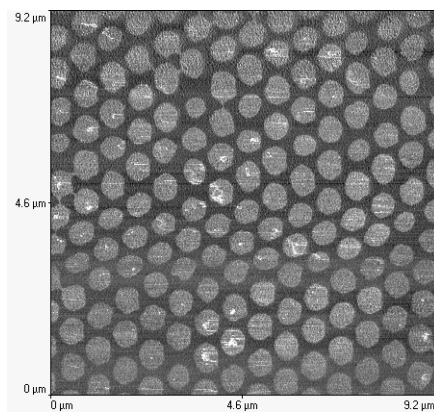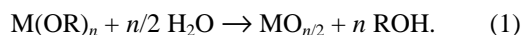$$M(OR)_n + n/2 \ H_2O \rightarrow MO_{n/2} + n \ ROH. \qquad (1)$$

Figure 1: Lateral force image of a chemically patterned gold surface where bright and dark areas indicate hydrophilic and hydrophobic domains, respectively. The structure was obtained by micro-contact printing using a monolayer of polystyrene spheres of 840 nm diameter as a master.

The basic advantage of the sol-gel process is its ability to form inorganic structures (semiconductors, ceramics and glasses) at relatively low temperatures. Furthermore, the process – being very similar to conventional coating techniques such as dip-, spin- or spray coating, does not require any vacuum steps, and is therefore a cost-effective way to produce thin homogeneous inorganic films on large scales.
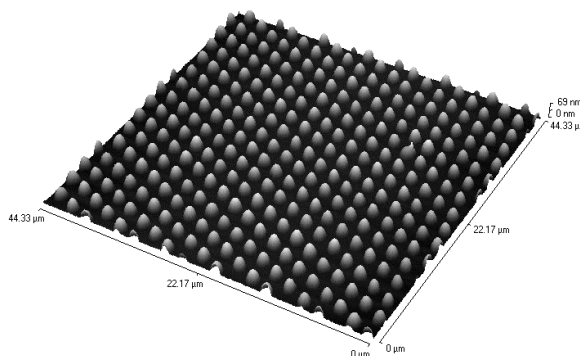

Figure 2: AFM image of an array of tungsten oxide dots obtained by dip coating of tungsten alkoxide to a chemically patterned surface. After an annealing step at 120°C, the liquid drops are transformed into solid dots [3].

In the following we will demonstrate that this technique - in contrast to homogeneous thin film deposition as it has been used so far - can also be employed for the fabrication of nanostructures on large scales which are useful for electronical, optical or catalytical applications. This is achieved by combining the benefit of the sol-gel process with micro-contact-printing (μ-CP), the latter comprising surfaces with well-defined periodic hydrophilic and hydrophobic domains, respectively [4] [5]. When a medium of low viscosity is applied to such patterned surfaces, spontaneous dewetting occurs and the fluid forms a droplet pattern which reflects the symmetry of the underlying substrate. The principle has been demonstrated already for simple liquids, polymers and other materials [6] [7] [8] [9] on homogeneous substrates. Additionally, fabrication of patterned sol-gel structures by means of micro molding is reported in the literature [10] [11]. In contrast to this, here we apply highly reactive liquids, i.e. alkoxides, to chemically patterned substrates. After the dewetting process an array of drops is obtained which can be considered as microscopic test tubes where a chemical reaction, namely the sol-gel process takes place, which eventually turns the liquid drops in solid dots.

When the sol is applied by dip-coating to a gold surface patterned with a stamp made from spheres of 3 μm in diameter, a periodic structure is formed as suggested already by the occurrence of interference colors which are visible with the bare eye and confirmed with an optical microscope. Fig.2 shows an atomic force microscope image of the sample after it was annealed at 120° C for about 30 minutes. Obviously, the sol dewetted completely the hydrophobic sites (see also Fig.1) , thus

producing monodisperse, hexagonally arranged drops where during the subsequent annealing step a chemical reaction, i.e. the sol-gel transition, takes place. As a result, one obtains WO_3 dots which strongly adhere to the surface and withstand an ultrasonic bath treatment of 1 M hydrochloric acid. In order to demonstrate that these droplets exhibit chromogenic properties we first evaporated a thin layer of palladium and then exposed the structure to hydrogen gas. We observed an immediate change in the reflected intensity which is typical for tungsten oxide thin films [12].

An array of WO_3 dots formed on a substrate prepatternd with a stamp molded from a monolayer of 600 nm PS spheres is shown in Fig.3 [3]. After the annealing process, the typical full width half maximum (FWHM) of the dots is in the order of 150 nm as can be seen from a cross section in the inset. The profile of the solid dots fits very well to a spherical cap function (solid line) which is typically obtained for liquid drops. Obviously the polycondensation does not alter the shape of the dot which is in agreement with the fact that tungsten oxide forms an amorphous network at these temperatures [13] [14]. Only above 350° C where crystallization occurs, deviations from a spherical shape are observed.
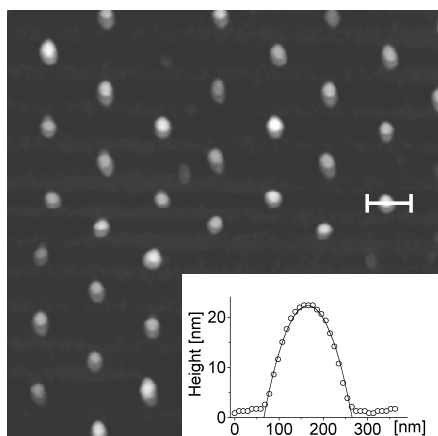

Figure 3: AFM image (3.73 x 3.75 μm^2) of tungsten oxide dots fabricated by dip coating on a gold surface prepatterned with stamps made from a monolayer of 600 nm micro spheres. The inset shows a cross section of a dot after the annealing process which can be fitted to a spherical cap (solid line). The typical size (FWHM) of the dots is about 150 nm [3].

Fig.4 shows an example where sol was allowed to rest on the substrate for about 15 seconds before it was removed by tilting the substrate. Although exactly the same recipe for the sol was used, now the "inverse" structure of Fig.2 is obtained. While the details of this process are not understood in detail yet, we believe that the formation of this geometry is due to micro-phase separation between the surfactant and the sol. When the sol rests at the substrate, the acetylacetone might preferentially wet the hydrophilic sites, thus leaving

entially wet the hydrophilic sites, thus leaving only the hydrophobic areas for the tungsten alkoxide. Thus, just by a the details how the sol is applied to the surface a
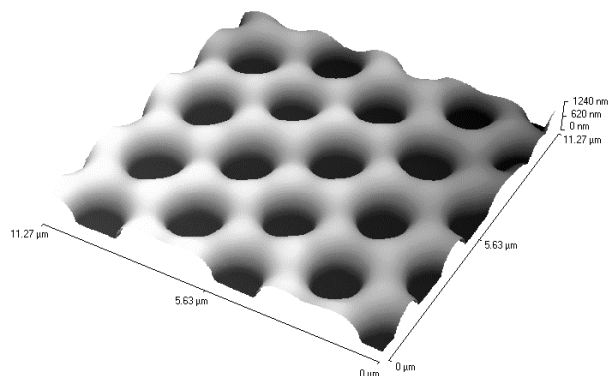
Figure 4: Inverse structure, which is obtained when the sol is not applied by dip coating but is allowed to rest on the chemically patterned substrate. The substrate prepattern was obtained by a colloidal monolayer of polystyrene spheres of 3 µm diameter [3].

[1] C. J. Brinker and G. W. Scherer, *Sol-gel science* (Academic Press, San Diego, 1990).

[2] C. J. Brinker, A. J. Hurd, G. C. Frye, K. J. Ward, and C. S. Ashley, J. Non-Cryst. Sol. **121,** 294 (1990).

[3] C. Bechinger, H. Muffler, C. Schäfle, O. Sundberg, and P. Leiderer, Thin Solid Films **366,** 135 (2000).

[4] Y. Xia, J. Tien, D. Qin, and G. M. Whitesides, Langmuir **12,** 4033 (1996).

[5] G. P. Lopez, H. A. Biebuyck, C. D. Frisbie, and G. M. Whitesides, Science **260,** 647 (1993).

[6] A. Kumar and G. Whitesides, Science **263,** 60 (1994).

[7] Z. Huang, P.-C. Wang, A. G. MacDiarmid, Y. Xia, and G. Whitesides, Langmuir **13,** 6480 (1997).

[8] M. Böltau, S. Walheim, J. Mlynek, G. Krausch, and U. Steiner, Nature **391,** 877 (1998).

[9] H. Yang, N. Coombs, and G. A. Ozin, Adv. Mater. **9,** 811 (1997).

[10] C. Marzolin, S. P. Smith, M. Prentiss, and G. M. Whitesides, Adv. Mater. **10,** 571 (1998).

[11] P. Yang, T. Deng, D. Zhao, P. Feng, D. Pine, B. F. Chmelka, G. M. Whitesides, and G. D. Stucky, Science **282,** 2244 (1998).

[12] K. Ito and T. Ohgami, Appl. Phys. Lett. **60,** 938 (1992).

[13] P. Judenstein, R. Morineau, and J. Livage, Solid State Ionics **51,** 239 (1992).

[14] M. Shiojiri, T. Miyano, and C. Kaito, Jap. J. Appl. Phys. **17,** 567 (1978).

B   Polymers

B1 Soft Ellipsoid Model for Polymers

F. Eurich and Ph. Maass

For many applications it is important to understand polymer dynamics on semi-macroscopic time scales corresponding to configurational changes of polymer chains on lengths scales comparable with or larger than the radius of gyration. A problem of active current research in nano-technology, for example, is the tailoring of thin polymer films on surfaces. Spontaneous phase separation processes of incompatible polymer blends may be used to translate a chemical pattern on the surface into a pattern of varying polymer compositions.

Investigation of such problems by means of molecular dynamics simulations of semi-microscopic bead-spring models is not feasible. To overcome this problem, one needs to introduce coarse-grained descriptions. For studying spontaneous phase separation processes in polymer blends the Cahn-Hilliard equation or generalized time-dependent Ginzburg-Landau equations are often used, but even within such treatments the exploration of long–time dynamics is hard. Nevertheless, a new implicit numerical procedure was recently developed by our group in collaboration with the group of Prof. Bohl (department of mathematics at the University of Konstanz) that allows one to explore the long–time kinetics [1].

Another way of treating slow kinetics being particularly adapted to polymers was suggested by Murat and Kremer [2]. They proposed a model, in which polymeric systems are described by inter-penetrating ellipsoids that can change their shape, position and orientation. The probability for a particular shape follows from an intramolecular free energy functional. A monomer density is assigned to each ellipsoid, and the interaction results from
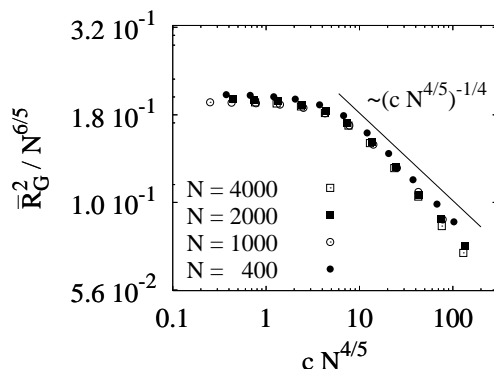
Figure 1: Scaling relation between the squared radius of gyration $\bar{R}_{\rm G}^2$ and the monomer concentration c for various polymerization degrees N at fixed temperature. For small c the chains are almost free and the master curve saturates, corresponding to Flory type behavior, $\bar{R}_{\rm G}^2 \sim N^{6/5}$. For large c, scaling arguments predict $\bar{R}_{\rm G}^2 \sim c^{-1/4} N$ in accordance with the data.
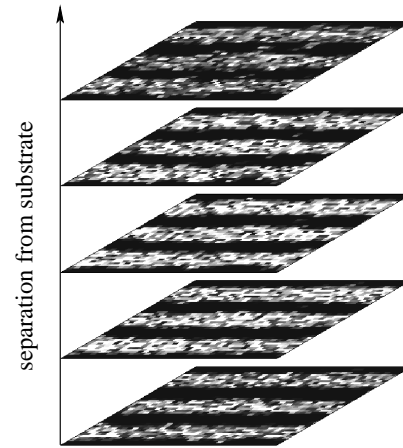
Figure 2: Concentration of one component of a binary polymer mixture in various planes above a substrate surface with a periodically modulated wall potential. For the parameters chosen in the simulation the structure propagates up to the top of the film.

the overlap of the respective densities. An important feature of the ellipsoid model is that the input parameters can be determined from microscopic models appropriate to describe the polymer system on short time scales.

In our work [3] we studied a soft ellipsoid model, where the input quantities are determined from ideal Gaussian polymer chains. For this "Gaussian ellipsoid model" (GEM) we determined the probabilities for the shapes and the associated monomer densities and expressed them by simple approximate formulae. Structural and kinetic properties were then investigated by Monte-Carlo simulations for both homogeneous systems and binary mixtures, and it was shown that the GEM provides a powerful approach for treating polymeric systems.

Figure 1 shows as an example the well-known scaling behavior of the radius gyration $\bar{R}_{\rm G}$ in homogeneous melts as a function of the monomer concentration c and the polymerization degree N. This scaling is rather difficult to obtain in more microscopic approaches as e.g. bead spring models. Similarly we could identify prominent features in blends, as e.g. the scaling of the coexistence curve with N and the Lifshitz–Slyozov late stage behavior of domain growth in spinodal decomposition.

Recently, we applied the GEM to study phase separation on chemically patterned surfaces. Figure 2 shows how, upon tuning the external parameters properly, a structure imprinted on a surface can be translated to a polymer film.

[1] R. Kenzler, F. Eurich, P. Maass, B. Rinn, J. Schropp, E. Bohl, and W. Dieterich, Comp. Phys. Comm. **133**, 139 (2001).

[2] M. Murat and K. Kremer, J. Chem. Phys. **108**, 4340 (1998).

[3] F. Eurich and P. Maass J. Chem. Phys., in press.

B2 Polymer ion conductors

O. Dürr, W. Dieterich

Chain polymers carrying electro-negative atoms (e.g. oxygen or nitrogen) in their repeat unit can act as solvents for certain salts. Well-known examples are Li-salts dissolved in polyethylene-oxide (PEO). At temperatures sufficiently above the glass-transition temperature these polymer-salt solutions show significant DC ionic (Li^+) conductivities. Such "polymer electrolytes" offer widespread applications in batteries, sensors and fuel cells. From the scientific point of view, an important goal is to improve our understanding of the electrical conduction mechanism in polymer electrolytes, and in particular to elucidate the interplay between ion diffusion and the polymer network dynamics.

Numerical simulation of these systems on a microscopic level is extremely demanding through the fact that time scales for motion of the chain molecules and time scales for ionic motions normally differ by orders of magnitude. This necessitates the design of appropriate coarse-grained models based on stochastic moves of chain segments and ions. In this project we investigate stochastic models on different levels of coarse-graining:

i) Dynamic Monte Carlo studies of lattice chains interacting with ions.
   From extensive simulations we obtained the diffusion constants of both chains and ions and their dependence on model parameters. In particular we were able to discuss important trends in the glass transition temperature as a function of the ion content. By combining simulations under constant volume with the quasichemical approximation for the equation of state we also deduced the conductivity as a function of pressure p. With increasing p the conductivity is found to decrease exponentially, in accord with many experiments [1].

ii) Dynamic percolation theory.
   Simulation of diffusion coefficients in the coupled system of ions and polymer chains is hampered by the need to move every monomer (polymer bead or ion) with the same probability. Therefore most of the computational time is spent moving the polymeric host without affecting the ionic configurations. On the other hand, earlier studies indicated that important features of ion diffusion within a dynamical matrix of chain molecules can be described by an even more coarse-grained model. The idea is to map the diffusion process onto dynamic percolation (DP)-theory [2,3] and to

determine the central quantity entering this theory, the renewal time distribution $\Psi(t)$, from the time dependence of the local occupational correlation function due to the polymer chain dynamics [4]. Tests of such a procedure for a hard-core lattice gas and for tracer diffusion in systems of athermal lattice polymers were carried out. Calculated tracer correlation factors $f(c)$, defined in terms of the tracer diffusion coefficient $D(c)$ by $f(c) = D(c)/D_0(1-c)$, are shown in Fig. 1. Here c and D_0 denote the overall concentration of occupied lattice sites and the diffusion coefficient for infinite dilution, respectively.
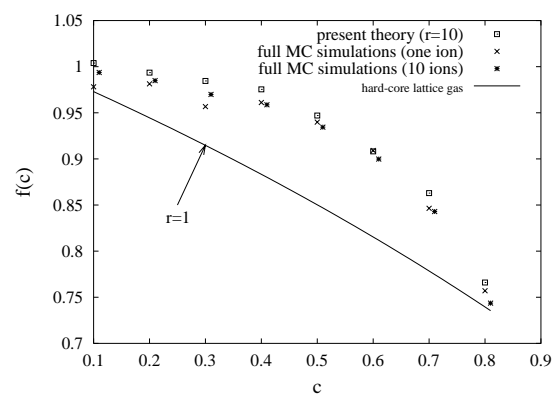
Figure 1: Comparison of tracer correlation factors from DP-theory and form full MC-simulation in an athermal system of point-particles diffusing through a network of polymer chains of length $r = 10$. The continuous line represents the tracer correlation factor of the hard core lattice gas, which corresponds to $r = 1$.

Furthermore, an attempt is being made to interpret recent measurements of the electrical conduction in stretched polymer ion conductors [5]. Thereby we start from the hypothesis that ions move through short helical channels formed by polyethylene-oxide chains and that long-range diffusion requires "interchannel hopping". This situation is mapped onto a random system of highly conducting ellipsoids embedded in a poorly conducting medium. Both dc and ac-conductance properties are worked out by applying differential effective medium theory, developed earlier for transport problems in porous media [6]. All the above projects are pursued in collaboration with A. Nitzan, Tel Aviv

A further question concerns the viscosity η of polymer electrolytes and its dependence on the ion concentration. For non-entangled chains and in the absence of hydrodynamic interactions the viscosity can be related to an effective local friction coefficient from knowledge of the fluctuations in the radius of gyration, when the chains are subjected to a Kramers potential [7]. In collaboration with H.L. Frisch (Albany) we apply this concept to the

coupled system of chains and ions. This should allow us to discuss the relationship between the friction coefficient and the degree of salt-induced crosslinking.

[1]   O. Dürr, P. Penzig, W. Dieterich, and A. Nitzan, J. Non-Cryst. Solids **748**, 235 (1998)

[2]   S. F. Druger, M. A. Ratner and A. Nitzan, Phys. Rev. B, **31**, 3939 (1985)

[3]   S. F. Druger and M. A. Ratner, Phys. Rev. B **38**, 12589 (1988)

[4]   O. Dürr, W. Dieterich and A. Nitzan in *Multiscale Computational Methods in Chemistry and Physics* edited by A. Brandt, J. Bernholc and K. Binder (IOS Press, 2001) p. 288

[5]   D. Golodnitsky and E. Peled, Electrochimica Acta, Vol 45, p. 1431-1436 (2000)

[6]   K. S. Mendelson and M. H. Cohen , Geophysics **47**, 257 (1982)

[7]   H. L. Frisch, N. Pistoor, A. Sariban, K. Binder und S. Fresjan, J. Chem. Phys. **89**, 5194

B3 DNA in front of an oppositely charged planar membrane: counterions evaporate and lead to an enthalpy-driven attraction

Christian Fleck and Hans Hennig von Grünberg

The possible occurrence of a phenomenon known as counterion condensation is perhaps the most prominent feature of polyelectrolyte suspensions. These chainlike macromolecules become charged, when solved in a liquid characterized by the Bjerrum length $\lambda_B = e^2/\epsilon kT$ (with e being the elementary charge, ϵ the dielectric constant of the solvent and kT the thermal energy). The counterions leaving the surface can either stay in the vicinity and thus under the influence of the charged polymer (bound counterions), or they can free themselves from the field of the polyelectrolyte (free counterions). If d, the mean distance between two charges on the polyelectrolyte, is large compared to λ_B, the number of free counterions in the suspension will increase in parallel with the line charge density $\tau = 1/d$. However, once the line charge density τ becomes so high that $\lambda_B \tau \geq 1$, i.e., $d \leq \lambda_B$, the number of free counterions ceases to grow with τ and remain constant. New counterions produced by further increasing τ, will now become bound counterions. This behavior is reminiscent of the coexistence of saturated vapor pressure and liquid in the usual condensation process. Therefore, the phenomenon is called "ion condensation".

This project is concerned with the question if the reverse process is possible, that is, if something like "counterion evaporation" or "counterion release" can occur, and if this can lead to an extra attraction between the polyelectrolyte and the object which is responsible for the evaporation. To answer these questions we have considered a model system consisting of an infinitely long, charged, cylindrical rod that is immersed in an unbounded electrolyte and brought into the external field of an oppositely charged, planar wall.

We have solved the Poisson-Boltzmann equation to obtain the mean-field electric potential $\phi(\mathbf{r})$ in the region filled by the electrolyte solution. The inset of Fig. (1.a) shows such a potential. With $\phi(\mathbf{r})$ one can then calculate quantities such as the total grand potential energy of the system, the total entropy, the number of particles in the system, and the enthalpy. Doing this for various distances h between the rod and the wall, one obtains the grand potential as a function of the distance $h - a$
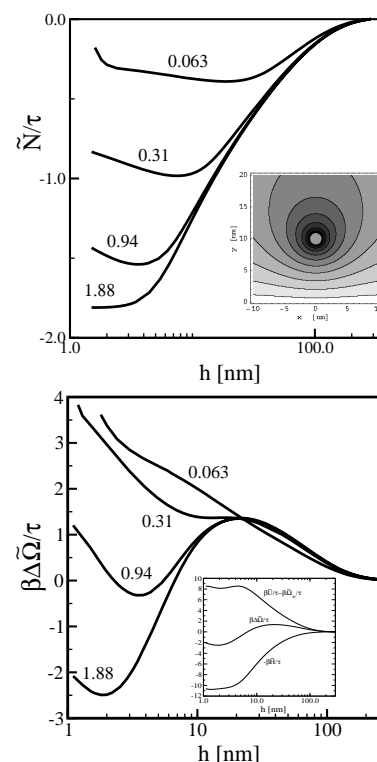
Figure 1: Change of a) particle number and b) grand potential of a system consisting of small electrolyte ions, a polyelectrolyte rod and a charged wall, as a function of the rod-wall distance h. The numbers labeling the curves are a measure of the surface charge density of the wall. Taken from Ref. (1).

function which may be regarded as the effective wall-rod interaction potential –, but also the entropy or particle number as a function of h.

All these quantities can now be used to analyze quantitatively the counter-ion release force. Fig. (1.a) shows for various different wall surface charge densities σ_w how the number of microions that are involved in the screening of the polyelectrolyte and the wall changes as a function of h. The counterion release is clearly visible: ions leave the system, they are "evaporated" due to the presence of the external field of the oppositely charged wall. Returning to the language of the gas-liquid phase-transition, the electric field strength of the wall charges here plays the role of the heat which one has to supply to transfer molecules from the liquid into the gas phase. In accordance with that picture, the total fraction of evaporated ions should grow with increasing "heat rate", that is increasing surface charge density σ_w of the wall, and the four curves in the Fig. (1.a) confirm that, indeed, this is the case.

Due to this evaporation, the whole system can gain a considerable amount of enthalpy and this gain for the system manifests itself as an attractive contribution to

the effective interaction between the polyelectrolyte and the wall. Fig. (1.b) shows the grand potential as a function of h, for four different values of σ_w. One can see how an additional minimum is formed on increasing σ_w. This additional attractive force is due to the release of counterions observed in Fig. (1.a). Ref. (1) is the first full mean-field study of this force. By analyzing the entropy and enthalpy as a function of h we could show on what mechanism this attractive force is exactly based. Contrary to what has been predicted by others, the counterion-release force is not a entropy-driven force. On the contrary: the total entropy of the system is considerably *reduced* due to the loss of particles, which alone would lead to repulsion. However, only parts of the total entropy are relevant for the grand-potential. This part is the entropy of only those microions that remain in the system which is in fact the enthalpy. This latter quantity now *increases* with decreasing h which is not surprising since the disappearance of ions leaves more space to the counterions remaining in the system. An increase of enthalpy means a lowering of the grand potential. Thus, the counterion release leads to an effective attraction due to a favorable change of enthalpy of the system: the counterion-release force is thus a enthalpy-driven force. This interaction, by the way, is in many respects reminiscent of the depletion interaction in a system consisting of small and large hard spheres where a gain of entropy of the whole system leads to an effective attraction between the large spheres.

That there is energy to be gained from the release of counterions is a fact long known in the theory of polyelectrolyte-ligand binding. Relatively new, however, is the incorporation of these ideas into a theory of polyelectrolyte adsorption. Our work as well as the current interest in counterion-release is triggered by a number of experiments of Rädler and coworkers on cationic lipid DNA complexation. We have chosen the parameters of our calculation so as to simulate the experiments of Rädler et al., i.e., a DNA in front of a cationic lipid membrane. Only recently a paper appeared where, for the first time, counterion-release has been observed directly. This study seems to confirm that the counterion-release force is a force that is of fundamental importance for our understanding of the adsorption behavior of DNA on oppositely charged membranes.

---

[1] C. Fleck and H.H. von Grünberg, PRE, in press, (2001).

C Colloids

C1   Monte Carlo studies of phase transitions of hard disks in external periodic potentials

W. Strepp, S. Sengupta, P. Nielaba

The liquid -solid transition in systems of particles under the influence of external modulating potentials has recently attracted a fair amount of attention from experiments [1-7], theory and computer simulations [8-13]. This is partly due to the fact that well controlled, clean experiments can be performed using colloidal particles [14] confined between glass plates (producing essentially a two -dimensional system) and subjected to a spatially periodic electromagnetic field generated by interfering two, or more, crossed laser beams. One of the more surprising results of these studies, where a commensurate, one dimensional, modulating potential is imposed, is the fact that there exist regions in the phase diagram over which one observes re -entrant [4-6] freezing/melting behaviour. As a function of the laser field intensity the system first freezes from a modulated liquid to a two dimensional triangular solid – a further increase of the intensity confines the particles strongly within the troughs of the external potential, making the system quasi -one -dimensional which increases fluctuations and leads to re -melting.

Our present understanding of this curious phenomenon has come from early mean -field density functional [8] and more recent dislocation unbinding [9] calculations. The mean field theories neglect fluctuations and therefore cannot explain re -entrant behaviour. In general, though mean field theories are applicable in any dimension, the results are expected to be accurate only for higher dimensions and long ranged potentials. The validity of the predictions of such theories for the system under consideration is, therefore, in doubt.

A more recent theory [9] extends the dislocation unbinding mechanism for two -dimensional melting [15] for systems under external potentials. For a two -dimensional triangular solid subjected to an external one -dimensional modulating potential, the only dislocations involved are those which have their Burger's vectors parallel to the troughs of the potential. The system, therefore, maps onto an anisotropic, scalar Coulomb gas (or XY model) [9] in contrast to a *vector* Coulomb gas [15] for the pure $2 - d$ melting problem. Once bound dislocation pairs are integrated out, the melting temperature is obtained as a function of the renormalized or "effective" elastic constants which depend on external parameters like the strength of the potential, temperature and/or density. Though explicit calculations are possible only near the two extreme limits of zero and infinite field intensities one can argue effectively that a re -entrant melting

transition is expected on general grounds quite independent of the detailed nature of the interaction potential for any two -dimensional system subject to such external potentials. The actual extent of this region could, of course, vary from system to system. In addition, these authors predict that the auto -correlation function of the Fourier components of the density (the Debye -Waller correlation function) decays algebraically in the solid phase with a universal exponent which depends only on the geometry and the magnitude of the reciprocal lattice vector.

Computer simulation results in this field have so far been inconclusive. Early simulations [10] involving colloidal particles interacting via the Derjaguin, Landau, Verwey and Overbeek (DLVO) potential [14] found a large re -entrant region in apparent agreement with later experiments. On closer scrutiny, though, quantitative agreement between simulation and experiments on the same system (but with slightly different parameters) appears to be poor [6]. Subsequent simulations [11-13] have questioned the findings of the earlier computation and the calculated phase diagram does not show a significant re -entrant liquid phase.

Motivated, in part, by this controversy, we have investigated [16,17] the freezing/melting behaviour of an unrelated system subjected to similar modulating external potentials. In Ref. [16,17] we have computed the phase behaviour of a two dimensional hard disk system in an external potential. The pair potential $\phi(r_{ij})$ between particles i and j with distance r_{ij} is:

$$\phi(r_{ij}) = \begin{cases} \infty & r_{ij} \leq \sigma \\ 0 & r_{ij} > \sigma \end{cases} \tag{1}$$

In addition a particle with coordinates (x, y) is exposed to an external periodic potential of the form:

$$V(x,y) = V_0 \sin\left(2\pi x/d_0\right) \tag{2}$$

The constant d_0 in Eq.(2) is chosen such that, for a density $\rho = N/S_x S_y$, the modulation is commensurate to a triangular lattice of hard disks with nearest neighbor distance a_s: $d_0 = a_s \sqrt{3}/2$ (see Fig. 1). The only parameters which define our system are the reduced density $\rho\sigma^2 = \rho^*$ and the reduced potential strength $V_0/k_B T = V_0^*$, where k_B is the Boltzmann constant and T is the temperature.

The pure hard disk system is rather well studied [18-21] by now and the nature of the melting transition in the absence of external potentials reasonably well explored. Also, there exist colloidal systems with hard interactions [14] so that, at least in principle, actual experiments using this system are possible. Finally, a hard disk simulation is relatively cheap to implement and one can make detailed studies of large systems without straining computational resources. The main outcome of our calculations, the phase diagram, is shown in Fig. 2. We

have shown results from our simulation of a system of $N = 1024$ hard disks (diameter σ) of density $0.86 < \rho^*(= \rho\sigma^2) < 0.91$ and the amplitude of the external potential $0 < V_0^*(= \beta V_0) < 1000$. Within our range of densities, one has a clear signature of a re-entrant liquid phase showing that this phenomenon is indeed a general one as indicated in Ref. [9]. We have determined phase transition points by the order parameter cumulant intersection method [22] applied to the order parameter ψ_{G_1} defined by: $\psi_{G_1} = \left| \sum_{j=1}^{N} \exp(-i\vec{G}_1 \cdot \vec{r}_j) \right|$, where $\vec{r}_j$ is the position vector of the jth particle, for $\vec{G}_1$ see Fig. 1.
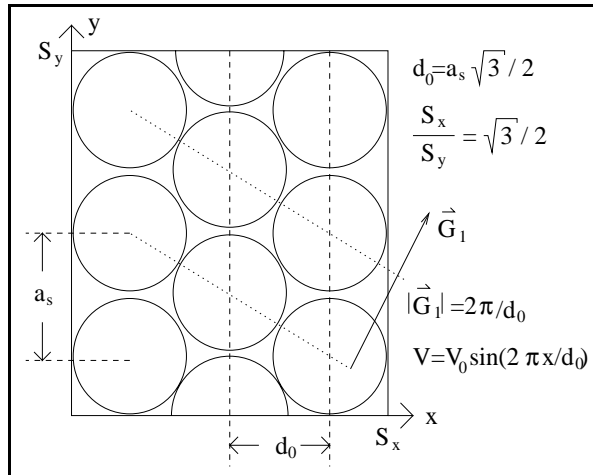

Figure 1: Schematic picture of the system geometry showing the direction $\vec{G}_1$ along which crystalline order develops in the modulated liquid. The four vectors obtained by rotating $\vec{G}_1$ anti-clockwise by $60°$ and/or reflecting about the origin are equivalent. The parameters d_0 and a_s are also shown. The size of the box is $S_x \times S_y$ and the modulating potential is V.
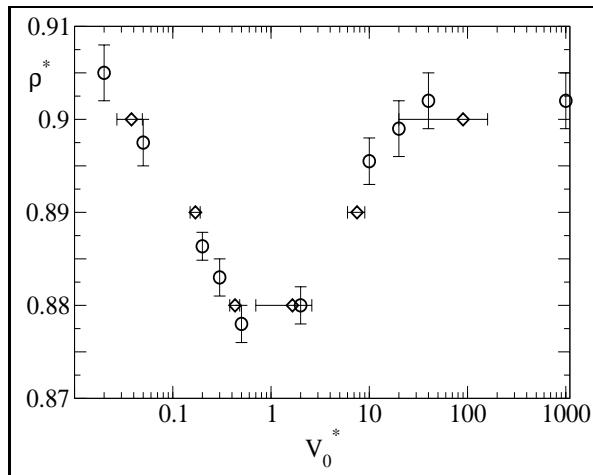

Figure 2: Phase diagram in the ρ^* / V_0^*- plane. Transition points for transitions from the solid to the modulated liquid have been obtained by the order parameter cumulant intersection method. In order to map the phase diagram we scanned in ρ^* for every V_0^*, starting from the high density (solid) region. The system size is $N = 1024$.

[1]   N.A. Clark, B.J. Ackerson, A. J. Hurd, Phys. Rev. Lett. **50**, 1459 (1983).

[2]   A. Chowdhury, B.J. Ackerson, N. A. Clark, Phys. Rev. Lett. **55**, 833 (1985).

[3]   K. Loudiyi, B. J. Ackerson, Physica **A 184**, 1 (1992); *ibid* 26 (1992).

[4]   Q. -H. Wei, C. Bechinger, D. Rudhardt and P. Leiderer, Phys. Rev. Lett. **81**, 2606 (1998).

[5]   C. Bechinger, Q.H. Wei, P. Leiderer, J. Phys.: Cond. Mat. **12**, A425 (2000).

[6]   C. Bechinger, M. Brunner, P. Leiderer, Phys. Rev. Lett. **86**, 930 (2001).

[7]   K. Zahn, R. Lenke and G. Maret, Phys. Rev. Lett. **82**, 2721, (1999)

[8]   J. Chakrabarti, H.R. Krishnamurthy, A. K. Sood, Phys. Rev. Lett. **73**, 2923 (1994).

[9]   E. Frey, D.R. Nelson, L. Radzihovsky, Phys. Rev. Lett. **83**, 2977 (1999).

[10]   J. Chakrabarti, H.R. Krishnamurthy, A.K. Sood, S. Sengupta, Phys. Rev. Lett. **75**, 2232 (1995).

[11]   C. Das, H.R. Krishnamurthy, Phys. Rev. **B58**, R5889 (1998).

[12]   C. Das, A.K. Sood, H.R. Krishnamurthy, Physica **A 270**, 237 (1999).

[13]   C. Das, A.K. Sood, H.R. Krishnamurthy, preprint.

[14]   For an introduction to phase transitions in colloids see, A. K. Sood in *Solid State Physics*, E. Ehrenfest and D. Turnbull Eds. (Academic Press, New York, 1991); **45**, 1; P. N. Pusey in *Liquids, Freezing and the Glass Transition*, J. P. Hansen and J. Zinn -Justin Eds. (North Holland, Amsterdam, 1991).

[15]   J. M. Kosterlitz, D. J. Thouless, J. Phys. **C 6**, 1181 (1973); B.I. Halperin and D.R. Nelson, Phys. Rev. Lett. **41**, 121 (1978); D. R. Nelson and B. I. Halperin, Phys. Rev. B **19**, 2457 (1979); A.P. Young, Phys. Rev. B **19**, 1855 (1979); K.J. Strandburg, Rev. Mod. Phys. **60**, 161 (1988); H. Kleinert, *Gauge Fields in Condensed Matter*, Singapore, World Scientific (1989).

[16]   W. Strepp, Ph.D-thesis, University of Konstanz (in preparation).

[17]   W. Strepp, S. Sengupta, P. Nielaba, Phys. Rev. **E** (2001) (in press).

[18]   K. W. Wojciechowski and A. C. Brańka, Phys. Lett. **134A**, 314 (1988).

[19]   H. Weber, D. Marx and K. Binder, Phys. Rev. **B51**, 14636 (1995); H. Weber and D. Marx, Europhys. Lett. **27**, 593 (1994).

[20]   A. Jaster, Phys. Rev. E **59**, 2594 (1999).

[21]   S. Sengupta, P. Nielaba, K. Binder, Phys. Rev. **E61**, 6294 (2000).

[22]   K. Binder, Z. Phys. **B43**, 119 (1981); K. Binder, Phys. Rev. Lett. **47**, 693 (1981).

C2 Phase Transitions of Colloidal Particles in strong Light Fields

M. Brunner, P. Leiderer, C. Bechinger

There has been considerable interest in the freezing and melting of colloidal particles during the recent years which has been largely motivated by the fact that colloidal particles provide ideal model systems for experimental studies of two-dimensional (2D) melting. Accordingly, such systems have been intensively investigated by several authors. While there exist numerous theoretical and experimental studies on 2D melting on homogeneous substrates, only little is known about 2D melting on corrugated surfaces, although the latter is much more relevant when modeling the substrate potential of a crystalline, i.e. atomically corrugated surface.

It was the experimental work of Chowdhury, Ackerson and Clark which originally demonstrated that periodic substrate potentials can cause interesting effects on the phase behavior of colloidal particles [1]. When they investigated a charge-stabilized colloidal liquid of polystyrene (PS) particles being confined between two glass plates and additionally exposed to a standing laser field (with its wave vector q tuned to the first peak of the direct correlation function), they observed a phase transition from a liquid into a crystal upon increasing the laser intensity. This phenomenon which has been termed laser-induced freezing (LIF) has been also theoretically analyzed employing Monte-Carlo (MC) studies and density functional theory (DFT) [2]. When Chakrabarti et al. [3] theoretically investigated the phase behavior of such a system as a function of the laser intensity, in addition to LIF which takes place at relatively small laser intensities, at higher laser intensities they found a reentrant laser-induced melting (LIM) transition where a remelting of the crystal back into the modulated liquid phase is observed. This effect has been also demonstrated to be in agreement with experimental studies [4,5].

In previous measurements the phase behavior was investigated only in a regime of fixed particle-particle interaction, i.e. constant particle number density and salt concentration, and only the laser intensity was varied. Here we present a systematic study where in addition to the depth of the light potential also the particle-particle interaction was varied [6]. Our data clearly show that reentrant melting from the crystalline state to a modulated liquid is only observed if the crystalline state had been formed by LIF (and not by spontaneous crystallization as has been theoretically suggested [3]). In addition, we observe LIF and LIM to take place at considerably higher laser fields and only in a relatively small region of particle number densities and salt concentrations.

We used aqueous suspensions of sulfate PS particles of 3 μm diameter and a polydispersity of 4% (Interfacial Dynamics Corporation). Due to sulfate-terminated surface groups which partially dissociate off when in contact with water, the suspended particles are negatively charged and experience a partially screened electrostatic repulsion. The experiments are performed in a closed circuit which is composed of the sample cell, a vessel of ion exchange resin and an electrical conductivity probe to control the ionic strength of the suspension [7]. A peristaltic pump is used to pump the highly deionized suspension through the circuit. The Debye screening length was estimated from the interparticle distribution of the colloids to be on the order of κ-1 ≈ 400 nm.

The sample cell consists of two horizontally aligned parallel glass surfaces with a distance of 1 mm. We first deionized the circuit almost completely as confirmed by the value of the ionic conductivity σ = 0.07 μS/cm. The laser potential was created by two slightly crossed laser beams of a linearly polarized Nd:YVO4 laser (λ=532 nm, Pmax = 2W) which overlapped in the sample plane thus forming an interference pattern. Due to the polarizability of the PS spheres this provides a periodic, one-dimensional potential for the particles. The periodicity could be adjusted by variation of the crossing angle. Due to the almost vertical incidence of the laser beams onto the sample the particles experienced additionally a vertical light pressure which pushed them towards the negatively-charged bottom silica plate of our cell. This vertical force is estimated to be in the range of pN and largely reduces vertical fluctuations of the particles, thus confining the system effectively to two dimensions. The sample, which was in addition illuminated with white light from the top, was imaged with a microscope objective onto a CCD camera chip connected to a computer for further analysis. The intense Nd:YVO4 laser light was blocked with an optical filter.

To distinguish different thermodynamic phases we first determined the particle center coordinates by means of a particle-recognition algorithm. From those data the time averaged single particle density $\rho(x,y)$ and the pair correlation function $g(x,y)$ were calculated, the latter being particular useful for differentiating the modulated liquid from the crystalline phase. Here, x and y denote the direction perpendicular and along the interference fringes, respectively. In addition, when fitting the decays $g(y)$ of the different phases, we find that the modulated liquid phases have always short range order and an exponential decay. In contrast, the decay in the

crystal extends over a much longer range and can be described by an algebraic function g(y)-1 ∝ y-η.

In contrast to earlier measurements, where the particle number density was held constant, here we measured systematically the phase behavior for different particle number densities as a function of the light potential amplitude V0. Particular attention was paid to the fact that the periodicity of the laser potential d was adjusted properly to obtain a hexagonal crystal, i.e. $d = \sqrt{3}a/2$. Otherwise a distorted lattice would have been observed. The range of d was between 6 μm and 8 μm. The result of more than 100 single measurements are shown in Fig.1 [6]. We plotted the vertical axis in units of (κa)-1 with a being the mean distance of next neighbor particles which has been measured for each particle concentration in the absence of the laser field. As can be seen, the value of (κa)-1 where the transition towards the crystal occurs decreases at small laser intensities as a function of V0. This is the characteristic feature of LIF. For larger values of V0, however, the separation line between the crystalline and the modulated liquid region is shifted back to higher (κa)-1- values and starts to saturate at the highest values which could be obtained with our setup. It is this up bending which gives rise to the LIM phenomenon. If (κa)-1 is in a range between 0.045 and 0.048, with increasing V0 one observes the following sequence of states: isotropic liquid – modulated liquid – crystal – modulated liquid which is in agreement with earlier results [4,5].

The experimental data suggest that LIF and LIM occur at higher V_0 than in the MC-simulations [2]. Possibly some deviations between theory and experiment stem from the fact that the latter were performed in finite size systems, whereas the simulation results were obtained by extrapolation to the thermodynamic limit. We believe, however, that this is not sufficient to explain such a large difference because our values for LIF are consistent with experimental and numerical results of other authors [1] [8] [9]. The second, and even more significant difference between our data and MC-simulations is the qualitative behavior of the phase separation line at high V0. The MC-simulations suggest that (κa)-1 at V0 = 0 is below the corresponding value at very high V0. This implies that LIM is not restricted to crystals formed by LIF but may also appear in systems where the particle concentration is above that for spontaneous crystallization. This is in contrast to our experiments, where LIM was only observed for light induced crystals. The latter is also supported by a recent theoretical work of Frey et al. where the qualitative phase behavior of a 2D system of charged colloids in the presence of a periodic light potential was reinvestigated [10]. Using the same concepts developed in the context of dislocation mediated melting theory

their data also support the existence of LIF and LIM. In contrast to ref. [2], however, the melting temperature of the reentrant modulated liquid is found to be higher than that of the modulated liquid at small V0. This directly corresponds to our finding that reentrant melting is only possible in a range of (κa)-1 values which allows for LIF and thus demonstrates the unique properties of the light-induced crystalline phase. In addition, because the region of (κa)-1-values where reentrance occurs is rather small, this might explain why such an effect has experimentally not been observed before although such a behavior should be also found in other 2D-systems with periodical, 1D potentials.
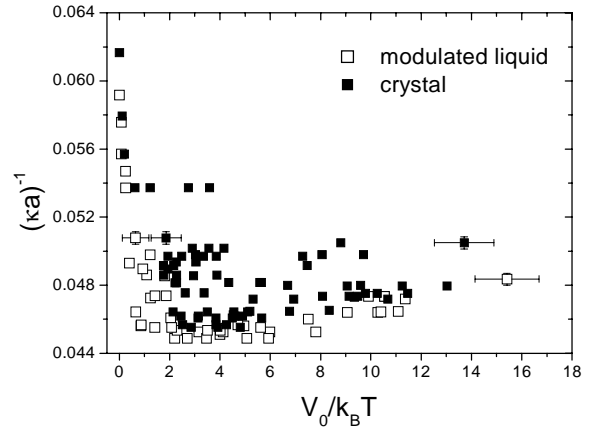
Figure 1: Experimentally determined phase diagram as a function of $(\kappa a)^{-1}$ vs. V_0/kT. The open symbols denote the modulated liquid, the closed symbols the crystalline phase, respectively. For clarity error bars are only plotted for a few data points.

[1] A. Chowdhury, B. J. Ackerson, and N. A. Clark, Phys. Rev. Lett. **55,** 833 (1985).

[2] J. Chakrabarti, H. R. Krishnamurthy, and A. K. Sood, Phys. Rev. Lett. **73,** 2923 (1994).

[3] J. Chakrabarti, H. R. Krishnamurthy, A. K. Sood, and S. Sengupta, Phys. Rev. Lett. **75,** 2232 (1995).

[4] Q.-H. Wei, C. Bechinger, D. Rudhardt, and P. Leiderer, Phys. Rev. Lett. **81,** 2606 (1998).

[5] C. Bechinger, Q. H. Wei, and P. Leiderer, J. Phys.:Cond. Matt. **12,** A425 (2000).

[6] C. Bechinger, M. Brunner, and P. Leiderer, Phys. Rev. Lett. **86,** 930 (2001).

[7] T. Palberg, W. Härtl, U. Wittig, H. Versmold, M. Würth, and E. Simnacher, J. Phys. Chem. **96,** 8180 (1992).

[8] K. Loudiyi and B. J. Ackerson, Physica A **184,** 1 (1992).

[9] K. Loudiyi and B. J. Ackerson, Physica A **184,** 26 (1992).

[10] E. Frey, D. R. Nelson, and L. Radzihovsky, Phys. Rev. Lett. **83,** 2977 (1999).

C3   Gas-liquid phase coexistence in colloidal suspensions: fact or fiction?

G. Klein, R. Klein, R. van Roij, H.H. von Grünberg

Suspensions of charged colloidal particles at low salt concentration have attracted much attention recently, mainly because of experimental claims of attractive interactions between like-charged colloids and the possibility of a gas-liquid phase transition [1]. Such phenomena cannot be explained by the standard and well-accepted DLVO theory. This theory predicts a repulsive effective interaction between the colloids which – according to the classical van-der Waals picture – cannot lead to a fluid-fluid phase-separation. Recent attempts to effectively take into account higher-body interactions in the form of density-dependent "volume terms" have provided a first theoretical explanation of the unexpected phase-separation [1]. In this project [2] we describe a charge-stabilized colloidal suspension within a Poisson-Boltzmann (PB) cell model and calculate the free-energy as well as the compressibility of the suspension as a function of the colloidal density. The PB equation for a 1:1 electrolyte is $\nabla^2 \phi(\mathbf{r}) = \kappa^2 \sinh \phi(\mathbf{r})$ where $\phi(\mathbf{r}) = e\psi(\mathbf{r})/kT$ is the normalized mean-field electric potential, and κ^2 the screening constant. The resulting boundary value problem can be linearized. The "traditional" (Debye-Hückel (DH) or DLVO) way to linearize the PB equation is to replace $\sinh \phi \approx \phi$ which is valid if $\phi \ll 1$. In [2], we have proposed an alternative, more general, linearization based on the expansion $\sinh[\phi(\mathbf{r})] = \sinh[\bar{\phi}] + \cosh[\bar{\phi}](\phi(\mathbf{r}) - \bar{\phi}) + \ldots$. Important is that we have not yet decided which linearization point $\bar{\phi}$ to choose. The linearized problem can now be solved analytically to obtain ϕ which in turn is used to calculate the free-energy and compressibility of the suspension. Both quantities are still functions of $\bar{\phi}$.

One important message of our investigation is that the success of linearization depends crucially on the choice of the linearization point $\bar{\phi}$. This can be systematically tested by comparing the free-energy that is based on the numerical solution to the full non-linear PB equation with the analytical expression for the $\bar{\phi}$-dependent free-energy obtained from the linear solution. Classical DH theory, for example, where $\bar{\phi}$ is taken to be zero, completely fails for suspensions of high volume fraction and typical colloidal charge. This is not surprising considering that in a concentrated colloidal suspension $\phi(\mathbf{r})$ hardly ever becomes zero, and a linearization point $\bar{\phi} = 0$ cannot be appropriate. We tested a number of different ways to choose linearization points, among them the idea to identify $\bar{\phi}$ with the Donnan potential. This choice turned out to be by far the best. Besides good agreement with the

free-energy of nonlinear theory, the Donnan linearization scheme has the additional advantage that the resulting expression for free-energy is identical to the free-energy Hamiltonian obtained in ref. [1], including both "volume-terms", whose physical origin can now be understood.

In ref. [1] these volume terms in the Hamiltonian have been shown to be responsible for the unexpected and exciting occurrence of a gas-liquid phase separation in colloidal suspensions. We, on the other hand, have a model system with a free energy expression in non-linear theory that after linearization about the Donnan potential leads to the same Hamiltonian as in [1]. We are thus in the position to check if the phase-separation predicted in [1] is due to nothing but the linearization of the problem, i.e., to check if the phase-separation is an artefact of the linearization. The answer is positive: within the limits of our model, we have come to the conclusion that, yes, indeed, this is an artefact. The criterion for such a
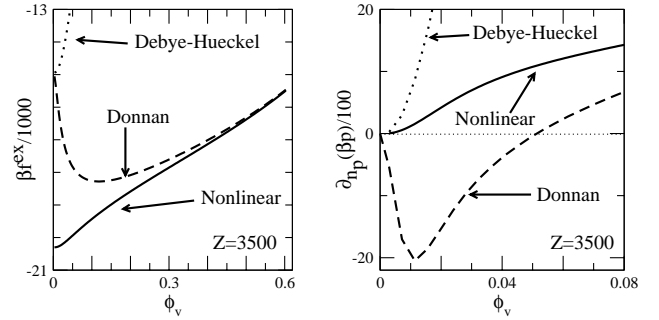

Figure 1: Excess free-energy per particle and compressibility as a function of the colloidal fraction ϕ_v for colloidal charge $Z = 3500$. The full curves stem from nonlinear Poisson-Boltzmann cell theory, the dashed and dotted one from Debye-Hückel and Donnan linearization.

fluid-fluid phase separation is that the compressibility $(\partial p/\partial n_p)_{\mu_s,T} < 0$, with p the osmotic pressure of the suspension. This negative compressibility can be seen in Figure 1 in the Donnan linearization scheme, but not in non-linear theory. The two values of ϕ_v where the compressibility changes sign are the spinodal points. Repeating such a calculation for various salt-concentrations leads to phase diagrams with a closed-loop spinodal, in perfect agreement with the predictions in [1]. By contrast, within the nonlinear theory *we do not find any indication of a phase instability* [2]. On the basis of these cell calculations one might therefore conclude that the failure of the linear theory at low ϕ_v is responsible for the gas-liquid phase separation found in [1].

[1] R. van Roij, M. Dijkstra, and J.P. Hansen, Phys. Rev. E **59**, 2010 (1999).

[2] H.H. von Grünberg, R. van Roij and G. Klein, submitted to EPL (2001).

C4   Elastic constants of 2D Colloids

A. Wille, K. Zahn, G. Maret

I. Optical tweezer measurements

Since the well known KTHNY-theory [1] of two-dimensional (2D) melting the close relation between the melting transition and elasticity of 2D systems is a well established fact. Recently a first complete study of both aspects on a 2D system made of hard discs was realized using Monte Carlo simulations [2]. The authors found a convincing agreement with KTHNY. In experimental systems, however, this dependency of the 2D melting scenario upon the elastic behavior has not been examined so far. This is mainly due to the problem of accessing the elastic constants of a 2D system. In the following we will propose two different methods for the determination of a complete set of elastic constants of a 2D colloidal system and will demonstrate that our results are well in agreement with theoretical predictions.

Our system consists of super-paramagnetic particles (diameter $2R_P = 4.5 \mu m$ and susceptibility $\chi = 7.37 \cdot 10^{-11}$ Am^2/T) in a water drop hanging from a glass plate. The drop is confined by a cylindrical hole, which is milled into the glass plate, of 8 mm inner diameter and 1 mm height. Due to their high specific density (1.7 g/cm^3) the colloidal spheres are subjected to strong sedimentation towards the water-air interface, where a single particles layer is formed. The curvature of the interface is adjusted automatically by computer controlling the drop's content of liquid using a micrometrical syringe: a height difference of less than 1 μm between the center and the border of the drop can be achieved. A magnetic field $\mathcal{B}$ perpendicular to the interface is applied and induces a magnetic dipole moment $\mathbf{M} = \chi \mathcal{B}$ in the spheres. This leads to a repulsive interaction: $u(r) = (\mu_0/4\pi) \chi^2 \mathcal{B}^\in / \nabla^\ni$, r denoting the distance between their centers. Since other contributions to the particle interaction were found to be negligible our system is entirely controlled by magnetic dipole interaction adjusted by the external field B [3]. In addition it was demonstrated that the setup is an almost ideal 2D system. Depending on the interaction strength $\Gamma = (\mu_0/4\pi) \chi^2 \mathcal{B}^\in (\pi\rho)^{\ni/\in}/\|\mathcal{T}$ (ρ being the 2D particle density) a two dimensional liquid, hexatic [1] or crystalline phase is found.

The first method to determine elastic constants in our 2D model system is based on relaxation measurements of deformations, which are induced by optical tweezers. As was shown by Ashkin [4] a highly focused laser beam can be used to manipulate colloidal particles individually. This tweezer effect is based on the fact that a particle with a higher refractive index than the surrounding suspension is pulled into the maximum of an electromagnetic field. Combined with two scanning galvanometer
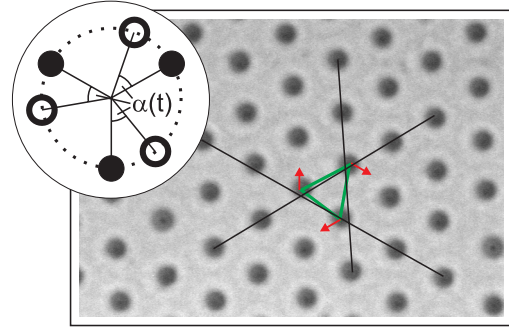

Figure 1: A section (165 x 110 μm) of a 2D colloidal crystal is shown. Three particles on a triangle are rotated out of their equilibrium position indicated by the arrows. The lines are guides to the eye and symbolize the lattice axes.
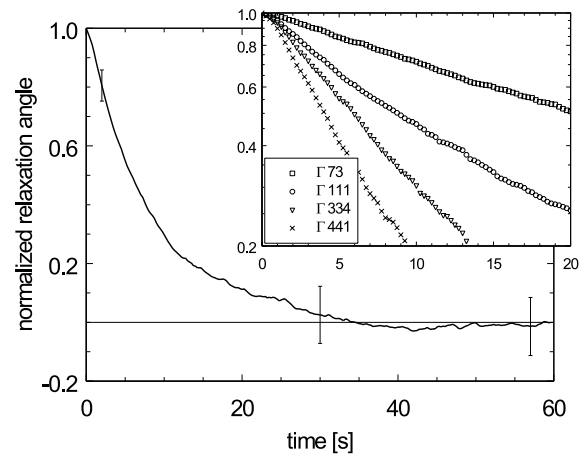

Figure 2: Time dependence of a normalized relaxation angle of three particles forming a triangle which were rotated out of their equilibrium position by 20 degrees (compare fig.1). The curve was obtained for an interaction strength of $\Gamma = 279$. The inset shows four curves in logarithmic scale corresponding to $\Gamma = 73, 111, 334, 441$ respectively.

mirrors we are able to position several particles simultaneously and precisely in the 2D sample plane against the repulsive magnetic particle interaction. In this way well defined local deformations in the 2D crystal can be induced. To probe the shear modulus of our system three particles forming a triangle were rotated by 20 degrees on a circle with constant radius (fig.1). Thereafter the tweezer was switched off and the particle relaxation was recorded in terms of the angle (line between a particle and the common center of the triangle compared to its equilibrium position) as a function of time. Fig.2 shows a typical angle relaxation as a function of time (normalized to one at $t = 0$) for $\Gamma = 279$. In the inset four relaxation curves are plotted in logarithmic scale for $\Gamma = 73, 111, 334, 441$ respectively. Clearly the increase of the relaxation time upon a decrease of Γ is demonstrated. We will develop a simple model to extract the shear modulus from the presented measurements: In the theory of elasticity the be-

haviour of an isotropic 2D systems is determined by two independent elastic constants, e.g. the bulk modulus B and the shear modulus μ. The analogy of our experiment in the elastic continuum is a disk of radius R_D [5] rotated by an angle α and relaxing due to the elastic forces. The energy which is necessary to rotate the disk by an angle α follow from basic elasticity theory:

$$E = 2\pi\mu\alpha^2 R_D^2. \tag{1}$$

This implies a repulsive force F_R proportional to the twist angle α: $F_R = -4\pi\mu R_D\alpha$. Obviously this experiment depends only on μ and not on B. If we assume that the colloidal movement is totally overdamped due to the high viscosity of the solvent and if we neglect hydrodynamic interactions we can equate F_R with the Stokes friction:

$$F_S = -6\pi\eta R_P \frac{a}{\sqrt{3}} \cdot \frac{\partial\alpha}{\partial t} \tag{2}$$

Here $a/\sqrt{3}$ denotes the particle distance to the center of the rotated triangle, a the lattice constant, $\eta = 0.0010 Nsm^{-2}$ the viscosity of water and $R_P = 2.25\mu m$ the particle radius. The resulting differential equation ($F_R + 3 \cdot F_S = 0$) has the solution:

$$\alpha(t) = \alpha_0 \cdot e^{-t/\tau} \qquad \tau = 2.86\frac{\eta R_P}{\mu} \tag{3}$$

This equation is fitted to the measured curves to determine the shear modulus. The dependence of μ on the interaction strength Γ is shown in fig.3. As expected μ increases with increasing interaction strength Γ. A linear least square fit to the data gives the relation $\mu = 0.30\,\Gamma$ compared to a slope of 0.346 from a zero temperature calculation (fig.3). This is a remarkable theoretical confirmation of our measurements.
Nevertheless, some points will have to be clarified in the future: The validity of elastic continuum theory on the
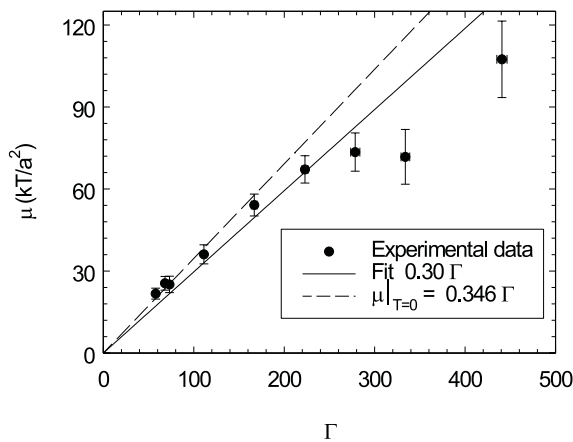

Figure 3: Shear modulus μ in units of kT/a^2 derived from the measured relaxation time τ (see fig.2). The data is compared to a zero temperature calculation.

scale of the lattice constant is questionable. On the one hand the value of the effective radius of the disc (R_D) is only determined up to a factor of order unity. On the other hand the measurements are performed on a local scale and even though we probe the shear modulus the precise relationship between our results and the macroscopic elastic constant μ is a priori not clear. However, this point can be clarified through the investigations described in the following part of this project.

The next step will be the determination of the bulk modulus B using a similar experiment. This will enable, for the first time, to establish experimentally the relation between the elastic constants and melting point of a 2D system.

II. Measurement of strain fluctuations

The second method proposed to determine elastic constants in our 2D colloidal system is based on the measurement of thermally induced strain fluctuations [6]. The basic idea of this method, which was so far only applied to simulations, will be explained by the following example. From statistical physics [7] the thermal volume fluctuations ΔV in a (p,T,N)-ensemble are known:

$$\langle(\Delta V)^2\rangle/V = kT/B \tag{4}$$

B denotes the bulk modulus and V the system size. In the following we will use the strains tensor ε_{ij}, which is defined through partial derivatives of components of the local displacement field $\mathbf{u}(x_i)$:

$$\varepsilon_{ij} = \frac{1}{2}\left(\frac{\partial u_i}{\partial x_j} + \frac{\partial u_j}{\partial x_i}\right) \tag{5}$$

In 2D systems we have $i, j = x, y$. The relative volume change can be expressed in terms of the strain tensor as $\Delta V/V = \varepsilon_{xx} + \varepsilon_{yy}$. Using this identity and the fact that our system is isotropic we can rewrite equation 4:

$$B = \frac{kT}{V}\frac{1}{2(\langle\varepsilon_{xx}\varepsilon_{xx}\rangle + \langle\varepsilon_{xx}\varepsilon_{yy}\rangle)} \tag{6}$$

Thus, if the strain fluctuations are known the bulk modulus can be determined. However, the strain fluctuations depend as $1/V$ upon system size and equ.6 holds only in the thermodynamic limit $V \to \infty$. To avoid measurements at different system sizes V and extrapolation to infinity a finite size scaling scheme was proposed recently and applied to Monte Carlo simulations of a 2D system made of hard discs [8]. Precisely the same methods will be applied in the following to our 2D colloidal system.
The strain fluctuations are determined from a set of particle configurations obtained by video-microscopy and image processing on a PC. Typically 700 configurations containing some 1000 particles each are gathered. The equilibrium position of each colloid is determined by an
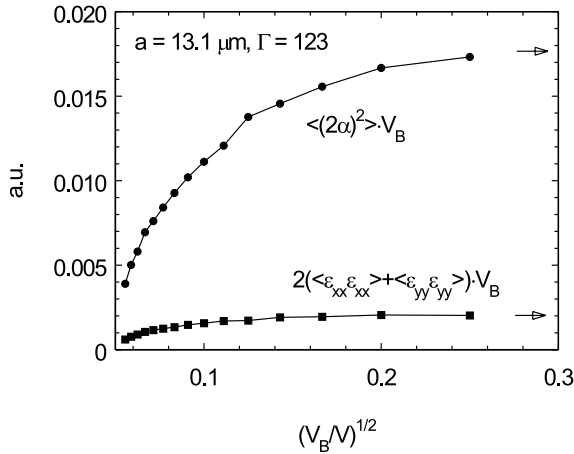
Figure 4: Scaling behaviour of $2(\langle \varepsilon_{xx}\varepsilon_{xx}\rangle + \langle \varepsilon_{xx}\varepsilon_{yy}\rangle) \cdot V_B$ and $\langle (2\alpha)^2 \rangle \cdot V_B$ as a function of the subsystem size V_B with respect to the total size V. The arrows denote the respective "infinite-system" values.
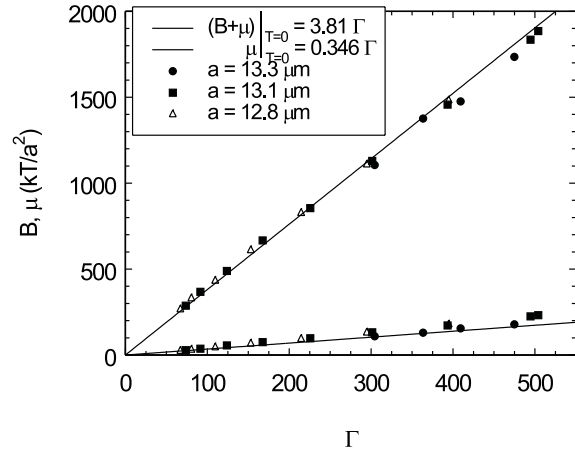
Figure 5: The comparison of the measured elastic constants (in units of kT/a^2) to the zero-temperature calculation reveals an very good agreement.

average over all configurations, and from that the displacement field $\mathbf{u}(x_i)$ (for every configuration and particle) is calculated. The strains are determined from equ.5 with the derivatives replaced by finite differences (e.g. $\partial u_i \rightarrow \Delta u_i$) calculated between nearest neighbors. Equ.6 together with the finite scaling analysis [8] already gives the result.

A similar expression as equ.4 can be found for the shear modulus μ. This is done by equating the mean energy of the twisted disc (equ. 1) to the thermal energy $kT/2$ and making use of $V = \pi R_D^2$:

$$\mu = \frac{kT}{V}\frac{1}{\langle (2\alpha)^2 \rangle} \qquad (7)$$

If the twist angle α is expressed in terms of the strain tensor $2\alpha = (\varepsilon_{xy} - \varepsilon_{yx})$ both B and μ are accessible through measurements of the local strain fluctuations. Yet, one subtlety concerning the determination of B has to be discussed. Equ.4 is obtained for a system in an (p,T,N) ensemble i.e. under a constant external pressure p. However our system (and sub-systems during the finite-size scaling) are part of an elastic continuum. The volume fluctuations do not only have to work against the external pressure – this is taken account of in equ.4 – but also against the elasticity of the surrounding medium. A precise analysis reveals that in equ.6 B has to be replaced by $B + \mu$. The final results are summarized in figs.4 and 5. In fig.4 the finite size scaling is illustrated. The rhs of equs.6 and 7 are shown as functions of the – linear – system size $\sqrt{V_B/V}$ for one given system at $\Gamma = 130$. V_B is the size of a sub-system during the finite size scaling analysis. The arrows denote the scaled "infinite-system" values. This analysis was performed for three different experimental systems (different lattice constants a) as a function of Γ. The final results of B and μ are drawn

in fig.5 in units of kT/a^2 (data points). In addition a zero-temperature calculation of B and μ has been included (solid line), which is obtained on the basis of the known interaction potential. Considering the fact that no adjustable parameter is used the agreement turns out to be very good. This demonstrates on the one hand the capabilities of the proposed method to predict elastic constants and on the other hand it clearly shows that the zero-temperature approximation works amazingly well even down to values of $\Gamma \simeq 70$, compared to the melting temperature of $\Gamma = 60$.

[1] J.M. Kosterlitz and D.J. Thouless, J. Phys. C **6**, 1181 (1973); A.P. Young, Phys. Rev. B **19**, 1855 (1979); D.R. Nelson and B.I. Halperin, Phys. Rev. B **19**, 2457 (1979).

[2] S. Sengupta, P. Nielaba and K. Binder, Phys. Rev. E **61**, 6294 (2000).

[3] K. Zahn, R. Lenke, and G. Maret, Phys. Rev. Lett. **82**, 2721 (1999).

[4] A. Ashkin, J. Dziedzic, J. Bjorkholm, and S. Chu, Opt. Lett. **11**, 288 (1986).

[5] We use an effective radius R_D for the disk which is obtained by equating the size of the disk and the area of the Voronoi cells of the three tweezed particles: $R_D = a \cdot \sqrt{3 \cdot \sqrt{3}/2\pi}$, a being the lattice constant.

[6] M. Parrinello and A. Rahman, J. Chem. Phys. **76**(5), 2662 (1982).

[7] L. Landau and E. Lifshitz, *Statistical Physics*, (Pergamon, Oxford, 1986).

[8] S. Sengupta et al., Phys. Rev. E **61**, 1072 (2000).

C5 Elasticity and orientational fluctuations in 2D colloids

G. Haller, A. Wille, K. Zahn, G. Maret

In the previous report C4 the elastic behavior of a 2D model system composed of super-paramagnetic colloidal particles (diameter $4.5\,\mu$m, susceptibility $\chi = 7.37 \cdot 10^{-11}$Am^2/T) confined to a water-air interface was studied. The micro-spheres interact via a repulsive dipole-dipole interaction adjusted by a magnetic field B applied perpendicular to the two-dimensional (2D) particle layer. In this report the melting scenario of the identical system will be analyzed using long time behavior of two dynamic correlation functions, the 2D Lindemann parameter $\gamma_L(t)$ and the bond-angular correlation function $g_6(t)$. The results are compared to predictions of the KTHNY-theory of 2D melting (see [1] of C4).

Real time video-microscopy and image processing on a PC were used to record complete positional data of typically 2000 particles over 5 decades in time. From these the desired correlation functions are calculated. In 3D the melting point is determined by the long time limit of the mean square displacement $\langle\Delta\mathbf{u}(t)\rangle$ (with $\Delta\mathbf{u}(t) = \mathbf{u}(t) - \mathbf{u}(0)$), which is finite in the crystalline and infinite in the liquid phase. However, for a 2D crystal $\langle\Delta\mathbf{u}(t)\rangle$ diverges and a modified "Lindemann" parameter $\gamma_L(t)$ has to be used. If j and $j+1$ denote neighboring particles $\gamma_L(t)$ is defined as [1,2]:

$$\gamma_L(t) = \langle(\Delta\mathbf{u}_j(t) - \Delta\mathbf{u}_{j+1}(t))^2\rangle/2a^2$$

where a denotes the lattice constant. In fig.?? $\gamma_L(t)$ is shown for different system temperatures which is the inverse of the interactionparameter Γ (compare C4) $\Gamma = (\mu_0/4\pi)\,\chi^2 B^2 (\pi\rho)^{3/2}/kT$ with ρ denoting the 2D particle density. The long time behavior clearly distinguishes between the solid ($\gamma_L(t)$ finite) and the liquid ($\gamma_L(t) \to \infty$ for $1/\Gamma \geq 0.0168$). In the inset the data are drawn on linear scale to illustrate the difference in behavior of $\gamma_L(t)$ observed at melting.

KTHNY theory predicts that the 2D solid phase melts into a so-called hexatic phase, characterized by an algebraic decay of orientational correlation – both in space and time. A second transition takes the system eventually into the isotropic liquid. This can be analyzed using the bond-angular correlation function (in time) $g_6(t) = \langle\exp[i6\theta(t)]\rangle$, where $\theta(t)$ denotes the angle fluctuation of a fixed bond over time t. Fig.?? shows $g_6(t)$ as a function of $1/\Gamma$ for the same data as fig.??. As predicted by KTHNY $g_6(t)$ tends to a constant in the crystal and in the hexatic and the isotropic liquid ($1/\Gamma \geq 0.0176$), respectively, an algebraic and an exponential decay is
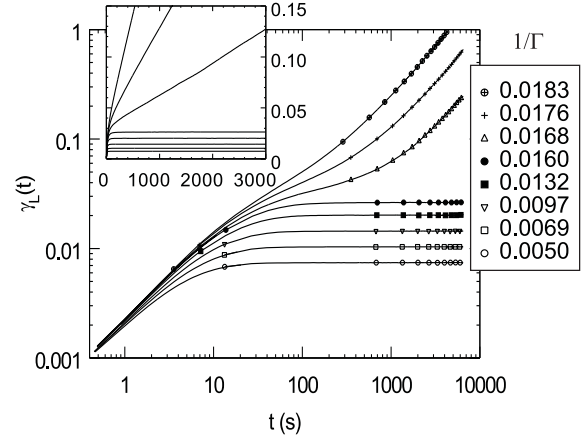

Figure 1: Dynamic Lindemann parameter as a function of time for various temperatures $1/\Gamma$. In the crystalline phase the long-time limit of $\gamma_L(t)$ is bounded while it diverges in the liquid phases ($1/\Gamma \geq 0.0168$). The inset shows the data in a linear plot to illustrate the change in the behavior of $\gamma_L(t)$.
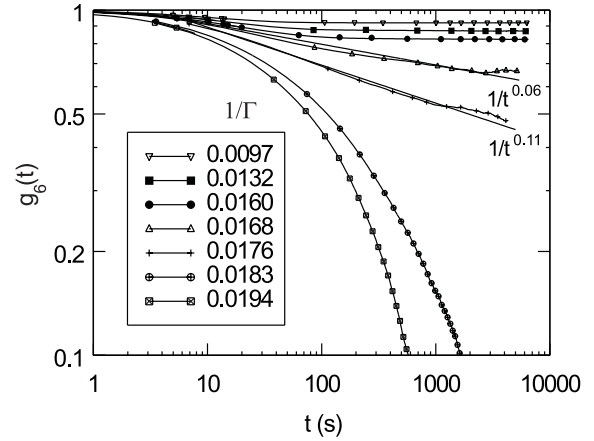
Figure 2: The bond-order correlation function in time $g_6(t)$ as a function of $1/\Gamma$. Clearly three long-time regimes of $g_6(t)$ can be distinguished: In the solid $g_6(t)$ tends to a constant; in the hexatic and the isotropic liquid, respectively, an algebraic and an exponential decay is found.

found. In addition, it was predicted that in the hexatic phase close to the isotropic liquid $g_6(t)$ decays proportional to $1/t^\eta$ with $\eta = 0.125$ [3]. This is well compatible with $\eta = 0.11$ at $1/\Gamma = 0.0176$, the latter being close to the hexatic-liquid transition at $1/\Gamma_i = 0.0178$ [2].

[1] V.M. Bedanov and G.V. Gadiyak , Phys. Lett. **109A**, 289 (1985).

[2] K. Zahn, R. Lenke, and G. Maret, Phys. Rev. Lett. **82**, 2721 (1999).

[3] D.R. Nelson, in: Phase Transitions and Critical Phenomena, Vol.7, eds by C. Domb and J.L. Lebowitz (Academic Press, London, 1983) p.1.

C6 Effective colloid/colloid forces in colloidal suspensions: non-pairwise pair-forces

H.H. von Grünberg, R. Klein, L. Belloni

Our headline is obviously nonsense: forces that depend on more than a pair of particles cannot be pair-forces. And still, the headline is well-chosen as it brings the apparent absurdity of the concept of "macroion-averaged" potentials to the point. What are these "macroion-averaged" potentials used to describe the colloid-colloid interaction in colloidal suspensions?

It is convenient to take the Wigner-Seitz cell radius R as a measure of the typical distance between colloids in a suspension, defined by $4\pi R^3 n_m/3 = 1$, where n_m is the colloid density. This distance has to be compared with the typical thickness of a double-layer which is given by $1/\kappa$, with $\kappa^2 = 8\pi\lambda_B c_s$. If $\kappa^{-1} >> R$ the colloids in the suspension are interacting with effectively an unscreened Coulomb law since the screening length is much greater than their mean distance. In this case it is reasonable to treat the colloids as a one-component plasma in a neutralizing background of electrolyte solution. If on the other hand, $\kappa^{-1} << R$, the screening length becomes much less than the distance between neighboring colloids, resulting in well separated double-layers around each colloidal particles. Here it makes sense to go over to a one-component description of the system with a pair-wise interaction between dressed colloids. This is the domain of DLVO theory. Things become complicated in the parameter regime in between these two limits, i.e., if $\kappa^{-1} \approx R$, because many simultaneously overlapping layers lead to an effective interaction that is essentially many-body in nature. Forces between two colloids then depend also on the positions of all other colloids, and the total interaction can, in principle, no longer be split into pairwise contributions. In practice, however, it is hard to come to terms without pair-potentials. One way out of this problem is to work with pair-potentials that depend on the colloid density. One calculates a pair-potential by averaging over all positions of the $N - 2$ colloids with the two colloids being held fixed at their position. This is a kind of effective potential; but it is not the microionic degrees of freedom that are averaged out, but those of the $N - 2$ neighboring colloids. Therefore, a better term for the volume-fraction dependent colloid/colloid interaction in suspensions is "macroion-averaged" effective potential where the attribute "macroion-averaged" refers to the macroion averaging and the word "effective" to the microion averaging. In [1] we proposed an eccentric Poisson-Boltzmann (PB) cell model with the aim of deriving such macroion-averaged potentials. We start
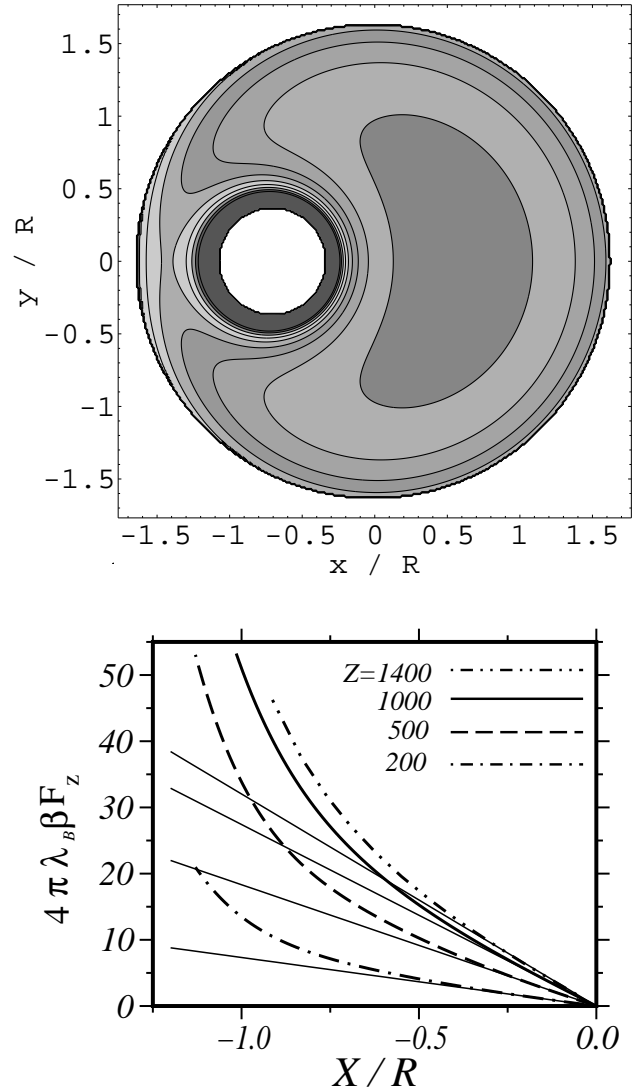
Figure 1: Upper picture: Typical ion density distribution for a shifted colloid in a spherical charged cage. Lower picture: Total force acting on a colloid which is shifted a distance X from the center of the cage of its nearest neighbors. Force curves for several charges of the macroion are shown, together with the linear forces (thin solid lines) calculated in the harmonic approximation.

from the assumption that all macroions are initially located at fcc lattice sites, and allow one colloid to be shifted a distance X from its center position. Calculating for each X the PB profiles, see Fig. (1.a), one can determine directly the force acting on the colloid, Fig. (1.b), something which is impossible in the standard centric cell model where the force on the colloid is always zero. From this total force we can subsequently derive "macroion-averaged" effective pair-forces.

[1] H.H. von Grünberg, J. Phys.: Condens. Matter, **12**, 6039 (2000); H.H. von Grünberg and L. Belloni, PRE, 62(2), 2493 (2000).

C7 Dynamic Scaling and related Freezing Criteria in Two and Three Dimensions

G. Nägele, R. Pesché, M. Kollmann, A.J. Banchio and J. Bergenholtz

In this project we have analyzed the static and dynamic scaling behavior of three-dimensional and quasi-two-dimensional (Q2D) colloidal dispersions with strong and long-range particle repulsions. Typical examples of such Q2D systems are monolayers of charged colloidal spheres between two glass plates interacting by long-range screened electrostatic interactions, and super-paramagnetic colloidal spheres located at a liquid-air interface and interacting by repulsive dipolar magnetic forces induced by a perpendicularly applied external magnetic field.

We have employed a Brownian Dynamics (BD) simulation method with the dominant far-field part of the hydrodynamic interactions (HI) included, to study the statics and dynamics of these Q2D systems with its implications on related static and dynamic freezing criteria [1,2]. For this purpose, various measurable quantities are calculated like the radial distribution function $g(r)$, the static structure factor $S(q)$, the mean squared displacement $W(t)$, the dynamic structure factor $S(q,t)$, and the distinct and self van Hove space-time correlation functions $G_d(r,t)$ and $G_s(r,t)$, respectively. An analogous study for three-dimensional salt-free dispersions of charge-stabilized particles was performed using a fully self-consistent mode-coupling scheme [3].

The radial distribution functions, $g(r) = G_d(r, t = 0)/n$, of these systems reveal a pronounced principal peak located at a radial distance, r_m, which is nearly equal to the geometric mean particle distance, $r_0 = n^{-1/d}$. Here, n is the number density of particles, and d denotes the system dimension. Since r_m is the only physically relevant static length scale, different systems sharing the same principal peak height $g(r_m)$ have radial distribution functions which superimpose nearly perfectly when plotted versus reduced distance r/r_0 (cf. Fig. 1). The static scaling behavior of the $g(r)$'s implies that the corresponding static structure factors nearly coincide when plotted versus the reduced wave number q/q_0 with $q_0 = 2\pi/r_0$. Without considering HI, there is a single characteristic time scale $\tau_0 = r_0^2/D_0$ associated with r_0. As a consequence there is dynamic scaling, i.e. colloidal systems with strong and long-range particle repulsion and identical peak heights $g(r_m)$ (likewise, identical $S(q_m)$) show nearly identical dynamical properties, e.g., nearly identical $G_d(r,t)/n$, , $W(t)/r_0^2$ and $S(q,t)$ as functions of reduced time $\tau = t/\tau_0$, distance $x = r/r_0$ and wave
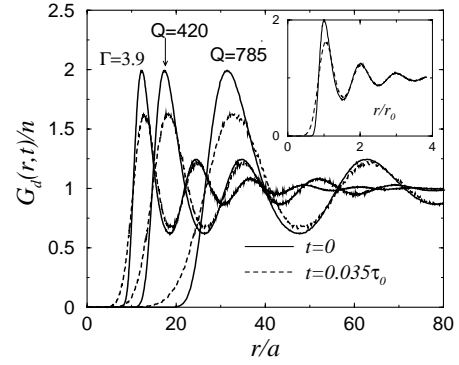

Figure 1: BD results for the distinct van Hove function $G_d(r,t)/n$ versus r/a of a magnetic dispersion with coupling parameter $\Gamma = 3.9$ and of two charge-stabilized Q2D systems of particle charge numbers $Q = 420$ and $Q = 785$, respectively. Note that $G_d(r, t = 0)/n = g(r)$ at $t = 0$. The inset exemplifies the static and dynamic scaling (from [1,2]).
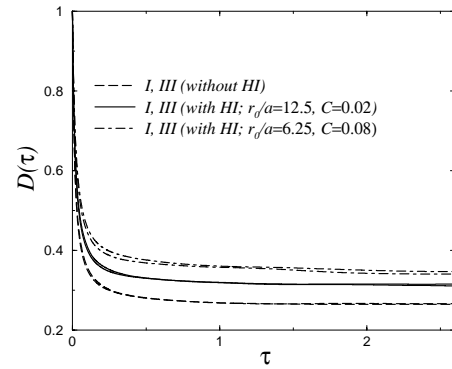
Figure 2: BD results with/without HI for the normalized self-diffusion coefficient $D(t) = W(t)/(D_0 t)$ of a magnetic systems, labeled by I, and a charged Q2D system, labeled by III, versus reduced time τ. Here, $C = \pi n a^2$ is the area fraction, and $S(q_m) = 2.2$ is constant for all systems considered in this figure (from [1,2]).

number $y = q/q_0$ (cf. Fig. 1 displaying $G_d(r,t)/n$ at time $t/\tau_0 = 0.035$).

Hydrodynamic interactions introduce the particle radius a as another relevant length scale since the particles are in contact with the solvent. With HI, a more restricted form of dynamic scaling holds where, e.g., the master curves for $G_d(x,\tau)/n$ and $D(\tau)$, defined by $D(\tau) = W(t)/(D_0 t)$, depend on the characteristic length ratio a/r_0. Furthermore, HI cause a modest enhancement of self-diffusion which becomes stronger with increasing a/r_0. The enhancement of self-diffusion is indicative of systems with prevailing influence of the far-field part of HI (cf. Fig. 2 showing $D(\tau)$).

The dynamic scaling behavior of systems with strong and long-range repulsion implies in particular a one-to-one correspondence between $S(q_m)$ and the

Figure 3: Reduced long-time self-diffusion coefficient D_S^L/D_0 vs. liquid static structure factor peak height $S(q_m)$. Mode-coupling results without HI (from [3]) for deionized three-dimensional bulk dispersions of charge-stabilized particles are include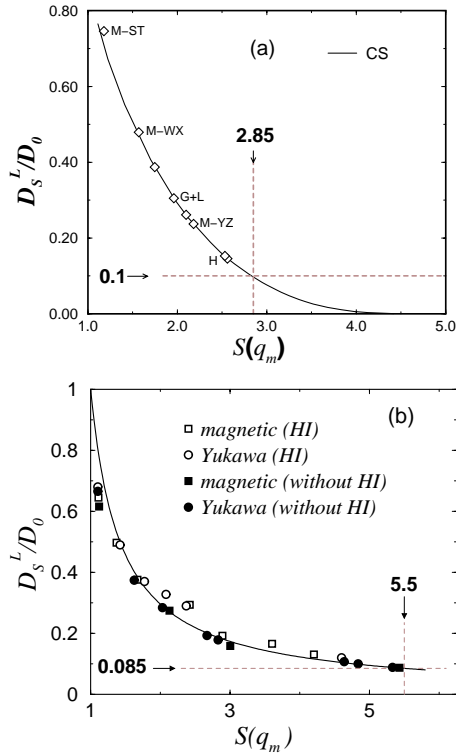d in (a). The particle interactions in (a) are described by a Yukawa-like screened Coulomb potential of DLVO type. BD results with/without HI for magnetic and charge-stabilized Q2D systems are shown in (b) (from [2,3]).

non-dimensionalized long-time self-diffusion coefficient $D_S^L/D_0 = D(t \to \infty)$. Fig. 3a includes the master curve for D_S^L/D_0 vs. $S(q_m)$ as obtained for deionized three-dimensional dispersions of charge-stabilized particles using a fully self-consistent mode-coupling scheme without HI. Note that a peak height of $S(q_m) = 2.85$ corresponds to $D_S^L/D_0 = 0.1$. This result is in accord with an empirical static freezing criterion of Hansen and Verlet [4], which states that the onset of freezing in three-dimensional systems should occur when $S(q_m) \approx 2.85$, and with a dynamic criterion of Löwen, Palberg and Simon [5], which localizes the freezing line of three-dimensional Brownian systems at $D_S^L/D_0 \approx 0.1$.

Our BD results of D_S^L/D_0 vs. $S(q_m)$ for magnetic and charged Q2D dispersions with and without HI are displayed in Fig. 3b. Without HI, there is for Q2D systems again a single master curve, but now with $D_S^L/D_0 \approx 0.085$ and $S(q_m) \approx 5.5$ at freezing. This finding is in excellent accord with an empirically found dynamic criterion for two-dimensional freezing of Löwen [6] stating that $D_S^L/D_0 \approx 0.085$ at the freezing line independent of the pair potential and the nature of the freezing process.

Moreover, a value of $S(q_m) \approx 5.5$ at freezing was indeed found from computer simulations of Broughton et al. [7]

For three-dimensional and Q2D dispersions with strong and long-range particle repulsion we have thus shown that dynamic scaling is at the origin of the equivalence of related static and dynamic freezing criteria. According to Fig. 3b, the value of D_S^L/D_0 close to freezing is only modestly enlarged by HI, indicating that the dynamic freezing rule of Löwen et al. applies also when far-field HI are considered.

For systems with strong near-field HI and lubrication forces acting between the particles like dispersions of colloidal hard spheres, $D_S^S < D_0$, where D_S^S is the short-time self-diffusion coefficient. The dynamic freezing criterion should then be restated in terms of D_S^L/D_S^S instead of D_S^L/D_0.

[1] R. Pesché, M. Kollmann and G. Nägele, submitted (2001).

[2] R. Pesché, M. Kollmann and G. Nägele, J. Chem. Phys., accepted for publication (2001).

[3] A.J. Banchio, G. Nägele and J. Bergenholtz, J. Chem. Phys. **113**, 3381 (2000).

[4] J. P. Hansen and L. Verlet, Phys. Rev. **184**, 151 (1969).

[5] H. Löwen, T. Palberg and R. G. Simon, Phys. Rev. Lett. **70**, 1557 (1993).

[6] H. Löwen, Phys. Rev. E **53**, R29 (1996).

[7] J. Q. Broughton, G. H. Gilmer and Y. D. Weeks, Phys. Rev. B **25**, 4651 (1982).

C8   Static and Dynamic Properties of Wall-Confined Colloids

R. Pesché and G. Nägele

The confinement of a dispersion of colloidal particles can lead to interesting static and dynamic features that are not observed in bulk systems. The aim of this work was to assess in a quantitative way the influence of the complicated many-body hydrodynamic interactions (HI) on the particle dynamics by calculating various dynamical properties and pointing to interesting hydrodynamic effects. To analyze the influence of HI on the dynamics of wall-confined charged and neutral colloidal particles, we have employed a Stokesian Dynamics (SD) simulation technique [1]. This powerful method can be applied to a variety of colloidal systems where HI effects need to be accounted for with good accuracy. To keep the numerical effort manageable, we have only considered the lateral diffusion of interacting colloidal particles within the midplane between the two parallel plates, separated by a fixed distance $h = 2\sigma$. Here, σ is the diameter of the particles. In the case of charged particles, we have used an effective pair potential of Yukawa type with a screening parameter depending on the plate separation [2].

The SD evolution equation for the trajectories of N identical spherical Brownian particles immersed in an incompressible fluid of shear viscosity η follows from a two-fold time integration (i.e. coarse-graining) of the many-particle Langevin equation. To describe the hydrodynamic influence of the two confining planes, we have used a superposition of the image force description for colloids in the presence of a single plane with stick boundary conditions [3,4]. In our SD simulations, typically $N = 200$ particles were equilibrated in a square replicated periodically. After equilibration, several thousand configurations were generated for calculating various properties.

To assess the importance of HI on the dynamics, we have analyzed the mean squared displacement (MSD) $W(t)$ of the particles, as well as real-space van Hove functions and the hydrodynamic function $H(q)$. We have further investigated static properties like the radial distribution functions, $g(r)$, and the static structure factor, $S(q)$, in two dimensions [4].

In Fig. 1, we present self-diffusion SD results for effective charge numbers $Z^* = 10^2$ and $Z^* = 10^3$, respectively, at plate separation $h = 2\sigma$ and area fraction $C = N\pi a^2 / A = 0.063$. We distinguish the case, labeled as full HI, where HI are accounted for (including the effect of the walls) from the case where particle-particle HI is neglected and where only particle-wall HI are accounted for (labeled as p-w HI). The MSD with full
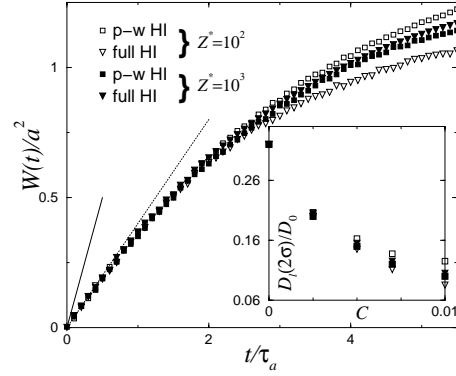

Figure 1: Lateral MSD $W(t)$ for a monolayer of charged spheres vs. reduced time for full HI and p-w HI only. Here $\tau_a = a^2 / D_0$, where a is the particle radius and D_0 the bulk self-diffusion coefficient of an isolated sphere. Two charge numbers are considered: $Z^* = 10^2$ and 10^3. Solid line segment indicates the slope, D_0, of the MSD for a free particle in the bulk fluid; the dotted line is the slope, $D_0(2\sigma)$, of the MSD for an isolated particle in the midplane between two walls separated by $h = 2\sigma$. Inset: long-time self-diffusion coefficient $D_l(2\sigma)/D_0$ vs. area fraction C. Shown are hard sphere results with full HI (open triangles) and with p-w HI (open squares), in comparison with results for charged particles of $Z^* = 10^2$ with full HI (filled squares) and p-w HI (filled triangles).

HI acting among the particles, and the particles and the walls, is compared with the corresponding result where particle-particle HI are disregarded. Consider first the system of less charged particles with $Z^* = 10^2$. As seen, inclusion of p-p HI gives rise to a hydrodynamic reduction of the MSD as observed also for neutral particles. In contrast, strongly charged particles with $Z^* = 10^3$ behave qualitatively different: far-field HI prevailing in systems of strongly repulsive particles support the diffusion of a particle out of its dynamic cage of neighboring particles. This leads to a hydrodynamic enhancement of $W(t)$ at intermediate and long times. Hard-sphere-like systems are most strongly affected by near-field HI, since the position r_m of the principal peak of $g(r)$ is close to the contact distance σ. Near-field HI always causes thus a slowing down of the particle motion. For $Z^* = 10^2$, the principal peak of $g(r)$ appears at a value significantly smaller than the geometrical mean interparticle distance, explaining thus the observed hydrodynamic reduction of $W(t)$. The long-time self-diffusion coefficient in the case where HI are completely neglected is significantly larger than when full HI are considered, since there is no retarding hydrodynamic influence of the confining walls.

We mention that hydrodynamic enhancement of the long-time self-diffusion coefficient, D_l, which is the long-time slope of the MSD, was theoretically predicted for three-dimensional charged-stabilized suspensions in [5], and experimentally verified subsequently [6].
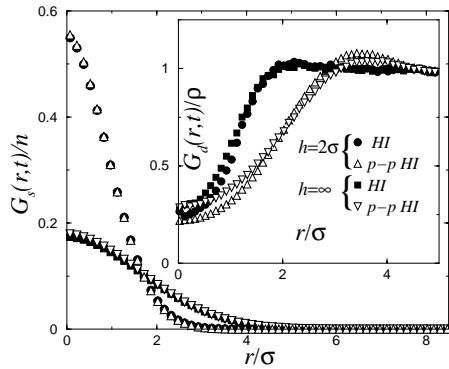
Figure 2: Reduced self and distinct (inset) van Hove functions, $G_s(r,t)/n$ and $G_d(r,t)/n$ for charged particles with $Z^* = 10^3$, area fraction $C = 0.063$, $t = 3.5\tau_a$ and $h = 2\sigma$.
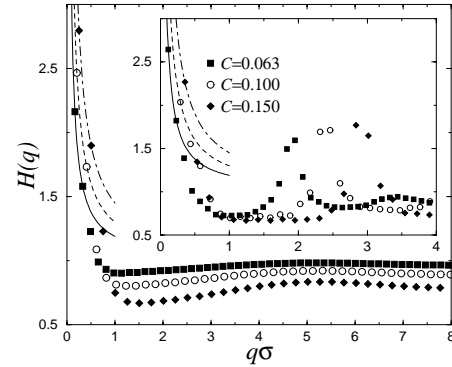

Figure 3: Hydrodynamic function at plate separation $h = 2\sigma$ for hard spheres and charged particles (shown in the inset) with $Z^* = 10^3$. Further shown is the asymptotic part, $1 + 3C/q$, of $H(q)$ for $C = 0.063$ (solid line), $C = 0.1$ (dashed line) and $C = 0.15$ (dashed-dotted line).

SD results for $D_l(h = 2\sigma)$ vs. area fraction are shown in the inset of Fig. 1 for the opposite cases of neutral hard spheres, and highly charged particles with $Z^* = 10^3$, for full HI and p-w HI. Inclusion of particle-particle HI leads to a visible increase (decrease) of D_l for highly charged (neutral) wall-confined colloidal spheres.

SD results for the self and distinct van Hove functions $G_s(r,t)$ and $G_d(r,t)$ with $Z^* = 10^3$ are included in Fig. 2. It is remarkable that self-motion (i.e. $G_s(r,t)$) is most strongly affected by p-w HI, whereas dynamic pair correlations (i.e. $G_d(r,t)$) are dominated by p-p HI.

Results for the two-dimensional hydrodynamic function $H(q)$ are shown in Fig. 3 for hard spheres and charged particles with $Z^* = 10^3$ (inset). The undulations in $H(q)$ grow larger for increasing C in case of hard spheres. The local maximum of $H(q)$ at wave-number $q = q_m$ is smaller than one and decreases with increasing C, with q_m shifted to slightly larger values of q. This behavior of $H(q)$ is similar to the one observed for the hydrodynamic function of three-dimensional suspensions of colloidal hard spheres. The q-dependence of $H(q)$ for charged systems is qualitatively different since $H(q_m)$ is now larger than one and increases monotonically with C. A monotonic increase in $H(q_m)$ for increasing concentration is further observed in three-dimensional charge-stabilized suspensions. As discussed in full detail in [7], $H(q_m)$ refers to particle pairs separated by the next-neighbor shell radius r_m and moving in opposite directions. Hard spheres are dominated by near-field HI since $r_m = \sigma$, which results in a reduction of the antagonistic motion of a particle pair due to the laminar friction in the thin coating of solvent sticking to the surfaces of both particles. Therefore, $H(q_m) < 1$ in case of hard spheres. The dynamics of charged particles, on the other hand, is dominated by far-field HI which favors the antagonistic motion of particle pairs separated by $r_m \geq 2\sigma$ due to a cumulative solvent back-flow effect. This leads for charged spheres at small C to values $H(q_m) > 1$. There is a strik-

ing difference in the small-q behavior of $H(q)$ between three-dimensional and quasi-two-dimensional colloids. Whereas $H(q \approx 0) < 1$ in the three-dimensional case, the SD results of Fig. 3 reveal a strong increase of $H(q)$ at small q, suggesting $H(q)$ to diverge as $q \to 0$. The unbounded increase of $H(q)$ for $q \to 0$ is due to the lateral confinement with no off-plane motion of the particles. By using a point force approximation for the mobility tensor, we find an expression for $H(q)$ with a first-order pole at $q = 0$ [8]. This divergence of $H(q)$ is a characteristic feature of two-dimensional systems. It depends not on the pair potential acting between the colloids. As a result, the two-dimensional dynamic structure factor $S(q,t)$ decays as $S(q,t)/S(q) \approx \exp[-(3CD_0(h)/\sigma)qt]$ for q and t small. In Fig. 3, we have included the graphs of the asymptotic term of $H(q)$ (of the form $1 + 3C/q\sigma$). The small-q part of the SD $H(q)$ is well described by this singular form even in the presence of the walls. The hydrodynamic influence of the walls on $H(q)$ becomes manifest only at intermediate values of q, where it gives rise to a small increase in $H(q)$.

[1] G. Bossis and J.F. Brady, J. Chem. Phys. **87**, 5437 (1987).

[2] E. Chang and D.W. Hone, Europhys. Lett. **5**, 635 (1988).

[3] R. Pesché and G. Nägele, Europhys. Lett. **51**, 584 (2000).

[4] R. Pesché and G. Nägele, Phys. Rev. E **62**, 5432 (2000).

[5] G. Nägele and P. Baur, Europhys. Lett. **38**, 557 (1997).

[6] W. Härtl, J. Wagner, Ch. Beck, F. Gierschner and R.R. Hempelmann, J. Phys.: Condens. Matter **12**, A287 (2000).

[7] A.J. Banchio, G. Nägele and J. Bergenholtz, J. Chem. Phys. **111**, 8721 (1999).

[8] A.J. Banchio, Ph.D. thesis, University of Konstanz (2000).

C9 Study of surface charge densities using total internal reflection microscopy.

L. Helden, H.H. von Grünberg, P. Leiderer,
C. Bechinger

Interactions that occur between charged objects immersed in an electrolytic solution, such as colloids, micelles, vesicles, and proteins, play an important role in many biological and physico-chemical systems [1] [2]. In the vicinity of charged surfaces in solution, a diffuse layer of electrolyte ions forms, with a thickness in the order of the Debye screening length κ^{-1}. Accordingly, if two such objects having like-charged surfaces approach each other closely, their double layers start to overlap which eventually leads to an increase of counter-ion density in the gap between them relative to the bulk solution. This results in a repulsive "double-layer" force [2] [3] being - except for small separations where dispersion and steric interactions become important - one of the principal long-range forces in such systems. The effective wall-colloid potentials are measured using the TIRM (total internal reflection microscopy) technique. In contrast to similar experiments which were performed by other authors before [4] [5] [6], here we measured the potentials at various salt concentrations using the same particle. This allows us to calculate its surface charge density with a very high accuracy.

A good approximation for the solution of the Poisson-Boltzmann equation in our experimental situation (polystyrene sphere of a=5µm radius in aqueous solution over a flat silica plate) is given by [7]:

$$\beta V_{DL(h)} = \frac{16a}{\lambda_B} \gamma_W \gamma_C \exp\{-\kappa(h-a)\} \qquad (1)$$

where h is the distance between the wall and the center of the colloid, $\lambda_B = e^2\beta/\varepsilon$ is the Bjerrum length, $\beta=1/kT$ and ε is the dielectric constant of the solvent, and κ is the inverse Debye screening length which depends on the salt concentration. This simple, and convenient analytical form is based on the Gouy-Chapman solution where the prefactor contains the charge renormalization factors γ_w and γ_c for wall and colloid respectively.

$$\gamma_{W/C} = \tanh\left[\tfrac{1}{2} \arcsin h\left(\frac{2\pi\lambda_B \sigma_{W/C}}{\kappa}\right)\right] \qquad (2)$$

Here the dependence of the prefactor on the surface charge densities σ_w and σ_c is explicitly spelled out and the idea of the following experiment is to measure the double layer interaction potentials for different salt concentrations (κ values) from which the surface charge densities from the prefactors can be derived.

The total interaction potential βV_{tot} between sphere and wall which has been experimentally obtained by employing total internal reflection microscopy [8] (for details of this technique we refer to C16) is a superposition of double layer repulsion $\beta V_{DL,}$ and gravity βV_{grav} that presses the particle against the wall.
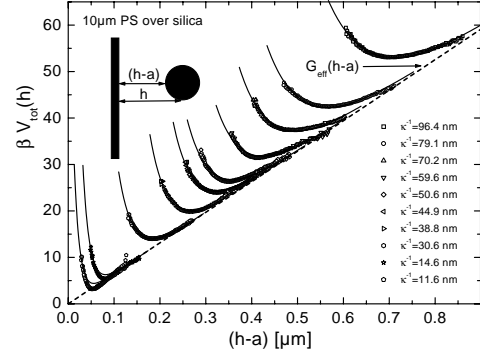

Figure1: Measured total potentials βV_{tot}, for a polystyrene sphere of 5µm radius, for ten different Debye lengths κ^{-1} ranging from about 10nm to 100nm. At higher salt concentrations the particles stick to the surface due to attractive dispersion forces. All the potentials have a very similar shape: towards larger distances the potentials increase linearly, because gravity is the dominant force acting on the particle. At smaller distances repulsive double-layer interaction and attractive dispersion forces between the particle and the wall become important [9].

As expected, the mean colloid-wall distance decreases with decreasing Debye length. In addition we observe that the left branch of each potential becomes steeper with decreasing Debye length, a feature that is to be expected from the exponential of Eq.1. As can be seen there is very good agreement between our data and theory (solid lines in Fig.1) , except for the two curves closest to the wall. These deviations are attributed to the short ranged attractive dispersion forces βV_{disp}, which will be neglected in the following because they play a rather marginal role here [9].

In the following we concentrate on the electrostatic repulsion, therefore we subtracted contributions due to gravitation (V_{grav}) and dispersion forces (V_{disp}) which are known without any open parameters in this case [10].

The closed symbols in Fig.2 correspond to the fitted prefactors of Eq.1 divided by the $16a/\lambda_b$. In principle the surface charge densities could be derived, from these data using Eq.2. However, to reduce the number of fit parameters, the same experiment was performed with an

a=1.5µm silica sphere over silica glass so that the two γ-factors cold be assumed equal ($\gamma_c = \gamma_w$). The Inset of Fig. 2 shows the prefactors found in this experiment using a single-parameter fit, which yields $\sigma_w = 0.0007 C/m^2$. The numerical value is in good agreement with literature [11]. With this value the surface charge density σ_c of the polystyrene sphere has been determined to $\sigma_c = 0.0001 C/m^2$ [9].
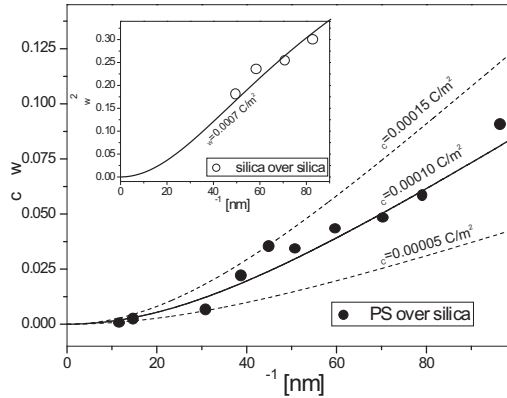

Figure 2: Prefactors of the exponential function in Eq.(1) divided by $16a/\lambda_B$, as obtained from a fit to the data in Fig.1. Shown are data for a PS sphere over silica, and for a silica sphere over silica (inset). To demonstrate the sensitivity of this method, the function $\gamma_w\gamma_C$ is plotted for three values of the colloidal surface charge density [9].

The fitted curve $\gamma_w\gamma_c$ from Eq.2 is displayed in Fig.2 as solid curve. To demonstrate the sensitivity of our measurements, we have added two curves of the same function with $\sigma_c = 0.00015 C/m^2$ and $\sigma_c = 0.00005 C/m^2$ as dashed lines. The theoretical and experimental data show in particular at higher values of κ^{-1} good agreement and indicate that in both experiments (PS and silica spheres) our data can be well described by the simple analytical form eq.1. We conclude that with the method proposed here, surface charge densities can be determined within ±30% accuracy [9].

The agreement observed in Fig.2 also implies that our measurements are in good agreement with the theoretical double-layer potential of Eq.1. This can be seen by dividing the potentials by their corresponding values of $\gamma_w\gamma_c$. According to Eq.1, it follows that the potentials scaled in this way should all have the same prefactor $16a/\lambda_B$. In a semi-logarithmic representation, this means that all curves should appear as straight lines with identical slopes and intersections. This is indeed confirmed by Fig.3 where we see all potentials collapsing onto one common master-curve. This proves that Eq.1 correctly describes the double-layer interaction between the wall and the colloid. The small deviations of the ex-

perimental data from the master curve are attributed to an approximate error of 5 % in the κ-values derived from our ionic conductivity measurements.
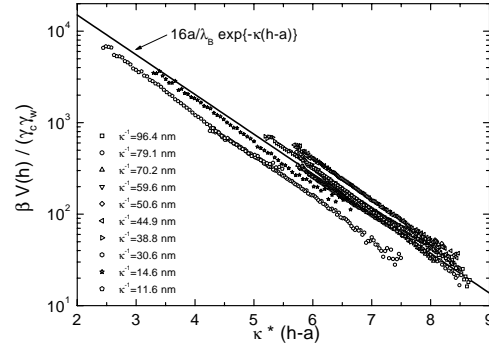
Figure 3: Master-plot of all measured potentials. For details we refer to the text [9].

[1] J. Israelachvili, *Intermolecular and Surface Forces* (Academic Press, London, 1992).

[2] D. F. Evans and H. Wennerström, *The Colloidal Domain: Where Physics, Chemistry, Biology, and Technology meet* (VCH, New York, 1994).

[3] H. Löwen and J. P. Hansen, Annu. Rev. Phys. Chem. **51,** 209 (2000).

[4] S. G. Bike and D. C. Prieve, Int. J. Multiphase Flow **16,** 727 (1990).

[5] S. G. Flicker, J. L. Tipa, and S. G. Bike, J. Colloid. Interface Sci. **158,** 317 (1993).

[6] S. G. Flicker and S. G. Bike, Langmuir **9,** 257 (1993).

[7] H. H. v. Grünberg and E. C. Mbamala, J. Phys.: Cond. Mat.**,** in press (2001).

[8] D. C. Prieve, F. Luo, and F. Lanni, Faraday Discuss. Chem. Soc. **83,** 297 (1987).

[9] H. H. v. Grünberg, L. Helden, P. Leiderer, and C. Bechinger, J. Chem. Phys.**,** (in press) (2001).

[10] M. A. Bevan and D. C. Prieve, Langmuir **15,** 7925 (1999).

[11] D. E. Dunstain, J. Coll. Int. Sci. **166,** 472 (1994).

C10 Charged colloids near dielectric interfaces

E.C. Mbamala, H.H. von Grünberg, R. Klein

The study of electric double layer forces and interactions of charged colloids in solutions has provided simple and convenient model systems for studying the interaction of more complex and important biological and chemical systems, among them, such prominent examples as the macromolecular DNA system. While in the bulk (far from any dielectric interfaces) charged-stabilized colloidal suspensions have been rigorously investigated, only few studies have been made for such suspensions near dielectric interfaces. This is surprising since the latter (interfacial suspension) should be well suited as a model system for studying, in general, the basic effect of dielectric discontinuity on the structural properties of suspensions of charged objects, be it an ion near a protein, or a single highly charged DNA molecule near a membrane.

In one of our studies [1], we have investigated suspensions of charged colloids near typical dielectric interfaces. Having a dielectric constant that is different from that of the suspension, the interface gives rise to image-charge-induced forces which compete with the usual double-layer forces acting between the colloids. Within the framework of Poisson-Boltzmann (PB) and Monte-Carlo (MC) cell model approximations in the salt-free limit, we calculated the total force acting on an interfacial charged colloid for a range of system parameters. These are: the ratio of the dielectric constants of the substrate wall and the solution, ϵ'/ϵ, the scaled macroionic charge, $Z\lambda_B/2a$ (a is the macro-sphere radius and λ_B is the Bjerrum length which contains the temperature), and the volume fraction of the suspension ϕ_{vol}.

Figure 1 shows the net force F_z acting on the interfacial colloid as a function of ϵ'/ϵ for various values of $Z\lambda_B/2a$ and ϕ_{vol}. The colloidal sphere is located at the center of the cell (other positions are also treated). We see remarkably from the figure, that the net force acting on the colloid at this specific configuration becomes attractive. This is so for all ϕ_{vol} and colloidal charge considered. The force is largest when the image charge vanishes, i.e. when $\epsilon' = \epsilon$, and it is zero if $\epsilon' = 0$, increasing with increasing ϵ'/ϵ, ϕ_{vol} and colloidal charge. This result can be explained in simple terms. The ions inside the interfacial cell are exposed not only to the image charges from the *image-cell* (see Fig.1 of [1]) but also to the real charges of the neighboring *real-cell*.
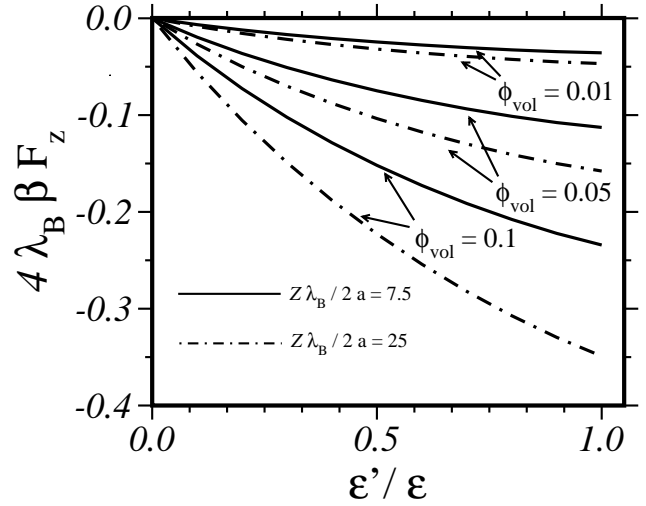

Figure 1: The total force acting on a colloid located at the center of an interfacial cell for varying ratios of ϵ'/ϵ. The force is attractive and grows with increasing volume fraction ϕ_{vol} and scaled colloidal charge $Z\lambda_B/2a$.

These charges are taken into account implicitly by the boundary conditions. A more detailed discussion is made in [1], where we have also calculated polarization surface charge densities at the wall and performed MC calculations to test the importance of finite-size effects of the counterions and investigate the question of colloid adsorption to the wall.

In another study [2] of the electric double-layer force between a charged colloidal sphere and a dielectric planar wall (charged and uncharged), we have derived and calculated effective wall-colloid potentials and compared them with exact numerical PB results. The major difference between this system and the previously discussed can be seen in that [1] is a study of a suspension of colloids near a wall, while it is the interaction of a single colloid with a wall that is considered in [2]. Also the important parameters of the calculation are different; they include (i) the salt content of a reservoir of electrolyte ions characterized by the inverse screening length κ, used as the dimension of all length scales, (ii) the colloidal sphere radius κa, (iii) the wall-colloid separation κh, and (iv) the surface charge densities on both the wall and the colloid, here represented by their surface potentials at isolation Φ_w and Φ_c.

One important result of this study among others, is that the attractive force observed in the cell model treatment of the salt-free solution [1] is not observed here, for any wall-colloid separation. Figure 2(a) shows the comparison of a derived effective potential (based on the Stillinger potential [3]) with exact PB potential for $\Phi_c = 1.0, 1.5, 2.0$, taking a fixed value for $\kappa a = 5.0$. Here $\Phi_w = 0$ (uncharged wall). The figure shows clearly that
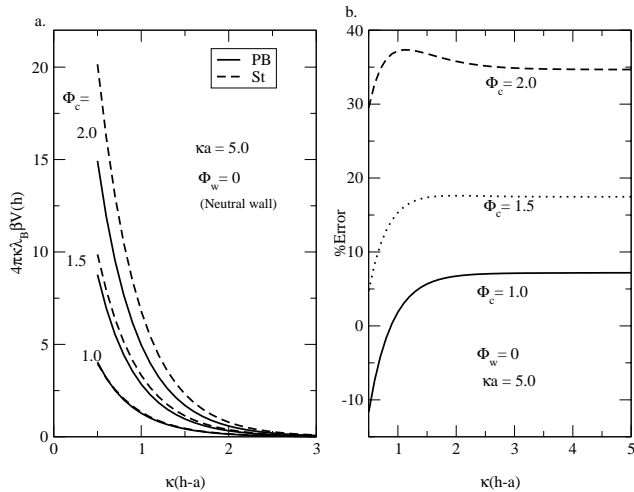
Figure 2: Comparison of the effective wall-colloid interaction potentials from, (i) approximate potential (based on the Stillinger potential), and (ii) exact numerical solution of the PB equation. Different values of the reduced surface potential Φ_c of the colloid are considered for a fixed sphere radius κa. (a) The interaction potential versus the wall-colloid minimum separation, $\kappa(h-a)$. (b) The accuracy of the effective potentials in (a), percentage error versus $\kappa(h-a)$. The potentials are repulsive for all separations.

both the derived effective and PB potentials (and hence the net force on the colloid) are repulsive for all minimum wall-colloid separations $\kappa(h-a)$. This is to be expected given the repulsive Coulomb interaction between the colloid and its image-charge beyond the wall. The attractive net force reported in [1] has been attributed to the influence of neighboring colloids in the suspension.

On-going studies [4] also show that the application of correct boundary conditions, namely, the inclusion of the image-charge contributions in treating charged colloids near and at dielectric interfaces may be applied to explain the observed trapping of colloids and other macromolecules at liquid-air interfaces.

[1] H.H. von Grünberg and E.C. Mbamala, J.Phys.: Condens. Matter **12** 10349 (2001).

[2] H.H. von Grünberg and E.C. Mbamala, J.Phys.: Condens. Matter **13** 1 (2001).

[3] F.H. Stillinger, J.Chem. Phys. **35** 1584 (1961).

[4] E.C. Mbamala and H.H. von Grünberg (in preparation).

C11 Electrokinetic Effects in Charged Colloids

M. Kollmann and G. Nägele

The dynamics of charge-stabilized dispersions consisting of highly charged colloidal particles (macroions) dispersed in a solution of weakly charged small counter- and coions (microionic atmosphere) has attracted considerable interest, both from the experimental and from the theoretical point of view. Theoretical work on charge-stabilized colloids has been mostly based on an effective macrofluid model of dressed macroions interacting by an effective pair potential of spherical symmetry, by integrating out the microionic degrees of freedom. To date, the screened Coulomb potential of Derjaguin-Landau-Vervey-Overbeek (DLVO) type is still the most widely used dressed macroion pair potential.

A major drawback of the dressed macroion model is that it does not account for the kinetic influence of the microionic atmosphere on the colloidal dynamics. The theoretical modeling and quantification of electrokinetic effects originating from the non-instantaneous relaxation of the microionic atmosphere is a demanding task even in case of a single spherical macroion diffusing in an unbounded multi-component electrolyte. In this case, light scattering experiments [1] have revealed that the diffusive motion of the microions relative to the large macroion give rise to an increase (decrease) in the friction coefficient (sedimentation velocity) of the tracer macroion. As a consequence, the long-time self-diffusion coefficient, D_T^L, of the tracer has a minimal value when the thickness of the microionic cloud, as measured by the Debye screening length κ^{-1}, is comparable to the radius a of the macroion (cf. Fig. 1).

The sedimentation velocity, U, of a slowly sedimenting macroion in the presence of its neutrally buoyant electrolyte atmosphere is related to the long-time self-diffusion coefficient, D_T^L, by

$$D_T^L = \frac{k_B T}{6\pi\eta a + \Delta\zeta_T} = D_T^0 \frac{U}{U^0}$$

where U^0 and D_T^0 are the Stokesian sedimentation velocity and the diffusion coefficient, respectively, of the tracer. Furthermore η is, essentially, the solvent viscosity. The effect of the microions relaxation is embedded in the excess friction contribution $\Delta\zeta_T$.

The statistical fluctuations of the microionic atmosphere around the colloidal tracer are coupled to the corresponding hydrodynamic fluctuations through the intervening solvent. Therefore, it appears to be necessary to treat the steric and electrostatic direct interactions (relaxation
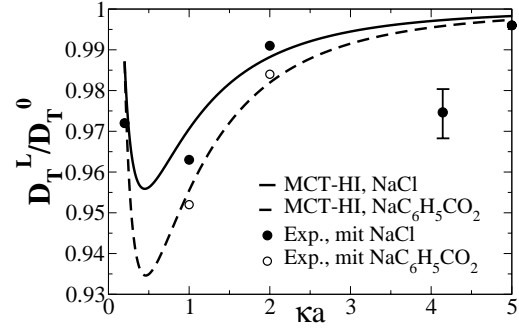

Figure 1: Normalized long-time self-diffusion coefficient D_T^L/D_T^0 versus reduced screening parameter, κa, for two different salts, NaCl and $NaC_6H_5CO_2$, respectively. Experimental data are taken from [1]. The lines are the results of our mode-coupling theory (MCT) with HI included [4,5].
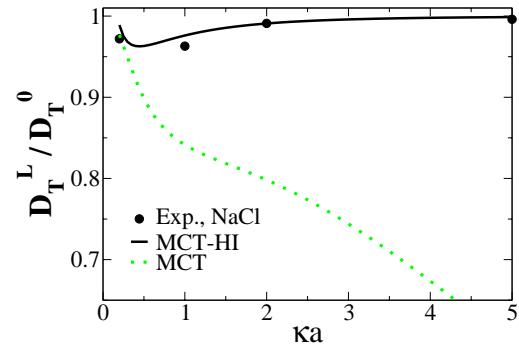
Figure 2: MCT results with HI (solid line) and without HI (dotted line) for D_T^L/D_T^0 vs. κa. Without HI, D_T^L/D_T^0 is monotonically decreasing, in conflict with experimental observation. Experimental data points are taken from [1].

effect), and the hydrodynamic interactions (HI) between tracer and microions (electrophoretic effect) on equal footing for a proper treatment of the experimentally observed colloidal electrolyte friction and sedimentation effect.

Based on a recently formulated mode-coupling scheme for Brownian systems where HI has been included [2,3], and where the macroion and the microions are treated on equal footing as charged hard spheres immersed in an unstructured solvent, we have derived new analytical expressions for the (time-resolved) self-diffusion coefficient and the sedimentation velocity of the tracer [4,5]. As seen from Fig. 1, use of these expressions yields good agreement with the experimental data for D_T^L. We have further derived analytical expressions for the time-dependent generalization, $\Delta\zeta_T(t)$, of $\Delta\zeta_T$. The friction function $\Delta\zeta_T(t)$ includes the non-instantaneous memory contributions to the mean squared displacement of the tracer.

An important conclusion drawn from our theoretical analysis is that the observed minimum of D_T^L at $\kappa a \approx 0.5$

Figure 3: Sketch of the Stokesian stream lines of a negatively charged macroion with its associated microionic atmosphere of counter- and coions. The macroion sphere is acted on by a weak external force F_T.

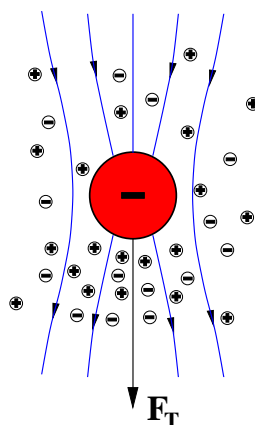is due to a combined effect of hydrodynamic and direct forces acting between macroion and microions. This fact should be contrasted with earlier approaches on electrolyte friction where it has been attempted to explain the minimum of D_T^L in terms of direct forces only (cf., e.g., [6,7]). In fact, the neglect of HI gives rise to a charge-independent contribution to $\Delta \zeta_T$. This additional friction contribution, in turn, leads to a monotonic decline of D_T^L with increasing ionic strength, as seen from Fig. 2, in conflict with experimental observation. The charge-independent friction contribution arises from the excluded volume interactions between the tracer and the point-like microions. With HI included, this excluded volume contribution becomes quite small [8] (i.e., it vanishes within the approximations made in [4,5]) since the microparticles are advected by the hydrodynamic flow field created by the moving tracer sphere (cf. Fig. 3).

Future extensions of this work will focus on electrokinetic effects in concentrated macroion dispersions with overlapping microionic atmospheres. This will allow to treat the primary and secondary electroviscous effects in a unified way.

[1]   G.A. Schumacher and T.G.M. van de Ven, Faraday Discuss. Chem. Soc. **83**, 75 (1987).

[2] G. Nägele and J.K.G. Dhont, J. Chem. Phys. **108**, 9566 (1998).

[3] G. Nägele and J. Bergenholtz, J. Chem. Phys. **108**, 9893 (1998).

[4] M. Kollmann and G. Nägele, J. Chem. Phys. **113**, 7672 (2000).

[5] M. Kollmann and G. Nägele, Europhys. Lett. **52**, 474 (2000).

[6] A. Vizcarra-Rendón, H. Ruiz-Estrada, M. Medina-Noyola and R. Klein, J. Chem. Phys. **86**, 2976 (1987).

[7] J.M. Schurr, J. Chem. Phys. **45**, 119 (1980).

[8] M. Kollmann, Ph.D. thesis, University of Konstanz (2001).

C12 Brownian Dynamics of Dipolar Colloids

B. Rinn and Ph. Maass

The Brownian dynamics of colloids suspended in liquids is a long–standing problem of considerable practical interest. While many results have been obtained for short–range interacting colloids in the past, much less is known in the case of long–range interactions. A system studied in detail by experiment is a two-dimensional colloidal suspension of superparamagnetic particles that interact via dipolar forces when an external magnetic field B is applied [1]. To understand the experiments we have performed extensive Brownian dynamics simulations. After verifying the static properties of the system, we have shown [2] that inclusion of hydrodynamic interactions (HI) are essential to quantify the diffusion of the colloids properly, see Fig. 1. As can be seen from the figure, the HI increase the self–diffusion on all time scales. This is in marked contrast to the behavior of short–range interacting colloids, where typically HI slow down the dynamics. The HI enhancement effect for long–range interactions becomes stronger for denser suspensions and is almost independent of the temperature [2].

Further experimental work on an analogous but confined system with a small number of 29 particles has been done by Bubeck *et al.* [3]. The colloids in this system are confined to a circular hard wall cavity and arrange into three concentric shells at sufficiently strong interaction strength $\Gamma \propto M^2/k_B T$, where M is the induced magnetization. By analyzing several particle trajectories monitored over 30 minutes an interesting "reentrant freezing phenomenon" was observed: While at large Γ the angular displacement of the colloids in the inner shell shows small fluctuations corresponding to some kind of "frozen state", this displacement was found to become larger than the angular separation of neighboring particles in the inner shell at intermediate Γ. Upon further decreasing Γ, however, the "frozen state" was found to reappear.
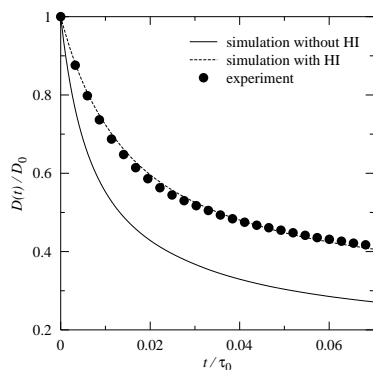

Figure 1: Time dependent diffusion coefficient of dipolar colloids with and without HI in comparison with experiment.
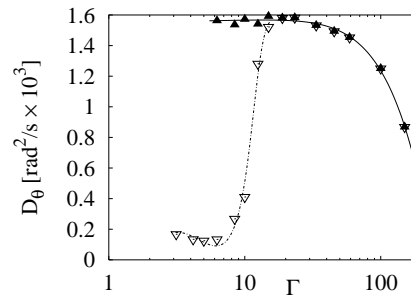

Figure 2: D_θ as a function of interaction strength Γ if shell jumps are taken into account (▲) and if they are ignored (▽).

Subsequently the effect was proposed to occur also in Brownian dynamics simulations [4]. In these simulations the authors considered a certain quantity as angular diffusion coefficient that exhibits a non–monotonous dependence on Γ in a Γ interval corresponding to that where the reentrant behavior was observed in the experiment.

In continuation of our former studies of the extended system [1] we have independently investigated the confined system [5]. Contrary to [4], however, we could not identify a non–monotonous behavior in the dynamics, when considering properly defined quantities. The diffusion coefficient defined in [4] is well–defined as long as the particles remain in the same shell while the trajectory is recorded. When, as it happens for small Γ, a particle changes its shell due to motion in the radial direction, other particles have to rearrange to build a new shell structure. Due to this fact the time averaging has to be restricted to times smaller than the time $t_\star$ of the first occurrence of a "shell jump". As a consequence, to determine the angular diffusion coefficient D_θ the trajectories between two shell jumps have to be long enough for reaching the long–time limit. We have shown [5] that, when taking shell jumps into account properly, D_θ decreases monotonously with increasing Γ as one would expect for ordinary physical situations. If, on the other hand, one evaluates D_θ by some other procedure involving inter–shell radial motions, one can obtain very different results. In an extreme case, where we analyzed the data by fully ignoring the occurrence of shell jumps, we found an even more pronounced increase of D_θ with Γ than Schweigert *et al.* For a comparison of the two procedures, see Fig. 2.

[1]   K. Zahn, J. M. Méndez–Alcaraz, and G. Maret, Phys. Rev. Lett. **79**, 175 (1997).

[2]   B. Rinn, K. Zahn, P. Maass und G. Maret, Europhys. Lett. **46**, 537 (1999).

[3]   R. Bubeck, C. Bechinger, S. Neser, and P. Leiderer, Phys. Rev. Lett. **82**, 3364 (1999).

[4]   I. V. Schweigert, V. A. Schweigert, and F. M. Peeters, Phys. Rev. Lett. **84**, 4381 (2000).

[5]   B. Rinn and P. Maass, Phys. Rev. Lett., in print.

C13 Diffusion and Rheology of Charged and Neutral Colloids

G. Nägele, A.J. Banchio, H. Zhang and J. Bergenholtz

A first principle calculation of rheological and diffusional properties of suspensions of spherical colloidal particles from the knowledge of their direct and hydrodynamic interactions (HI) is a major theoretical challenge. It is important to develop an understanding for the microscopic origin of the transport properties of these systems since they can serve as model systems for more complex colloids relevant to chemical and pharmaceutical industry.

In a series of recent articles, we have formulated and employed a fully self-consistent mode coupling theory (MCT) adjusted to describe the over-damped dynamics of neutral and charged colloidal particles. For concentrated hard-sphere dispersions, we used a short-time hydrodynamic rescaling procedure to approximate the strong many-body influence of the HI on the particle dynamics. Experimentally accessible dynamical quantities determined using the (rescaled) MCT comprise the suspension viscosity η, dynamic elastic storage and viscous loss moduli $G'(\omega) = \omega\eta''(\omega)$ and $G''(\omega) = \omega\eta'(\omega)$, mean-squared displacement $W(t)$, dynamic structure factor $S(q,t)$, long-time collective and self-diffusion coefficients, and collective and self-memory functions. Comparison of our MCT results with experiment and computer simulations leads to good agreement, particularly for systems with strong particle correlations (cf. [1,2]).

Fig. 1a shows MCT results for the volume fraction (i.e. Φ-) dependence of the reduced suspension viscosity η/η_0, where η_0 is the solvent viscosity. The HI-rescaled MCT is in good accord with the experimental data for η by Segrè et al. (Phys. Rev. Lett. **75**, 958 (1995)). There is also decent qualitative agreement between the MCT result for η without HI, and Brownian dynamics (BD) simulation results of Strating (Phys. Rev. E **59**, 2175 (1999)). Notice the strong hydrodynamic contribution to the viscosity at larger Φ. MCT results for the reduced dynamic viscosities $R(\omega)$ and $I(\omega)$ without HI of a concentrated hard-sphere dispersion are included in Fig. 1b and compared with BD data of Heyes and Mitchell (J. Chem. Soc. Faraday Trans. **90**, 1931 (1994)), and a non-equilibrium HNC closure scheme of Lionberger and Russel (J. Rheol. **41**, 399 (1997)). The MCT is seen to be in better agreement with the simulation data than the HNC scheme. In Fig. 1c, MCT results for the reduced mean squared displacement $W(t)/(D_0 t)$ of hard spheres are compared with BD data of Cichocki and Hinsen (Physica A **187**, 133 (1992)). The agreement between MCT and BD improves with increasing Φ, with nearly coincident results for $\Phi = 0.45$.
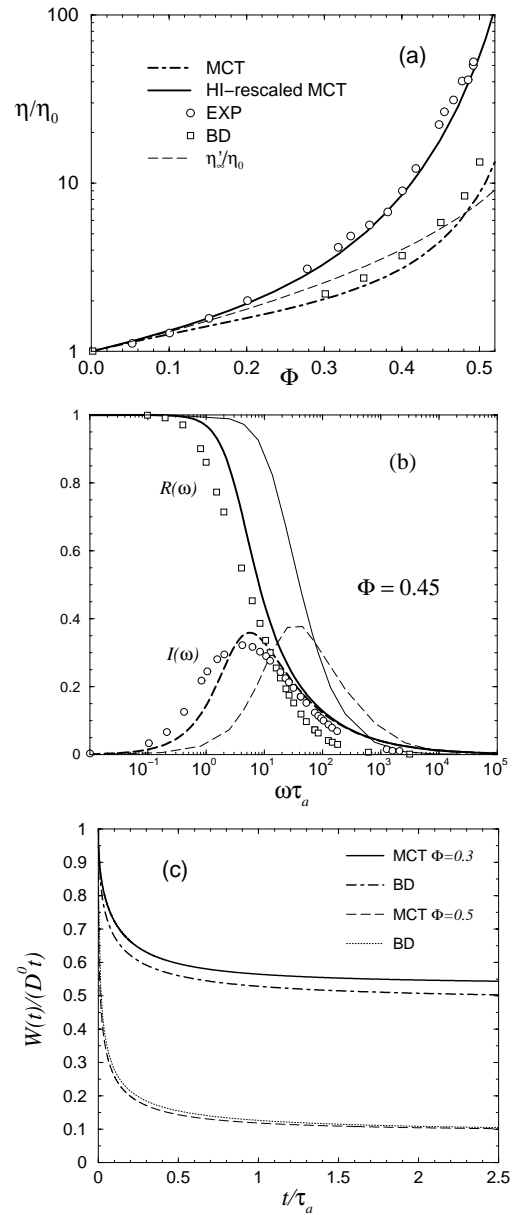
Figure 1: (a) Hard-sphere reduced viscosity η/η_0 in MCT with and without HI-rescaling vs. experimental data (Segrè et al.) and BD results without HI (Strating). Dashed line: high-frequency limiting viscosity η'_∞, normalized by η_0. (b) Real part $R(\omega) = (\eta'(\omega) - \eta'_\infty)/(\eta - \eta'_\infty)$ and imaginary part $I(\omega) = \eta''(\omega)/(\eta - \eta'_\infty)$ of the reduced dynamic viscosity for a concentrated hard-sphere suspension vs. reduced frequency $\omega\tau_a$, with $\tau_a = a^2/D_0$. Thick lines: MCT results; open symbols: BD data of Heyes and Mitchell; thin lines: non-equilibrium HNC closure scheme of Lionberger and Russel. (c) Reduced mean squared displacement for hard spheres at $\Phi = 0.3$ (upper two curves) and $\Phi = 0.5$ (lower two curves). Figures taken from [1,2].

From our MCT calculations we were further led to interesting predictions concerning the validity of certain empirically found generalized Stokes-Einstein (GSE) relations linking low-shear viscoelastic properties to diffusion coefficients. Most of these GSE relations were shown to hold fairly well for hard-sphere dispersions, whereas the violation of the same GSE relations is predicted in case of charge-stabilized suspensions with long-range interactions (cf. [1]).

For an application of the fully self-consistent MCT scheme to charge-stabilized dispersions consider Fig. 2. This figure demonstrates the damping out of density fluctuation correlations with increasing correlation time t, quantified by the dynamic structure factor $S(q,t)$. The system parameters used for the results shown in the figure are typical of deionised aqueous dispersions of highly charged colloidal spheres. Our MCT results for $S(q,t)$ are compared with BD data of Gaylor et al. (J. Phys. A **13**, 2513 (1980)), and with results of López-Esquivel et al. (J. Chem. Phys. **96**, 1651 (1992)) derived from a two-exponential approximation (SEXP) of $S(q,t)$ based on exact short-time moments. The MCT $S(q,t)$ is in excellent agreement with the BD results of Gaylor et al. even for the largest time $t = 1.6$ ms considered. The SEXP predicts a too rapid progression of structural relaxation.

It should be noted that charge-stabilized dispersions are qualitatively different from hard-sphere systems regarding the short-time and long-time transport properties, due to the combined influence of long-range electrostatic and hydrodynamic interactions. An important example is provided by the Φ-dependence of the sedimentation velocity U. For dilute suspensions of charged particles at low salinity, the reduced sedimentation velocity is well represented by the non-linear form $U/U_0 = 1 - p\,\Phi^\alpha$, with $\alpha = 1/3$ in case of strongly charged spheres and $\alpha = 1/2$ for weakly charged particles [3]. The exponent $1/3$ has indeed been observed in sedimentation experiments on strongly charged particles.

Aside from translational motion, colloidal spheres perform rotational Brownian motion which can be investigated experimentally by depolarized dynamic light scattering, time-resolved phosphorescence anisotropy (TPA), and NMR. So far, rotational diffusion is much less understood than translational diffusion, sedimentation and viscoelasticity. In a joint theoretical/experimental project, we have studied the (short-time) rotational diffusion of colloidal tracer spheres in a dense colloidal host fluid (cf. [4,5]). Experimental/theoretical results for the rotational diffusion coefficient, D_s^r, of a neutral tracer sphere in a hard-sphere host dispersion, normalized by its limiting value D_0^r at infinite dilution and multiplied by η_∞'/η_0 are displayed in Fig. 3. Note the approach towards a generalized Stokes-Einstein behavior $D_s^r \propto (\eta_\infty')^{-1}$, and $D_l^r \propto \eta^{-1}$, with increasing tracer/host diameter ratio λ.
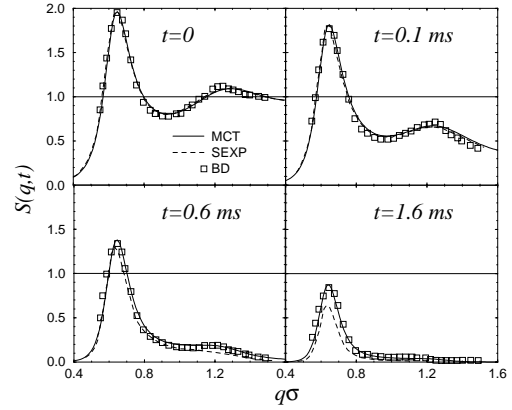
Figure 2: Dynamic structure factor of a deionized charge-stabilized dispersion. Solid lines: MCT results; dashed lines: SEXP results of López-Esquivel et al.; open squares: BD data (Gaylor et al.). Figure reproduced from [2].
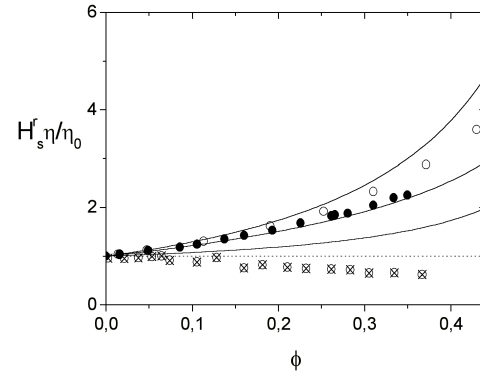
Figure 3: Experimental values for $H_s^r = D_s^r/D_0^r$ times semi-empirical results for η_∞'/η_0 at tracer/host size ratio $\lambda = 0.33$ and 1, and, for $\lambda = 10$, times the rescaled MCT result for η/η_0 (cf. Fig. 1a). Solid lines: theoretical predictions for $H_s^r\eta_\infty'/\eta_0$; the dotted line represents $H_s^r\eta_\infty'/\eta_0 = 1$. Figure taken from [4].

The TPA data are qualitatively well described by our approximate theory, which accounts only for the asymptotically leading three-body HI, provided λ is not too different from one.

[1] A.J. Banchio, G. Nägele and J. Bergenholtz, J. Chem. Phys. **111**, 8721 (1999).

[2] A.J. Banchio, G. Nägele and J. Bergenholtz, J. Chem. Phys. **113**, 3381 (2000).

[3] M. Watzlawek and G. Nägele, J. Colloid Interface Sci. **124**, 170 (1999).

[4] G. H. Koenderink, H. Zhang, M.P. Lettinga, G. Nägele and A.P. Philipse, submitted (2001).

[5] H. Zhang and G. Nägele, submitted (2001).

C14 Glass transition of binary mixtures of 2D colloids

H. König, R. Hund, K. Zahn, G. Maret

A glass can be considered as a supercooled melt which forms a solid without long-range periodic order. The various glass-formers qualitatively reveal the same universal physical properties, but the details of the glass features depend on the particle interaction [1,2]. Various types of glasses can be distinguished by their temperature dependence of the *viscosity* $\eta(T)$ and of the *structural relaxation time* $\tau_\alpha(T)$ in the supercooled liquid. The covalent binding network glasses on the one hand exhibit an *Arrhenius*-like behavior (1), colloidal glasses with hard-sphere-interaction on the other hand are quite well described by a *Vogel-Fulcher-law* (2). Most of the other glass-formers lie in between these extreme cases. A classification of the glass-formers by Angell [3], [4] defines glasses described by (1) as strong and others represented by (2) as fragile.

$$\eta(T), \ \tau_\alpha(T) \ \sim \ \exp(E/k_BT) \qquad (1)$$

$$\eta(T), \ \tau_\alpha(T) \ \sim \ \exp(E/k_B(T - T_{VF})) \qquad (2)$$

Initially, the fragile three-dimensional hard-sphere colloidal glasses were investigated by Bragg reflection of light [5]. More recently, such systems are examined by confocal microscopy providing also information of the particle trajectories and their cooperative relaxations, e.g. [6]. Furthermore, two-dimensional simulations try to understand the heterogenic relaxation behavior of fragile glasses with short-range interactions in supercooled liquids and the glassy phase, e.g. [7].

In this project we study a binary mixture of superparamagnetic colloidal particles (diameters 4.5μm and 2.8μm) confined by gravity to the water-air interface of a hanging suspension droplet. The micro-spheres interact via a repulsive long-range dipole-dipole interaction adjusted by a magnetic field B applied perpendicular to the two-dimensional (2D) particle layer (see also C4). The interaction strength is characterized by the dimensionless *plasma parameter* Γ defined as the ratio of the average repulsive *magnetic interaction energy* to the *thermal energy* k_BT:

$$\Gamma = \frac{\mu_0}{4\pi}B^2\rho^{3/2}[\chi_{small}\varphi + \chi_{big}(1 - \varphi)]^2/k_BT \qquad (3)$$

Here φ denotes the fraction of the small colloids, $\chi_{small} \approx 6 \cdot 10^{-12}\mathrm{Am^2/T}$ and $\chi_{big} \approx 6.2 \cdot 10^{-11}\mathrm{Am^2/T}$ the magnetic susceptibilities of the small and big spheres, respectively, and ρ the (total) 2D particle density.
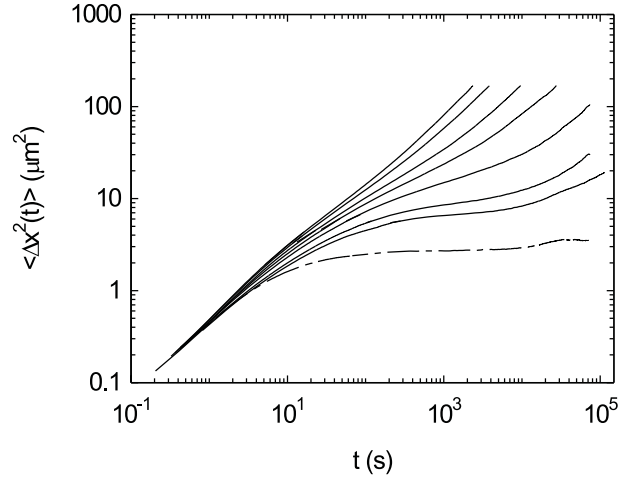

Figure 1: Time-dependent mean-square displacement of a binary mixture (solid lines) with $\varphi = \rho_{small}/\rho = 0.41$ for different interaction strengths Γ (from above: 19.1, 24.9, 30.8, 42.1, 52.0, 78.8, 96.3) in comparison with a system of only big colloids (dashed line) at $\Gamma = 54.3$ forming a hexagonal crystal. Note the logarithmic time-scale and that the here used Γ-value has to be multiplied by $\pi^{3/2}$ in order to correlate with that defined in C4.

The diameter of the circular solvent drop was 8 mm containing approximately 10^5 homogeneously dispersed colloids. Using real time video-microscopy and image processing on a PC about 1000 particles in the center of the drop were studied in real time: Complete positional data were obtained for more than 6 decades in time and from these data various time-correlation functions were calculated.

In fig. 1 mean-square displacements $\langle\Delta x^2(t)\rangle$ are plotted for several interaction strengths featuring all relaxation time-scales relevant for glassy systems. The short-time behavior which is also denoted as fast β-relaxation and corresponds to the linearly increasing free diffusion in isotropic liquids, merges into the cage-effect. This motion slows down on account of blocking restrictions caused by the repulsive interaction of the nearest neighbors. The strength and the duration of the cage-effect amplifies with rising interaction strength. Subsequently, $\langle\Delta x^2(t)\rangle$ increases again and the particles eventually leave the cage. In super-cooled liquids it is expected that hopping or slow β-relaxations are responsible for this process. Finally long-time structural relaxation processes take over. These involve a complete reorganization of the neighborhood of the particles and cause the ultimate increase of $\langle\Delta x^2(t)\rangle$. The time scale τ_α corresponding to these so-called α-relaxations depends upon temperature according to eqs. (1) and (2).

For comparison, we have included in fig. 1 the mean-square displacement of a 2D colloidal crystal consisting of big particles only (see C4/C5). As expected the particles are always caged apart from a small long-time relax-
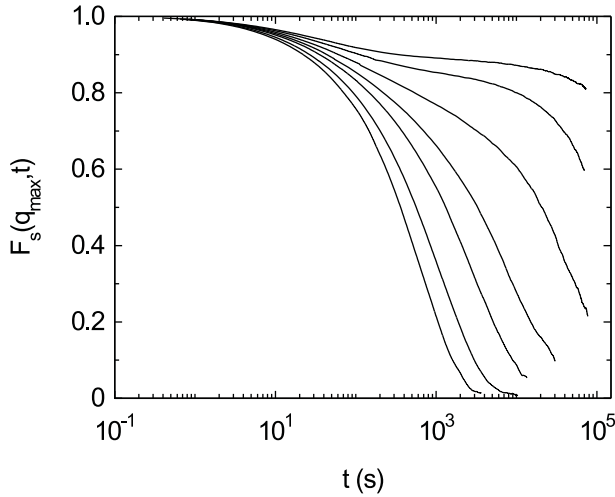
Figure 2: Time-dependent self-intermediate scattering function $F_s(q_{max}, t)$ of a binary colloidal mixture with $\varphi = 0.41$ for different interaction strengths Γ (from above: 96.3, 78.8, 52.0, 42.1, 30.8, 24.9, 19.1). q_{max} corresponds to the inverse distance of the first maximum of the radial pair-correlation function g(r).

Figure 3: Long-time structural relaxation time τ_α of a binary mixture with $\varphi = 0.41$ as a function of $\Gamma(B)$ corresponding to an inverse temperature. The experimental data agrees well with a fit representing an Arrhenius-like behavior $\tau_\alpha \sim \exp(\Gamma/\Gamma_0)$ with a fitting constant Γ_0 (compare with eq. (1)).

ation. The latter is due to the softness of 2D crystals and some residual convectional flow of the solvent. Nevertheless, the mean-square displacement of the binary mixture cannot be directly compared with that of the crystal because of different cage sizes due to different densities.

The self-intermediate scattering function $F_s(q, t)$ corresponding to the mean-square displacement is shown in fig. 2. This function describes the relaxation processes in the Fourier-space and can be obtained by scattering experiments. The relaxation spectrum can be explained in the same way.

The structural relaxation time τ_α has been determined from the long-time limit of the self-diffusion coefficient $D_s^l = 1/4 \lim_{t \to \infty}(d\langle x^2 \rangle/dt)$ using the relation $\tau_\alpha = 1/(D_s^l \rho)$. In fig. 3 the values of τ_α are shown as a function of the interaction strength $\Gamma(B)$ corresponding to an inverse system temperature $1/T_{sys}$. As the plot is in logarithmic y-scale the straight line behavior corresponds well to an Arrhenius-like law (1). Thus the data reveal strong evidence that the long-range repulsive magnetic dipole-dipole-interaction in this 2D colloidal system produces a strong glass.

To our knowledge this binary mixture is the first colloidal system which can be interpreted as a strong glass. We plan further measurements at even higher interaction strengths Γ and for other mixture ratios (small/big = $\varphi/(1 - \varphi)$) in order to explore how general this behavior is.

[1]   J. Jäckle, Rep. Prog. Phys. **49**, 171 (1986).

[2]   M.D. Ediger, C.A. Angell and S.R. Nagel, J. Phys. Chem. **100**, 13200 (1996).

[3]   C.A. Angell, in Relaxation in Complex Systems, ed. K.L. Ngai and G.B. Wright, Naval Res. Lab., 3 (1984).

[4]   R. Böhmer, C.A. Angell, in Disorder Effects on Relaxational Processes, edit. R. Richert and A. Blumen, Springer-Verlag, 11 (1994).

[5]   P.N. Pusey, W. van Megen, Nature **320**, 340 (1986).

[6]   E.R. Weeks, J.C. Crocker, A.C. Levitt, A. Schofield, D.A. Weitz, Science **287**, 627 (2000).

[7]   D.N. Perera, P. Harrowell, J. Chem. Phys. **111**, 12, 5441 (1999).

C 15 Magnetic field assisted colloidal masks

P. Keim, K. Zahn, G. Maret

Close packed two-dimensional (2D) arrays of colloidal particles (so-called Colloidal masks) provide a "parallel" method to structure substrates on sub-micron scale. Therefore they represent an interesting alternative to linear sequential processing steps like electron or ion beam lithography. Different attempts to build a hexagonal closed packed monolayer of colloids have been made using the attractive interaction caused by the interfacial tension of an evaporating solvent layer [1,2]. However, true long range order could only partially be achieved. Here a novel approach for improving the long range order of colloidal masks will be proposed based on the application of external fields.

The systems consists of monodisperse superparamagnetic polystyrol spheres with diameter $d = 4.5\,\mu$m and mass density $1.7\,$g/ cm^3 confined by gravity to a water/air interface. The interface is formed by a cylindrical drop suspended by surface tension in a top-sealed ring [3] (see also C4, C5). This liquid/air interface is free of impurities and provides the smoothness necessary for a high mobility of the colloids at the surface which can not be reached on a solid substrate. Fig. (1) shows a schematic setup of the system. Applying an external magnetic field vertically to the 2D layer causes a tunable repulsive interaction between the colloids acting as an inverse temperature. Depending on the strength of the field and the particle density the system can be driven from the fluid to the crystalline phase.
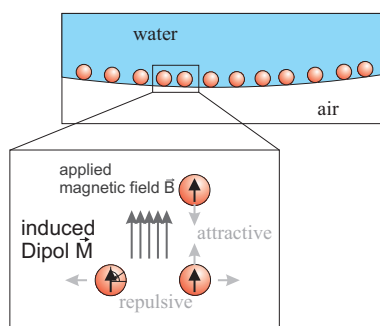

Figure 1: Colloids confined to a water/air interface.

Unlike in a closed packed hexagonal crystal dislocations and disclinations can easily migrate through the crystal. An in-plane field is used to define a preferential direction and to temper imperfections of the droplet. Lowering the surface in the center of the droplet causes a curvature which adds an additional component of the gravitational force parallel to the surface and leads to an isotropic compression of the crystal Fig. (2). If the colloidal system
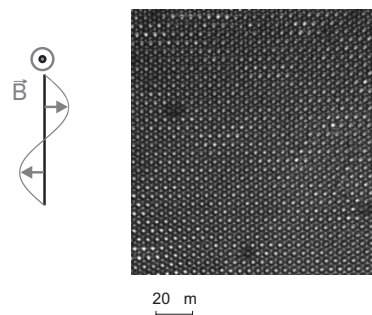
Figure 2: Enlarged view of a part of a hexagonal closed packed monolayer of colloids at liquid-vapor interface.

is scaled down to reach a periodicity on the nanometer length scale sedimentation of the particles into a 2D plane will no longer occur because of increased thermal agitation. A different method has to be used to confine the colloids at the interface. As was applied in the case of proteins [4] we want to use the electrostatic interaction of a charged lipid monolayer at the water-air interface with oppositely charged colloids. The charge density of the lipid monolayer can be adjusted by the mixture of ionic and non-ionic lipids. Fig. (3) shows an schematic picture of small colloids attached by electrostatic interaction to the surface. To circumvent the small choice of commer-
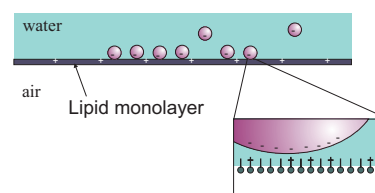
Figure 3: Electrostatic interaction between particles and lipid monolayer at the interface.

cial available super-paramagnetic microspheres with suitable size and susceptibility distribution we are also working on a magnetically inverted system of diamagnetic colloids dispersed in a ferrofluid. This enables the use of the large variety of commercially available polystyrene colloids. Using water-based ferrofluids all chemical technics including lipid monolayer covering should be adoptable.

[1] F. Burmeister and P. Leiderer, Ad. Mat. **10**, 495 (1998).

[2] Q.-H. Wei, D.M. Cupid and X.L. Wu, App. Phys. Lett. **77**, 1641 (2000).

[3] K. Zahn, R. Lenke, and G. Maret, Phys. Rev. Lett. **82**, 2721 (1999).

[4] C. Venien-Bryan, Biophys. **74**, 2649 (1998).

C16 Entropic Forces beyond Entropy

D. Rudhardt, P. Leiderer, C. Bechinger

The stability of systems like polydisperse mixtures of colloids, natural rubbers, micelles, or polymer coils is known to be strongly influenced by depletion forces. In addition, such forces may also play an important role in biological systems, e.g. in the aggregation of red blood cells [1,2]. Therefore, the understanding of these forces is highly demanding from both the experimental but also from a theoretical point of view [3] [4].

The principal phenomenon of depletion interaction is easily understood when, e.g. a hard sphere of radius R suspended in a fluid containing smaller spheres of radius r in front of a wall at distance z is considered. If z decreases below 2r they are excluded from the region between the sphere and the wall. Consequently, the concentration of smaller spheres becomes depleted in this region compared to that of the bulk and an effective osmotic pressure causing a net attraction between the large sphere and the wall occurs [5].

This, however, is only true for small concentrations of the small spheres where they can be treated as an ideal gas to good approximation. When their volume fraction increases, correlation effects become important which are predicted to lead to an oscillatory behavior of depletion forces containing attractive and repulsive parts [6]. So far the interpretation of the corresponding experiments has been based on assuming hard-sphere macromolecule and hard-wall interactions which is, however, not always justified under experimental conditions. This is most evident in the case of highly charged macromolecules where even at volume fractions below 2% long-range repulsive and short-ranged attractive depletion potentials between an sphere and a wall have been measured. But even for systems of uncharged macromolecules or in the high salt limit, the model of hard spheres and a hard wall is not always applicable within the range of attractive dispersion forces.

In our experiments we use the so called total internal reflection microscopy (TIRM), to measure the potential of a freely (!) suspended colloidal sphere close to a wall [7]. As smaller spheres we employed nonionic polymer coils of poly(ethylene oxide) (PEO). The principle of TIRM is easily understood when considering a light beam which is reflected at a solid/fluid interface above the critical angle of total internal reflection Θ_c. The intensity of the electric field does not drop instantaneously to zero above the interface but decays exponentially (as an evanescent wave) with a characteristic decay length β^{-1} perpendicular to the surface. When an object which scatters light, e.g. a colloidal sphere, approaches the surface close enough to enter the evanescent field, frustrated total reflection will occur. The scattering intensity I of the sphere is then proportional to that of the evanescent wave. Measuring I (which fluctuates due to Brownian motion of the sphere) as a function of time thus provides a sensitive and non-intrusive method to determine z. In thermal equilibrium the sphere-wall-interaction potential $\Phi(z)$ can be calculated as a function of z by using the Boltzmann-distribution $p(z) = \exp(-\Phi(z)/kT)$.
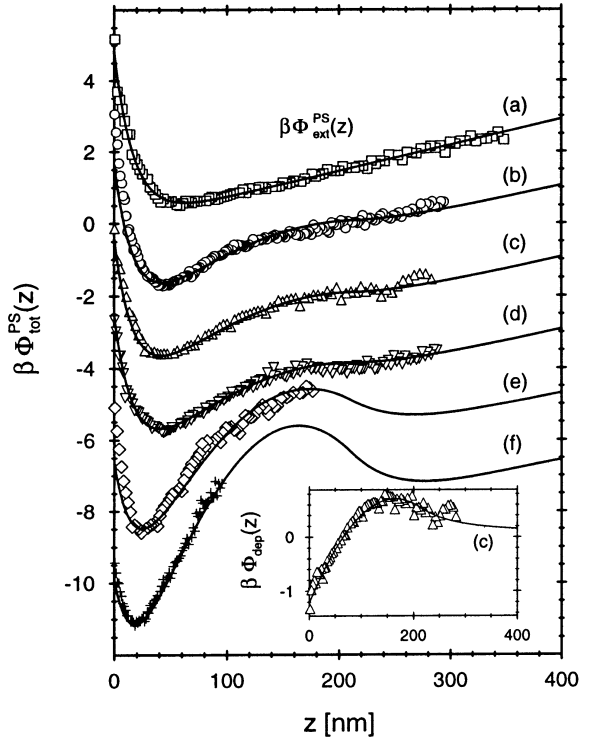
Figure 1: Measured potential curves (symbols) of a PS sphere as a function of its distance z from a flat surface for polymer concentrations n = 0 (a), 4.1 μm^{-3} (b), 6.3 μm^{-3} (c), 8.7 μm^{-3} (d), 16.4 μm^{-3} (e), and 23.4 μm^{-3} (e). The solid lines are calculations according to a density functional theory

The symbols in Figs.1a-f shows the measured effective potential of a PS sphere of 10μm diameter in a solution of PEO molecules of various concentrations [8]. Curve a corresponds to the case where no PEO is added. In the absence of depletion forces the potential of a negatively charged PS sphere above a glass plate is composed of two parts [9]: towards larger distances z the potential increases linearly, because the dominant force acting on the particle is due to gravity. At smaller z the potential increases exponentially due to the electrostatic interaction between the sphere and the likewise negatively charged glass plate. This contribution to the total potential has been assumed to be constant when polymer was added. With increasing polymer concentration one observes on top of this potential an additional attractive

part below about 100nm. In the inset of Fig.1 we plotted the difference between curve c and a, i.e. only the depletion potential. As can be seen there is a repulsive barrier around 200 nm which is followed by an attractive part towards smaller distances. In order to understand this behavior, we compared our results to density functional theory (DFT) calculations of Roland Roth (group of Prof. S. Dietrich/MPI Stuttgart). To obtain good agreement between theory and the experimental data, it is not sufficient to consider only hard sphere interactions. At the concentrations used in our experiments this would highly underestimate the repulsive depletion potential. In contrast, it is essential to include also the dispersion forces and the electrostatic interaction energy between the PEO and the charged glass surface which gives rise to an external potential

$$\Phi_{ext}^{PEO}(z) = C \exp[-2\kappa(z+r)] - A\left(\frac{r}{z+r}\right)^3 \quad (1)$$

with the Hamaker constant $A = 5*10^{-20}$ J and

$$C = 12\pi[\kappa r \cosh(\kappa r) - \sinh(\kappa r)]\frac{\varepsilon\varepsilon_0(\varepsilon - \varepsilon_1)}{\varepsilon_1 + 2\varepsilon}\frac{E_0^2}{\kappa^3} \quad (2)$$

with $\varepsilon_1 \approx 5$, the surface electric potential of the glass plate $E_0 \approx 50$ m, and ε_0 the permittivity of vacuum. Estimates indicate that for the densities considered here the attractive dispersion forces among the macromolecules and between them and the PS spheres are not important.
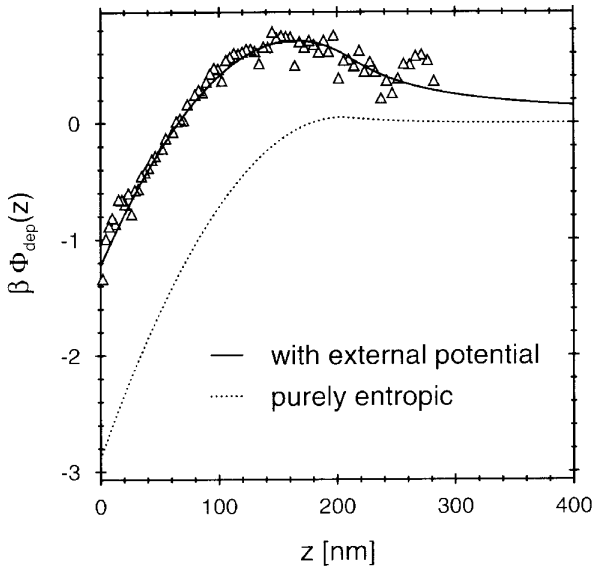

Figure 2: The depletion potentials between the wall and a big PS sphere calculated from the corresponding PEO density profiles. For details refer to the text.

Taking this external potential into account the solid curves in Fig.1 have been obtained by a novel and ver-

satile DFT approach [10]. The remarkable agreement between theory and the experimental data clearly demonstrates hat even in systems with uncharged macromolecules a hard sphere and hard wall interaction is not always justified.

We emphasize that the potential barriers in Fig.1 cannot be explained in terms of a hard-sphere and hard-wall model, i.e. by purely entropic arguments. This conclusion is demonstrated in Fig.2 by the discrepancy between the actual depletion potential (solid line) and the one close to a hard wall (dotted line). At the low concentrations of PEO polymer which have been used in our experiments an entirely hard sphere- hard wall interaction produces only a very small potential barrier which can be hardly seen in Fig.2.

An important conclusion which can be drawn from our calculations is that, although the dispersion attraction seems to be mainly responsible for the potential barrier, the soft electrostatic repulsion plays an important role as well. By changing the salt concentration and hence the inverse screening length, one can experimentally tune the range of the electrostatic repulsion and thus modify the potential barrier. This explains why in an earlier experiment with a lower salt concentration no repulsive depletion forces were found [11].

[1] J. Martin and F.-U. Hartl, Proc. Natl. Acad. Sci. **94,** 1107 (1997).

[2] A. P. Minton, Current Opinion in Biotechnology **8,** 65 (1997).

[3] C. Bechinger, H. H. v. Grünberg, and P. Leiderer, Phys. Blätt. **55,** 53 (1999).

[4] H. H. v. Grünberg and C. Bechinger, Spektrum d. Wissenschaft **6,** 16 (2000).

[5] S. Asakura and F. Oosawa, J. Polymer Sci. **33,** 183 (1958).

[6] D. L. Sober and J. Y. Walz, Langmuir **11,** 2352 (1995).

[7] D. C. Prieve, Adv. Coll. Int. Sci. **82,** 93 (1999).

[8] C. Bechinger, D. Rudhardt, P. Leiderer, R. Roth, and S. Dietrich, Phys. Rev. Lett. **83,** 3960 (1999).

[9] D. Rudhardt, C. Bechinger, and P. Leiderer, Prog. Colloid Polym. Sci. **110,** 37 (1998).

[10] B. Götzelmann, R. Roth, S. Dietrich, M. Dijkstra, and R. Evans, Europhys. Lett. **47,** 398 (1999).

[11] D. Rudhardt, C. Bechinger, and P. Leiderer, Phys. Rev. Lett. **81,** 1330 (1998).

C17 Single-File-Diffusion of Colloidal Particles in 1D-Channels

Q.-H. Wei, P. Leiderer, C. Bechinger

A unique physical phenomenon, widely termed single-file diffusion (SFD), arises when individual pores of a medium are so narrow that particles are unable to pass another, and thus the sequence of particles remains unchanged over time. The mechanism of SFD was originally introduced more than 40 years ago in biophysics to account for the transport of water and ions through molecular sized channels in membranes [1]. Besides biological systems, SFD is also discussed in the context of the transportation of adsorbate molecules through the long, parallel 1D pores of zeolites, charge carrier migration in 1D polymer and superionic conductors, and even the motion of monomers of reptating polymers [2].

It is well known that in two or three dimensions, the mean-square displacement (MSD) of a tagged particle is proportional to the observation time for long times. In contrast, when the mutual passage of particles is prohibited as typical for SF-systems, the movements of individual particles are correlated even at long times. This is due to the fact that the displacement of a particle along one direction is facilitated if the motion of its neighbors occurs in the same direction. This correlation effect strongly influences the long-time transportation of a labeled particle, and is reflected in the long-time behavior of the MSD which has been predicted for an infinite system to be [3]

$$< \Delta x^2 >= 2F \sqrt{t} \qquad (1)$$

where F is the SF mobility.

In order to test the validity of SFD in colloidal systems, we confined super paramagnetic particles of 3.6 µm diameter in a system of circular trenches fabricated by photolithography. In contrast to atomic systems where SFD has been reported previously, here the channels are well characterized, and the particle-particle interaction can be precisely adjusted by an external magnetic field. Since the time and length scales in such a colloidal system are easily accessed with video microscopy, we are able to follow the trajectories of individual particles over long times. These advantages enable us to demonstrate unambiguously the non-Fickian behavior of SFD. In particular, our measurements confirm for the first time the theoretically predicted gaussian distribution of particle displacements [4].

Our sample cell was composed of two optical flats separated by an O-ring of 1 mm thickness. The bottom plate was first coated with a thin layer of polymethylmethacrylate (PMMA) to prevent the colloidal particle from sticking to the glass surface. On top of this film, a 5 µm thick layer of transparent photo resist material was deposited. Afterwards a set of concentric circular channels was etched into the photo resist by means of photolithography (Fig.1).
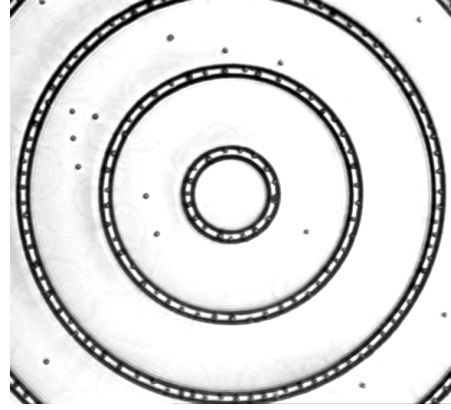
Figure 1: Optical microscope image of three concentric channels with a width of about 7 µm and diameters between 33 and 1608 µm. Dark objects are the colloidal particles. The channels are narrow enough to meet the condition for SFD.

When an external magnetic field is applied perpendicular to the sample plane, a magnetic dipole moment M is induced in the colloids which increases linearly with B for the weak field strengths used in our experiments. This gives rise to a dipole-like pair interaction potential of the form $V(r) \propto M^2/r^3$. In order to characterize the interaction strength between particles we introduce the plasma parameter Γ, which is the mean diplole interaction energy normalized by the thermal energy k_BT. The particle-wall interaction can be considered hard sphere-wall like to a good approximation.

After the cell was assembled, the particles sediment to the bottom plate and are trapped in the micro channels. Due to the high particle density (1.20 g/cm³) the channels can be regarded as pores where the diffusion of the particles takes place. After most of the particles were trapped in the channels, the sample was carefully adjusted horizontally before the experiments.

The dynamics of colloidal particles was monitored with an inverted transmission optical microscope which is connected to a CCD camera and a computer. The instantaneous particle coordinates and their trajectories were extracted from digitized pictures with an image-processing algorithm and saved in a computer for later analysis. To obtain the long time behavior, we recorded the coordinates of colloidal particles for about 8 hours, with a time interval of 8 seconds between two adjacent pictures. From those data the MSD were calculated.

Fig.2 shows MSD in a double logarithmic plot for five different magnetic field strengths, corresponding to Γ = 0.66, 1.10, 2.34, 4.03 and 7.42. The solid lines correspond to best fits according to Eq.1 with F as the only adjustable parameter. Our data clearly agree with the predicted $t^{1/2}$ - behavior over more than two decades of time [4]. The small deviations from the solid lines at small time scales correspond to the crossover between the long-time diffusion and the short-time diffusion of the particles. As indicated by the arrows in Fig.2 the crossover time from the short-time behavior to SFD is significantly shifted to larger values when the magnetic dipole repulsion between the particles decreases.
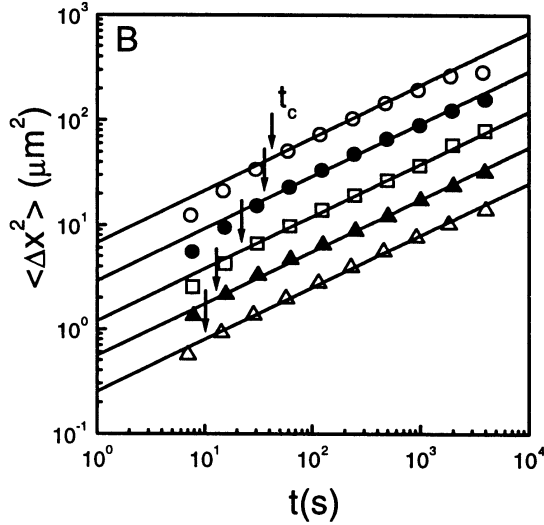

Figure 2: Log-log plot of MSD´s vs. time t for five particle interaction strengths Γ (top to bottom): 0.66, 1.1, 2.34, 4.03, 7.42. The data points were shifted vertically by ln2 for clarity.

From the particle trajectories one can also calculate the distribution function of displacements p(x,t), which is defined as the conditional probability of finding a particle at position x after time t with the particle located for t=0 at x=0. Despite the apparent simplicity of the physical situation describing SF conditions, the theoretical treatment remains a highly sophisticated task. Analytical results are only obtained for long time limits for hard rods hopping in an infinite one-dimensional chain (called one-dimensional exclusion model). It has been predicted that p(x,t) follows [5] ,

$$p(x, t) = \frac{1}{\sqrt{4\pi\, F} t^{1/4}} \exp(-x^2/4Ft^{1/2}) \quad (2)$$

This form, however, is suggested to remain valid under more general conditions whenever the single-file effects become important. To compare our data with Eq.2 we plotted the experimentally determined particle distribution function as shown in Fig.3. It can be seen that all data points collapse to a master curve after rescaling of the axis [4]. In addition, a gaussian function fit (solid line) shows good agreement with the data. From the only adjustable parameter of the gaussian fit, the single-file mobility can be derived, which is in agreement with the value obtained from the mean-square displacement data. This observation is also true for the p(x,t) for the other magnetic fields. It should be emphasized that Eq. 2 has never been experimentally observed before. In fact, the data analysis of the earlier mentioned PFG NMR and Neutron scattering experiments, relies on the validity of Eq. 2.
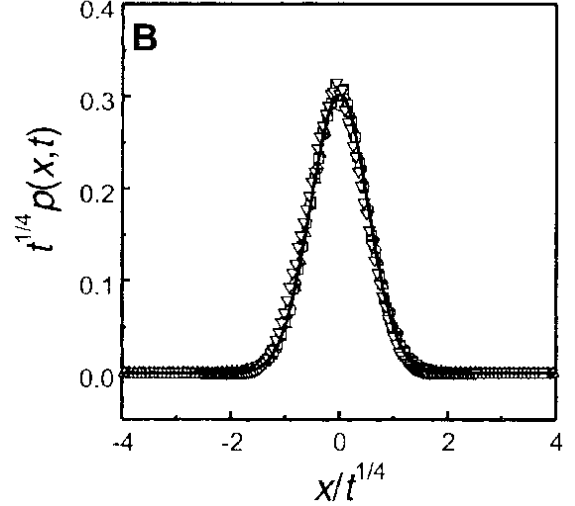
Figure 3: Distribution function p(x,t) multiplied with $t^{1/4}$. The solid line is a Gaussian fit with Eq.(2) with the fitting parameter F = 0.14 $\mu m/s^{1/2}$.

Because of the flexibility and ease of varying the channel geometry and the interaction potential form of colloids, the system allows for systematical experimental investigations of many other interesting aspects of SFD, such as finite size effect, boundary effect, hydrodynamics interaction effect, collective dynamics and multi-species system. The success of our one-dimensional colloidal system in demonstrating the non-Fickian behavior of SFD opens a new avenue not only for the SF systems, but also for particle transport through disordered micro porous mediums, e.g. self-similar percolating pores. Furthermore, the method of confining the particles by using structured surfaces may be useful to experimental study of the basic colloidal interactions under confined geometry.

[1] A. L. Hodgkin and R. D. Keynes, J. Phys. **128,** 61 (1955).

[2] K. Hahn, J. Kärger, and V. Kukla, Phys. Rev. Lett. **76,** 2762 (1996).

[3] D. G. Levitt, Phys. Rev. A **8,** 3050 (1973).

[4] Q.-H. Wei, C. Bechinger, and P. Leiderer, Science **287,** 625 (2000).

[5]H. v. Beijeren, K. W. Kehr, and R. Kutner, Phys. Rev. B **28,** 5711 (1983).

C18 Adhesion induced deformation of submicrometer PS spheres on silicon surfaces

M. Mosbacher, M. Engelke, B.-U. Runge, and P. Leiderer

The adhesion and removal of submicrometer particles on solid surfaces is of great interest both from a scientific point of view as well as technologically. Some examples for such technological questions are the adhesion of medicinal particles to specific sites in the pharmaceutical industry or the adhesion of contaminating particles on silicon wafers in the semiconductor industry.

The importance of the adhesion of fine particles to surfaces has stimulated a lot of research on the underlying physical processes. As early as in the 1930's Hamaker computed the attractive force between a hard, undeformable sphere and a flat surface from the Van der Waals-forces between the two bodies, and later his approach was improved by Lifshitz. While this theory assumes the particles to stick to the surface as a perfect sphere, a direct observation of the contact zone between the adhering bodies showed that the contact takes place not at a single point but in a contact area of finite size. This turned out to be a consequence of the deformation of particle and substrate due to surface forces.

The first model which took into account these surface forces was suggested by Johnson, Kendall and Roberts (JKR) [1]. Assuming a particle-substrate interaction only in the contact zone the authors predict a dependence of the contact radius a_{JKR} on the particle radius R given by

$$a_{JKR} = \frac{R^{2/3}}{K} \left(\frac{\zeta_{123}}{8\pi\varepsilon_0^2} + 3\gamma\pi + \left(\frac{3\gamma\zeta_{123}}{4\varepsilon_0^2} + 9\gamma^2\pi^2 \right)^{\frac{1}{2}} \right)^{\frac{1}{3}} \tag{1}$$

i.e. proportional to $R^{2/3}$. In equation (1) γ denotes the energy of adhesion of *both* surfaces, ζ_{123} the Lifshitz-Van der Waals-constant for the system PS-vacuum-SiO$_2$ [1] and ε_0 the equilibrium distance between particle and surface. K is defined as the effective module of elasticity

$$\frac{1}{K} := \frac{3}{4} \left(\frac{1-\nu_1^2}{E_1} + \frac{1-\nu_2^2}{E_2} \right) \tag{2}$$

with the Young's moduli E_i and the Poisson ratios ν_i of particle and substrate, respectively.

---

[1]Which is the system experimentally under consideration here. Due to the native oxide layer 2nm in thickness the substrate's contribution to the adhesion forces must be described by the Lifshitz-Van der Waals-constant of SiO$_2$ rather than those of Si

According to investigations by Muller, Derjaguin and Toporov (MYD) [2] the JKR theory is the limiting case of a more general theory of adhesion and the induced deformations, valid for "soft" particles on "hard" substrates, such as PS on silicon wafers.

Whereas the JKR theory assumes a totally elastic deformation of the particles, an estimation of the pressure in the contact zone [3] yields an order of magnitude of 10^9 Pa. This value is close to the elastic modulus of polystyrene and well in excess of its yield strength, therefore also plastic deformation of the particles may occur. This plastic deformation was described by Maugis and Pollock (MP) [4] as an extension of the JKR model. They obtain a contact radius of

$$a_{MP} = \frac{R^{1/2}}{H^{1/2}} \left(\frac{\zeta_{123}}{8\pi^2\varepsilon_0^2} + 2\gamma \right)^{1/2} \tag{3}$$

and hence a proportionality to $R^{1/2}$. Here H denotes the hardness of the particle-substrate system.

It is possible, therefore, by measuring the contact radius of the deformed particles to distinguish between elastic and plastic deformation by the power law dependence of the contact radius as function of the particle radius. Additionally the determined contact radius can be compared to the one predicted by JKR or MP.

Several experimental determinations of the contact radius a have been published in the recent years (see e.g. [3,5]) for various combinations of particle and substrate materials. However, these investigations used spherical particles with diameters above or only slightly below 1μm. However, for industrial applications even smaller particles are relevant, as they are found, for example, as contaminants on silicon wafers. For this reason our research focused on the adhesion induced deformation of particles with diameters down to 140nm.

As substrate we used $\langle 100 \rangle$ industrial silicon wafers [?] that were cleaned in isopropanol (IPA) in an ultrasonic bath. The spherical colloidal polystyrene particles (PS, Interfacial Dynamics Corporation, size distribution $\pm$ 5%) were rarified with IPA and deposited as isolated particles onto the silicon sample in a spin coating process. Immediately after the deposition of the particles the samples were further processed.

For the determination of the contact radius we used two different techniques. On one hand we applied a scanning electron microscope (SEM) to directely observe the contact area. This method was also employed by Rimai et al. [3,5]. Before imaging the samples in the SEM we evaporated a thin gold film (thickness 10-20nm) onto the sample. This evaporation process caused a delay between particle deposition and imaging of several hours. In contrast to Rimai et al. we observed the adhering particles

(a) Determination of the contact radius by SEM

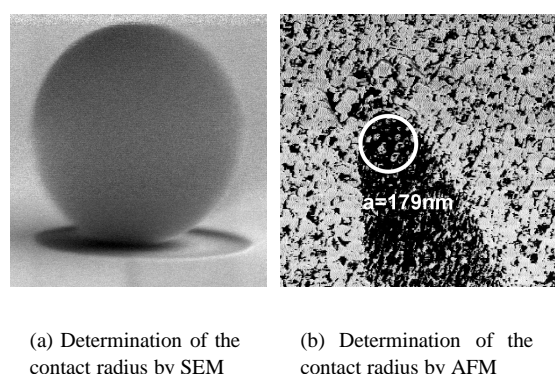(b) Determination of the contact radius by AFM

Figure 1: A comparison of two methods for the determination of the contact area of PS spheres on silicon. Fig. 1(a) shows a sphere 1700nm in diameter, the contact area as well as the crater formed by the gold evaporated onto the sample can be seen. In Fig. 1(b) the shadow created by the contact area of a particle (diameter 800nm) adhering to the silicon surface when evaporated with gold at grazing incidence can be seen. The thickness of the gold film is approx. 10nm. A white circle symbolizes the contact area. The image shows the phase signal of an AFM in contact mode.

at an angle of about 82-85° to the surface normal. This allows a better imaging of the contact region as one can look into the crater around the particle formed by the gold film (thickness 10-20nm). A typical example of a picture obtained by this SEM method is shown in Fig. 1(a).

As one can also see from this figure it is not easy to determine the contact radius accurately in this way. This is a consequence of the fact that the SEM cannot resolve the contact area, therefore it is not possible to determine its value for particles smaller than about 300nm in diameter. For this reason we developed a new technique, which is based on imaging the contact area by evaporating gold at grazing incidence (about 85°) onto the sample. After the evaporation the samples were dropped in an ultrasonic bath for 15 minutes in toluene. This process dissolved the PS solloids. Using an AFM in contact mode we then imaged the shadow created during the evaporation by the particle - surface contact. As can be seen from Fig. 1(b) this technique allows the determination of the contact radius with a good contrast. We applied it successfully even for particles with diameters as low as 140nm.

When comparing the contact radii obtained by the two methods (Fig. 2) we found that the values obtained from the AFM-shadow technique are about a factor of two smaller than those measured by the direct SEM imaging. In addition the AFM data show good quantitative agreement with the predictions of the JKR theory. A fit of a $a \propto R^x$ power law revealed values of x=0.71±0.01 for the SEM method and x=0.72±0.06 for the AFM method. These values are different from the value of 0.5 expected
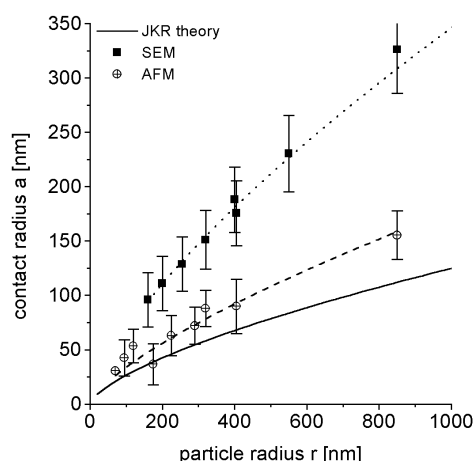
Figure 2: Contact radius of PS spheres on a Si substrate as function of the sphere diameter. The contact radius was determined both by direct SEM observation and the imaging of evaporation shadows using an AFM.

for plastic deformation, a value that has been found experimentally after allowing the samples to rest for 14 days [3]. It should be noted, that some groups reported on 3/4 power law for submicron particles [3]. From the experimental data obtained so far this as well as the 2/3 power law (JKR) is within the error bars of our experiment. However, the origin of the exponent of 3/4 is still under debate and further experimental investigation is needed.

From our experiments we conclude that PS spheres on silicon wafers are deformed elastically within the first few hours after deposition. The adhesion by surface forces and the particle deformation induced by these forces are described by the JKR theory quantitatively in good agreement, an important observation for the modeling of particle adhesion in industrial applications. For the smallest particles the ratio of the radius of the contact area and the particle radius is about 30-40%.

[1] K.L. Johnson, K. Kendall and A.D. Roberts, Proc. R. Soc. Lond. A **324**, 301 (1971).

[2] V.M. Muller, V.S. Yushenko, B.V. Derjaguin, J. Coll. Interface Sci. **92**, 92 (1983).

[3] D.S. Rimai, L.P. DeMejo, R.C. Bowling, in Fundamentals of Adhesion and Interfaces, K.L. Mittal (Ed.), VSP Publishing (1995).

[4] D.H. Maugis, H.M. Pollock, Acta Metall. **32**, 1323 (1984).

[5] D.S. Rimai, D.Q. Quesnel, A.A. Busnaina, Colloids and Surfaces A **165**, 3 (2000).

D Biological Systems

D1 Low-frequency phonons in protein crystals

R. Weissenborn, T. Gisler, and G. Maret

Understanding the structure and dynamics of proteins is a central issue in molecular biology. In particular the questions of how proteins fold and what determines the catalytic activity of a protein are still unresolved problems, mainly due to the enormous structural complexity of proteins. Very much unlike synthetic macromolecules, proteins show a great degree of structural organization despite their complex amino acid sequences. Secondary structural elements such as α-helices or β-sheets, being rather rigid themselves, are connected by flexible loops which allow large-amplitude collective motions of entire structural units. These large-amplitude collective vibrations lead to exchange between neighboring conformations which are characterized by local minima in the free energy surface of the protein. These transitions between different conformational substates are believed to be essential for the catalytic activity of a protein.

As these conformational fluctuations in a substate modulate the polarizability of the molecule, one expects these fluctuations to lead to quasielastic or inelastic scattering of light at frequencies that correspond to normal mode frequencies for a given conformational substate. Transitions between different conformational substates are also expected to give rise to light scattering, however at much smaller frequencies than normal-mode fluctuations.

We have performed light scattering experiments from hen-egg-white lysozyme single crystals grown by the vapour diffusion method. As a light source we used a diode-pumped frequency-doubled $\mathrm{Nd}:\mathrm{YVO_4}$ laser operating in a single longitudinal mode at $\lambda_0 = 532\,\mathrm{nm}$; scattered light was analyzed using a scanning Fabry-Pérot interferometer and detected using a cooled photomultiplier tube. During the scan through the laser line the photomultiplier tube was protected from over-exposure by a shutter. Operating the interferometer at a finesse of typically $F = 50$ in 5-pass geometry allowed to enhance the instrumental contrast to $C > 10^7$. Measurements in backscattering geometry and at scattering angles around $90°$ show rather broad inelastic lines (see Fig. **??**) whose frequency shifts $\Delta\omega$ scale roughly linearly with the wave vector q, indicating that the observed peaks are pertinent to (longitudinal) acoustic phonons of the protein crystal lattice. The observed frequency shifts are indeed consistent with a sound speed of $(2001 \pm 38)\,\mathrm{ms^{-1}}$, if we assume a refractive index of the crystal of 1.6 which is likely to be an overestimate. Taking into account the large water content of the lysozyme crystals (typically 80% by weight), the effective refractive index can be es-
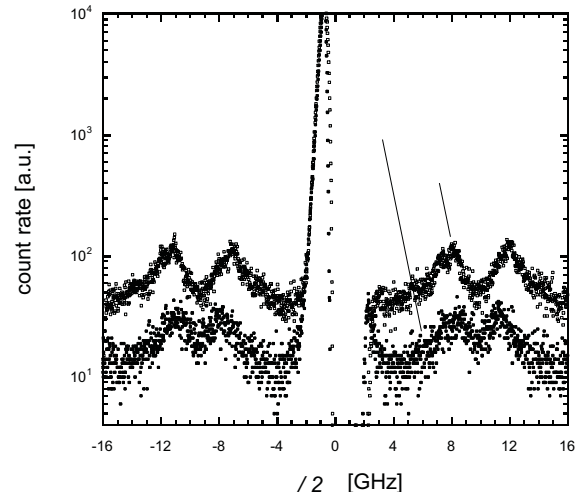
Figure 1: Inelastic light scattering spectra from a single hen-egg-white lysozyme crystal. The broad inelastic lines at $7.66\,\mathrm{GHz}$ and $8.31\,\mathrm{GHz}$ were taken at scattering angles $\theta = 80°$ (lower curve) and $\theta = 85°$ (upper curve), respectively; the laser wavelength was $\lambda = 532\,\mathrm{nm}$; the Fabry-Pérot interferometer was operated in 5-pass geometry with a free spectral range of $19.5\,\mathrm{GHz}$. The doubled lines in each spectrum are due to neighboring orders of interference; the asymmetry of the central part of the spectrum is due to the delayed opening of the shutter after scanning through the laser line.

timated to be around 1.38, resulting in a sound speed of $(2328 \pm 44)\,\mathrm{ms^{-1}}$ which is in the range obtained for collagen fibers of varying hydration [1].

Apart from the acoustical phonons, we have, however, not been able to detect any underdamped, q-independent modes in lysozyme crystals, even when working with a greatly enhanced contrast of up to 10^{12} using a six-pass tandem Fabry-Pérot interferometer. A possible qualitative explanation for this result may be that low-frequency conformational fluctuations are overdamped by the hydration shell.

[1] R. Harley, D. James, A. Miller, and J. W. White, Nature **267**, 285 (1977).

E   Multiple Light Scattering

E   Light propagation in disordered media

Ralf Lenke, Ralf Tweer, Stefanie Eiden, Christoph Eisenmann, Roman Lehner and Georg Maret

We are studying the propagation of light in multiple scattering media, i.e. in materials which appear white or turbid. These materials represent the most common 'aggregate state' in nature, examples ranging from paint, paper, bio-materials, milk, rock to clouds. It is thus of general interest to obtain a better understanding of light propagation in such media and to develop new measuring techniques for their characterization. In very strongly scattering media even new, non-classical 'photon states' are predicted. This is of particular interest as those states are not only restricted to classical waves but are also predicted for quantum mechanical waves, such as for electrons in the conducting band (*Anderson localization*).

E 1   Material characterization by coherent backscattering [1, 2]

Light scattering by particles much larger than the wave length λ is well explained by ray optics. The same is true for disordered media, in which however, this model essentially reduces to a random walk model of light paths with the characteristic average step length $\ell^\star$, the so-called transport mean free path.

In the exact backscattering direction (reversed direction of the incident light beam), the scattered intensity of a single spherical particle is coherently enhanced due to the constructive interference of all light rays which are symmetric by rotation around the optical axis. This phenomenon is known as the 'Glory'. In a disordered medium, this class of light rays reduces to a multiple scattered light path and its reversed path. It leads to an interference enhancement of a factor of two with respect to the incoherent background to which the intensity de-

Figure 1:   CB-enhancement (renormalized) of an oil/water emulsion. With increasing stirring time and speed, the oil droplet size decreases leading to an increasing effective scattering strength and to a broader CB-cone.

creases with increasing deviation from exact backscattering. In the diffusion approximation, the following angular dependence for the coherence $\mathcal{C}$ between the direct and reversed path is obtained:

$$\mathcal{C}(\vec{q_b}) = \frac{1 - \exp[2(1+\gamma)|\vec{q_b}|\ell^\star]}{2(1+\gamma)|\vec{q_b}|\ell^\star} , \qquad (1)$$

$q_b \approx 2\pi\theta_b/\lambda$ being the back-scattering vector for a given back-scattering angle θ_b with respect to the reversed direction of the incident light. With (1), the shape of the coherent backscattering (CB) cone (normalized to the incoherent background) is given by $1 + \frac{I_{ms}}{I_{ms}+I_{ss}} \mathcal{C}(\vec{q_b})$. I_{ms} and I_{ss} are the (incoherent) intensities of the multiple scattering light paths and of single scattering, respectively. The pre-factor containing these intensities is necessary as single scattering does not contribute to CB and consequently reduces the enhancement factor below two. Its precise value depends on the incident and detected polarization state, the kind of scattering and on absorption. According to eq. (1), the angular width of this cone is proportional to $\lambda/\ell^\star$, thus giving the possibility to experimentally determine the transport mean free path $\ell^\star$. From eq. (1), it can also be seen that the cone has a triangular tip. This is no longer the case for absorbing samples. Then, the cone is rounded off because the long light paths, which are responsible for the tip of the cone, are suppressed by absorption. In terms of scattering vectors q, this corresponds to a lower cut-off vector q_a which enters in eq. (1) by the replacement $q_b^2 \rightarrow q_b^2 + q_a^2$. With ℓ_a the absorption length, one finds $q_a^2 = 3/\ell^\star\ell_a$. However, absorption does not destroy the enhancement factor of 2 as it reduces the coherent and incoherent part to the same extent, i.e. (1) must be renormalized accordingly. The factor γ in (1), which is of order unity, reflects the fact that a multiple scattering light path does not end exactly on the interface of the sample, normally, but at a certain distance of order $\ell^\star$ outside the sample. The average value of this distance is just $\gamma\ell^\star$ [1].

A standard experimental setup measuring the coherent backscattering cone essentially consists of an enlarged parallel laser beam, a beam splitter permitting observation in the exact backscattering direction and a CCD-camera whose optic is adjusted to infinity. Thus, comparative measurements of $\ell^\star$ are easily possible. Fig. 1 shows the evolution of the CB-cone for an oil/water emulsion with decreasing droplet size. Quantitative evaluation is best done by comparison with Monte-Carlo simulations, where experimental conditions can be incorporated easily (see fig. 2). The precise evaluation of $\ell^\star$ is limited by the details of the light propagation close to the interface which may cause additional scattering and internal reflections. These effects are not very dramatic for samples with a moderate contrast of the index of refraction, such as the above emulsions, but they become substantial for high index particles and samples with a very small $\ell^\star$.
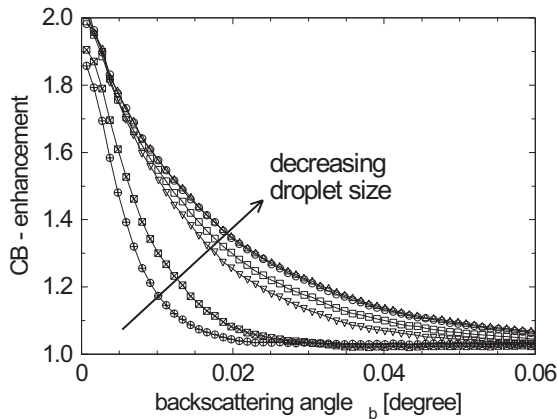
It is worth noting that while diffusing wave spectroscopy - a technique commonly used nowadays on suspensions to determine $\ell^\star$ - CB-measurements are also possible for solid samples.

As can be seen from fig. 2, the precise shape of the CB-cone depends on the type of scattering, on absorption and on polarization. In fact, full coherence between direct and reversed paths is only achieved if incident and detected polarization states are identical. This is guaranteed by the theorem of reciprocity which states that the scattering matrices describing direct and reversed paths are the transposed matrices of each other. However, as these matrices are not symmetric in general, especially for long light paths, no or only a small CB-cone exists in case of orthogonal polarizers and analyzers. By decomposing the scattering matrices M in a symmetric and antisymmetric part, the coherent backscattering enhancement in the orthogonal channels can be described as following:

$$\mathcal{C}_{q_b=0}^{\perp} = \frac{\langle |\vec{P}^{\perp} M^s \vec{P}|^2 - |\vec{P}^{\perp} M^a \vec{P}|^2\rangle}{\langle |\vec{P}^{\perp} M^s \vec{P}|^2 + |\vec{P}^{\perp} M^a \vec{P}|^2\rangle}, \qquad (2)$$
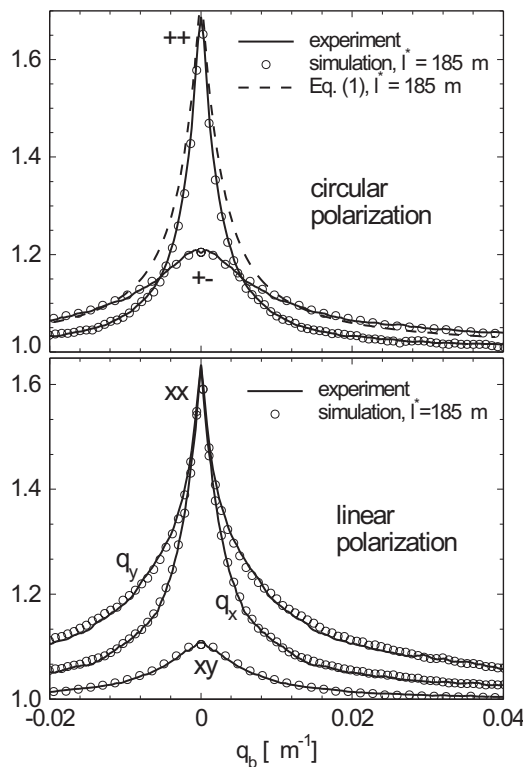

Figure 2: CB-enhancement of colloidal polystyrene spheres (diameter 100nm, wavelength 514nm) in water for different polarization channels. In case of circular polarization, the cone is symmetric by rotation around the maximum. For linear polarized light, the cone is larger for q_b parallel to the incident polarization (y) than perpendicular to it. The value $\ell^\star$ can be determined from the width of the cone. Moreover, the precise cone shape - as a function of polarization - gives qualitative informations on the type of scatterers as well. If absorption is present, it can be determined by the rounding of the cone tip.

where $\vec{P}$ and $\vec{P}^{\perp}$ are vectors representing the orthogonal polarizer and analyzer. More useful, eq. (2) can be transformed to a relation between $\mathcal{C}^{\perp}$ and the depolarization of the backscattered intensity 'I' by the sample. For the linear crossed (xy) and circular orthogonal ($\pm$) channel we find [1]:

$$\mathcal{C}_{q_b=0}^{\pm} = \left.\frac{2\mathcal{P}_l}{1 - \mathcal{P}_c}\right|_{ms} \quad \text{and} \quad \mathcal{C}_{q_b=0}^{xy} = \left.\frac{\mathcal{P}_c + \mathcal{P}_l}{1 - \mathcal{P}_l}\right|_{ms} \qquad (3)$$

with $\mathcal{P} = (I^{\parallel} - I^{\perp})/(I^{\parallel} + I^{\perp})$ reflecting the degree of remaining polarization after backscattering. Note, that the equations are only valid for the multiply scattered (ms) part of the light. Fig. 2 also shows the CB-cones in the crossed channels for Rayleigh scattering.

At the moment we study the influence of the interface on the shape of the CB-cone by investigation of the deformation of the cone with increasing inclination angle of the sample [1].

E 1.1   A large angle CB-setup

The CB-setup described in **E1** using a beam splitter and a CCD-camera permits relatively fast (on-line) measurements in and around the exact backscattering direction. However, the maximum angle range is limited to about $\pm 5°$. This is not sufficient in the context of the research for localization [2] where one looks for very strongly scattering samples with a very large CB-cone. Therefore we built up a completely new kind of setup which operates from $0.05°$ to $\pm 90°$. This setup does not operate with parallel but with divergent incident light. Here, use is made of the fact that CB acts, to some extent, like a phase conjugating mirror. When using divergent light, originating from a point-like light source - for example the focus of a laser beam - an image of the CB-cone reproduces exactly around this source. No lens system is needed. Our setup is shown in fig. 3. The focus of the laser beam is at a distance of about 1m from the sample which is placed at the center of a goniometer. A single mode fiber is mounted on a goniometer arm such that the circle it describes passes through the focus of the incident laser beam. This position corresponds to exact backscattering. The laser light is linearly or circularly polarized. The an-
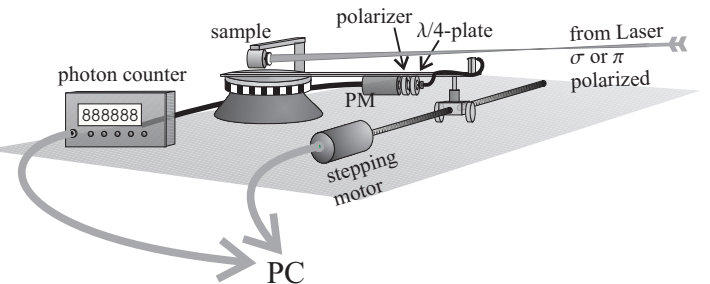

Figure 3: see text

alyzer is placed between fiber and photomultiplier. The whole setup is controlled by a PC.

Fig. 4 shows the experimental results of two wide-angle CB-cone measurements for a commercially available, colloidal TiO_2 powder and for a sample of colloidal silica spheres coated with TiO_2 that we have fabricated ourselves. The $\cos(\theta_b)$-like behaviour (*Lambert's law*) of the incoherent background as well as the triangular shape of the cone tip are clearly visible. By fitting the curves to the theoretical line shape given by eq. (1), we find $\ell^\star \approx 1\mu m$ for TiO_2 and $\ell^\star \approx 1.7\mu m$ for the coated spheres.
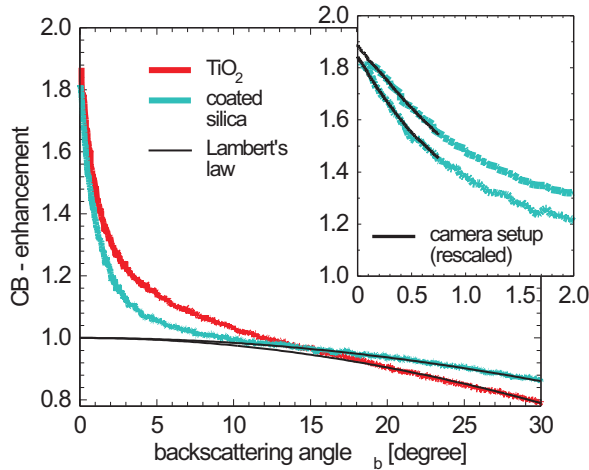

Figure 4: Measurements of the CB-enhancement with a 'wide-angle-setup' (see text). The inset shows the same curves at smaller angles completed by the measurements with a 'standard' setup (CCD camera, parallel laser). Here, no curve reaches the theoretically predicted enhancement factor of 2. This is due to experimental artifacts which, moreover, depend on the experimental setup. In fact, as the experimentally obtained enhancement factors of the camera setup were different from those of the wide-angle-setup, the curves had to be rescaled accordingly. The $\cos(\theta_b)$-like behaviour for the incoherent background is only a rough estimation. In our case, the base lines were fitted to $\cos(1.02\,\theta_b)$ and $\cos(1.26\,\theta_b)$, respectively. Wavelength 514nm.

E 2   CB and localization [2]

Light propagation in 2D and 3D random media is well described by the random walk model. It explains, for example, the *Ohm*-like behaviour that the transmitted intensity of a non-absorbing sample is inversely proportional to its thickness L. So far, experimentally measured deviations from this behaviour can - to our opinion - be completely explained by absorption. In one dimensional samples, however, the random walk model is completely inappropriate because the transmitted intensity decreases exponentially with sample thickness (such an exponential decrease is or would be an indication for localization). Immediately the question arises, if and to what extent the 1D behaviour is also inherent

to 2/3D samples. However, there are basic differences between the different dimensions, for example, wave propagation in 1D is determined by transmitting and reflecting planes (which can cause resonances), whereas in 2/3D the (differential) cross section of the scatterers is the relevant parameter. Since the famous paper of *P.W. Anderson* in 1958 on (quantum) wave localization there is a never-ending discussion especially on the 2/3D problem. Essentially two different theoretical concepts are put forward: One considering the eigenstates of the disordered system and predicting localization in the case where the dimensionless conductance [1] $g = (\text{sample diameter} * \pi/\lambda)^2/(L/\ell^\star)$ is very small. However, to our understanding this only applies to the case of (quasi-) 1D-samples. The other theoretical *Ansatz* is based on CB. Because of CB part of the light is scattered back to the source. As each scatterer in a disordered medium can be considered as source, the diffuse light propagation is slowed down by CB and we have a deviation from the 2/3D random walk model. CB cannot be cast in terms of a modified structure factor - and thus described by a renormalized random walk - as it is not destroyed with increasing length of the light paths. The second theoretical *Ansatz* predicts light localization in any 2D sample and in very strongly scattering 3D samples when $\ell^\star \lesssim \lambda/2\pi$. Until nowadays no such behaviour could be unambiguously observed, neither by other groups nor by us [2] In fact, even the 'classical' description of light propagation in strongly disordered media is an important field of research on its own. Actually, we study the meaning and the value of $\ell^\star$ in samples where the scatterers can no longer be considered as optically independent: Is there a lower limit to $\ell^\star$? Moreover, as the existing localization theories cannot help making important simplifications and thus are very unclear, we are actually testing out a completely different theoretical *Ansatz*, describing multiple sacttering plus CB by a self-attracting random walk model of light.

E 3   Magnetic field effects on CB [1-5]

Magnetic field induced Faraday rotation (FR) destroys the reciprocity of light paths as it introduces a phase difference of $2\sigma V\vec{B}\cdot\vec{r}$ between the direct and the reversed path; $V\vec{B}\vec{r}$ being the Verdet constant, the magnetic field and the propagated distance, respectively; $\sigma=\pm1$ is the handedness of the circular polarization. Let us first assume that the light is not depolarized. With $\vec{R}$ the distance vector between starting and end point of the random walk, this results in a total phase shift of $2\sigma V\vec{B}\cdot\vec{R}$ and finally in the substitution $\vec{q}_b \to \vec{q}_b + 2\sigma V\vec{B}$ in eq. (1). Consequently, without depolarization, the CB enhancement is not destroyed but only shifted out of the exact backscattering direction if $\vec{R}\|\vec{B}$. But normally, especially on the long light paths, the light is depolarized (circular

polarization). Then, the FR-induced phase shifts are assumed to be independent of each other after a distance $\ell_{FR}^\star \approx \ell^\star$ and decorrelated of $\vec{R}$, resulting in the substitution $q_b^2 \rightarrow q_b^2 + \ell_{FR}^\star/\ell^\star \cdot (2VB)^2$ in eq. (1). Therefore, the coherence $\mathcal{C}^{++}$ between direct and reversed paths is destroyed by FR ('++' for same incident as detected circular polarization channel). The considerations made above basically hold as well for the parallel linear channel 'xx'. More precise evaluations of the scattering matrix M give the result [4]:

$$\mathcal{C}(VB)^{xx} = \underbrace{\frac{\mathcal{P}_l + \mathcal{C}(VB)^{++}}{1 + \mathcal{P}_l \mathcal{C}(VB)^{++}}\Bigg|_{ms}}_{= \,\mathcal{P}_l(VB)}. \qquad (4)$$

Again, the light must be depolarized, i.e. $\mathcal{P}_l < 1$, otherwise the CB-cone is not destroyed. For the crossed polarized channels we find:

$$\mathcal{C}(VB)^{\pm} = \frac{2\mathcal{P}_l}{1 - \mathcal{P}_c}\Bigg|_{ms} \qquad (5)$$

$$\mathcal{C}(VB)^{xy} = \frac{\mathcal{P}_l + \mathcal{P}_c \mathcal{C}(VB)^{++}}{1 - \mathcal{P}_l(VB)}\Bigg|_{ms}. \qquad (6)$$

Why is it necessary to introduce the length $\ell_{FR}^\star$? When a circular polarized wave is reflected by a single Rayleigh scatterer in the exact backward direction, the product $\triangle\alpha = \sigma V\vec{B}\vec{r}$ does not change sign and the FR induced phase shift $\triangle\alpha$ is not randomized. The sign is not changed because the polarity flip of σ is compensated by the reversion of the vector $\vec{r}$ before and after scattering. Consequently, for the randomization of $\triangle\alpha$, exact back- and forward scattering are identical and we can make the replacement $(\sigma, \vec{r}) \rightarrow -(\sigma, \vec{r})$ for the scattered light. The same is true also for other directions for the part of the light which was scattered in the opposite circular polarization state. This picture gives a modified 'scattering cross section' with respect to the decorrelation of FR, which is more forward pointed, i.e. non-isotropic, than the real scattering cross section (see fig. 5). This non-isotropy is responsible for a larger FR-decorrelation length $\ell_{FR}^\star$ with respect to $\ell^\star$. Quantitatively, one obtains $\ell_{FR}^\star/\ell^\star = \langle 1 - \cos(\theta_{FR})\rangle^{-1}$. For Rayleigh scattering, the value $\ell_{FR}^\star/\ell^\star$ equals 2. With increasing size of scatterers $\ell_{FR}^\star$ decreases to about the same value as $\ell^\star$.

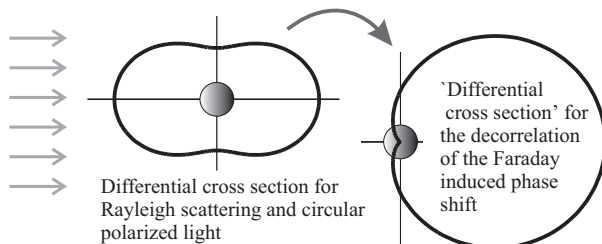Eqs. (4-6) have only been proofed for non-correlated scattering matrices. The model leading to the length $\ell_{FR}^\star$
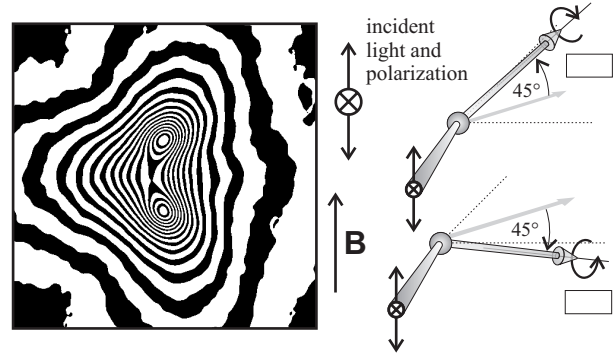

Figure 6: Contour lines of a CB-cone with FR (simulation). Magnetic field, incident (=detected) polarization as indicated. The bean-like, i.e. transverse asymmetry is clearly visible.

seems to be in very good agreement with reality as it was demonstrated by numerical simulations; however, only for segments of light paths deep inside a multiple scattering medium. In any case, these models cannot reproduce the hole shape of the CB-cone. This can only be done by Monte-Carlo simulations. Experimental results, and their comparison to simulations, of the destruction of the CB-cone, cone shifts and the appearance of double cones are given in refs. [2-5]. A great, recent success of the simulations was their contribution to the explanation of an experimentally observed transversal asymmetry of the cone, i.e. a photon flux perpendicular to the incident light and perpendicular to the applied magnetic field [2, 3, 5]. Fig. 6 shows a numerical simulation of this experiment. The explanation is the following: Mie scatterers with an index of refraction smaller than the embedding material act, to some extent, like phase retarding plates: Linearly polarized light that is scattered in a plane including an angle of say $+45°$ with respect to the incident polarization gets partially circular polarized. The circular polarized light experiences a phase shift of $\sigma V\vec{B}\vec{r}$, where $\vec{B}$ and $\vec{r}$ include an angle of $45°$ as well. If the scattering plane includes an angle of $-45°$ with the incident polarization, both σ and $\vec{B}\vec{r}$ change sign. Consequently, independent of the orientation of the path segment, part of the light experiences a net phase shift perpendicular to $\vec{B}$ resulting in the transversal asymmetry.

At the moment we are performing experiments where we want to verify and evaluate quantitatively the new correlation length $\ell_{FR}^\star$.

Figure 5:

Differential cross section for Rayleigh scattering and circular polarized light

'Differential cross section' for the decorrelation of the Faraday induced phase shift

[1] R. Lenke, G. Maret, *Scattering in Polymeric and Colloidal Systems*, Gordon and Breach Scientific (2000), Eds. W. Brown and K. Mortensen, pp. 1-72

[2] Annual report *Soft condensed matter*, University of Konstanz (1998), Ed. T. Gisler.

[3] Annual report *Quantum Optics*, Uni. of Konstanz (1999)

[4] R. Lenke, G. Maret, Euro. Phys. J. B **17**, (2000) pp. 171-85

[5] R. Lenke, R. Lehner, G. Maret, Euro. Phys. Lett. **52**, (2000) pp. 620-6

Publications

Publications

Dieterich Group

R. Kenzler, F. Eurich, P. Maass, B. Rinn, J. Schropp, E. Bohl, and W. Dieterich
Implicit Numerical Method for Solving the Cahn-Hilliard Equation with Automatic Time Step Control
Comp. Phys. Comm. **133**, 139 (2001).

B. Rinn and P. Maass
Comment on ''Radial fluctuations induced stabilization of the ordered state in two-dimensional classical clusters''
Phys. Rev. Lett., to appear in April 2001.

B. Rinn, K. Zahn, P. Maass, and G. Maret
Influence of Hydrodynamic Interactions on the Dynamics of Long-Range Interacting Colloidal Particles,
Europhys. Lett. **46**, 537 (1999).

Klein Group

H.H. von Grünberg,
Non-linear screening in concentrated colloidal suspensions,
J. Phys.: Condens. Matter, **12**, 6039, 2000.

H.H. von Grünberg, L. Belloni
Eccentric Poisson-Boltzmann cell model,
PRE, **62**(2), 2493, 2000.

H.H. von Grünberg, E.C. Mbamala
Colloidal suspensions at dielectric interfaces,
J.Phys.: Condens. Matter, **12**, 10349, 2000.

H.H. von Grünberg, E.C. Mbamala
Charged colloids near interfaces,
SPECIAL ISSUE: LIQUID INTERFACES,
J.Phys.: Condens. Matter, to appear in May 2001.

H.H.von Grünberg, R. van Roij, G. Klein
Poisson-Boltzmann theory, the Donnan potential, and gas-liquid phase coexistence in colloidal suspensions,
submitted to EPL, 2001.

C. Fleck, H.H.von Grünberg
Counterion evaporation,
in press, PRE, 2001.

G. Nägele, J. Bergenholtz, and R. Klein
Dynamics of Colloidal Suspensions,

Proceedings of the Yamada Conference L on Polyelectrolytes, Editors: I. Noda, E. Kokofuta, 199-204, Yamada Science Foundation, 1999.

G. Nägele, J. Bergenholtz, and J.K.G. Dhont,
Cooperative Diffusion in Colloidal Mixtures,
J. Chem. Phys. **110**, 7037 (1999).

A. Banchio, J. Bergenholtz, and G. Nägele,
Dynamics and Rheology of Colloidal Suspensions,
Phys. Rev. Lett. **82**, 1792 (1999).

M. Watzlawek, and G. Nägele,
Sedimentation of Strongly and Weakly Charged Colloidal Particles: Prediction of Fractional Density Dependence,
J. Colloid and Interface Sci. **214**, 170 (1999).

A.J. Banchio, G. Nägele, and J. Bergenholtz,
Viscoelasticity and Generalised Stokes-Einstein Relations in Colloidal Dispersions,
J. Chem. Phys. **111**, 8721-8740 (1999).

A.J. Banchio, G. Nägele, and J. Bergenholt
Collective Diffusion, Self-Diffusion and Freezing Criteria of Colloidal Suspensions,
J. Chem. Phys. **113**, 3381 (2000).

R. Pesché and G. Nägele,
A Stokesean Dynamics Study of Quasi-two-dimensional Suspensions Confined Between Two Parallel Walls,
Phys. Rev. E **62**, 5432 (2000).

M. Kollmann and G. Nägele,
Colloidal Electrolyte Friction and Sedimentation: a Mode-coupling Approach,
J. Chem. Phys. **113**, 7672 (2000).

R. Pesché and G. Nägele,
Dynamical Properties of Wall-confined Colloids,
Europhys. Lett. **51**, 584 (2000).

M. Kollmann and G. Nägele,
The Role of Hydrodynamic Interactions in Colloidal Electrolyte Friction and Sedimentation,
Europhys. Lett. **52**, 474 (2000).

R. Pesché, M. Kollmann, and G. Nägele,
Brownian Dynamics Study of Dynamic Scaling and Related Freezing Criteria in Quasi-two-dimensional Dispersions,
J. Chem. Phys. **114**, in press (2001).

G. H. Koenderink, H. Zhang, M. P. Lettinga,
G. Nägele, and A. P. Philipse,
Rotational Tracer-Diffusion in Binary Colloidal Sphere Mixtures,
submitted (2001).

R. Pesché, M. Kollmann, and G. Nägele,
Dynamic Scaling and Freezing Criteria in Quasi-two-dimensional Dispersions,
submitted (2001).

H. Zhang and G. Nägele,
Short-time Translational and Rotational Diffusion in Binary Colloidal Dispersions.
submitted (2001).

J.M. Mendez-Alcaraz and R. Klein,
Depletion forces in colloidal mixtures,
Phys. Rev. E **61**, 4095(2000).

R. Klein,
Colloids as model systems for condensed matter,
in: Frontiers of Neutron Scattering, ed. by A. Furrer (Singapore, 2000), p.89.

Leiderer Group

Q.-H. Wei, C. Bechinger, and P. Leiderer,
Experimental observation of single-file diffusion of Brownian particles
Progr. Colloid Polym. Sci. **112**, 227 (1999).

D. Rudhardt, C. Bechinger, and P. Leiderer,
Entropic interactions in mixtures of colloids and non-ionic polymers,
Prog. Colloid Polym. Sci. **112**, 163 (1999).

D. Rudhardt, C. Bechinger, and P. Leiderer,
Repulsive depletion interactions in colloid-polymer mixtures,
J. Phys: Cond. Matt **11**, 10073 (1999).

C. Bechinger, H.H.v. Grünberg, and P. Leiderer,
Entropische Kräfte,
Phys. Blätt. **55**, 53 (1999).

C. Bechinger, D. Rudhardt, P. Leiderer, R. Roth, and S. Dietrich,
Understanding depletion forces beyond entropy,
Phys. Rev. Lett. **83**, 3960 (1999).

C. Bechinger, Q.H. Wei, and P. Leiderer,
Reentrant melting of two-dimensional colloidal systems,
J. Phys.:Cond. Matt. **12**, A425 (2000).

C. Bechinger, H. Muffler, C. Schäfle, O. Sundberg, and P. Leiderer,

Submicron metal oxide structures by a sol-gel process on patterned substrates,
Thin Solid Films **366**, 135 (2000).

Q.-H. Wei, C. Bechinger, and P. Leiderer,
Single-file-diffusion of colloids in one-dimensional channels
Science **287**, 625 (2000).

H.H.v. Grünberg, and C. Bechinger,
Die Attraktivität von Unordnung,
Spektrum d. Wissenschaft **6**, 16 (2000).

C. Bechinger,
Physik mit kolloidalen Suspensionen,
Phys. Blätt. **56 (7/8)**, 75 (2000).

C. Bechinger, M. Brunner, and P. Leiderer,
Phase behavior of two-dimensional colloidal systems in the presence of periodic light fields,
Phys. Rev. Lett **86**, 930 (2001).

H.H.v. Grünberg, L. Helden, P. Leiderer, and
C. Bechinger,
Measurement of surface charge densities on Brownian particles using total internal reflection microscopy,
J. Chem. Phys. **144**, 10094 (2001).

K. Mangold, R. Bubeck, P. Leiderer, and C. Bechinger,
Substrate-induced phase transitions in 2D-colloidal systems,
J. Phys: Cond. Mat. (in press) (2001).

C. Bechinger, and E. Frey,
Phase behavior of colloids in confined geometry,
J. Phys. Cond. Mat. **13**, 12321 (2001).

M. Mosbacher, V. Dobler, J. Boneberg, P. Leiderer,
Universal threshold for the steam laser cleaning of submicron spherical particles from Silicon,
Appl. Phys. A **70** (2000), 669-672.

P. Leiderer, J. Boneberg, V. Dobler, M. Mosbacher,
H.-J. Münzer, T. Fourrier, G. Schrems, D. Bäuerle,
J.Siegel, N. Chaoui, J. Solis, C.N. Afonso,
Laser-Induced Particle Removal from Silicon Wafers,
Proc. SPIE 4065, 249-259 (2000).

T. Fourrier, G. Schrems, T. Mühlberger, J. Heitz,
N. Arnold, D. Bäuerle, M. Mosbacher, J. Boneberg,
and P. Leiderer,
Laser Cleaning of Polymer Surfaces,
Appl. Phys. A **72**, 1-6 (2001).

M. Mosbacher, H.-J. Münzer, J. Zimmermann, J. Solis,
J. Boneberg, and P. Leiderer,
Optical field enhancement effects in laser-assisted particle removal,
Appl. Phys. A **72**, 41-44 (2001).

V.P. Aksenov, G.N. Mikhailova, J. Boneberg,
P. Leiderer, and H.-J. Münzer,
*The modification of the substrate roughness spectrum
by means of power laser ablation,*
Proc. SPIE, to be published

H.-J. Münzer, M. Mosbacher, M. Bertsch,
J. Zimmermann, P. Leiderer, and J. Boneberg,
*Local field enhancement effects for nanostructuring of
surfaces,*
Journal of Microscopy 202, 129 (2001).

Maret Group

T. G. Mason, T. Gisler, K. Kroy, E. Frey, and D. A.
Weitz,
*Rheology of F-actin solutions determined from
thermally driven tracer motion,*
J. Rheol. **44**, 917-928 (2000).

J. C. Crocker, M. T. Valentine, E. R. Weeks, T. Gisler,
P. D. Kaplan, A. G.Yodh, and D. A. Weitz,
*Two-point Microrheology of Inhomogeneous Soft
Materials,*
Phys. Rev. Lett. **85**, 888-891 (2000).

R. Lenke, R. Lehner and G. Maret,
*Magnetic-field effects on coherent backscattering of
light in case of Mie spheres,*
Europhys. Lett. **52**, 620-626 (2000).

R. Lenke and G. Maret,
*Magnetic Field Effects on Coherent Backscattering of
Light,*
Europ. Phys. J. B. **17**, 171-185 (2000).

R. Lenke and G. Maret,
*Multiple Scattering of Light: Coherent Backscattering
and Transmission in Scattering in Polymeric and
Colloidal Systems,*
W.Brown Ed., Gordon and Breach Science Publishers,
Reading U.K. 1-72 (2000).

F. Scheffold, R. Lenke, R. Tweer and G. Maret,
Localization or classical diffusion of light?,
Nature, scient. corr.: Vol.**389,** 206-207 (1999).

B.Rinn, K.Zahn, P.Maass, and G.Maret,
*Influence of hydrodynamic interactions on the
dynamics of long-range interacting colloidal particles
in solution*, Europhys. Lett.**46**, 537 (1999).

K.Zahn and G.Maret,
Dynamic criteria for melting in 2D,

Phys. Rev. Lett. **85**, 3656 (2000).

K.Zahn, and G.Maret,
2D Colloidal structures responsive to external fields,
Current Opinion in Colloid & Interface Science, **4**, 60-
65 (1999).

Nielaba Group

W. Strepp, S. Sengupta, and P. Nielaba,
*Phase transitions in hard disks in external periodic
potentials: A Monte Carlo study;*
Phys. Rev. E **63**, 046106 (2001).

P. Nielaba,
Quantum effects in adsorption at surfaces;
in ''Computational Methods in Surface and Colloid
Science'',edited by M. Borowko, Marcel Dekker, Inc.,
New York, 77-131 (2000).

S. Sengupta, P. Nielaba, and K. Binder,
*Defect fugacity, spin-wave stiffness and T_c of the 2d
planar rotor model,*
Europhys. Lett. **50**, 668 (2000).

S. Sengupta, P. Nielaba, and K. Binder,
Elastic moduli, dislocation core energy and melting of
hard disks in two dimensions,
Phys. Rev. E **61**, 6294 (2000).

S. Sengupta, P. Nielaba, M. Rao, and K. Binder,
Elastic constants from microscopic strain fluctuations,
Phys. Rev. E **61**, 1072 (2000).

H.L. Frisch, S. Puri, and P. Nielaba,
*Enrichment of surfaces in contact with stable binary
mixtures: The case with long-ranged surface fields,*
J. Chem. Phys. **110**, 10514 (1999).

Chr. Rickwardt, M. Presber, D. Löding, M. Reber, and
P. Nielaba,
*Path Integral Monte Carlo Simulations in Materials
Science,*
in: *Path-integrals from peV to TeV,*
R. Casalbuoni, R. Giachetti, V. Tognetti, R. Vaia, P.
Verrucchi (Eds.),World Scientific, Singapore (1999),
pp. 446.

M. Reber, D. Löding, M. Presber, Chr. Rickwardt, and
P. Nielaba,
*Quantum simulations in materials science: molecular
monolayers and crystals,*
Comp. Phys. Commun. **121-122**, 524 (1999).

Diploma, Doctoral Theses, and Habilitations

Klein Group

Adolfo J. Banchio,
Diffusion, Rheology, and Polydispersity Effects in Three-dimensional and Quasi-two-dimensional Colloids,
June 1999, PhD thesis

Christian Fleck,
Counterion-Release: Elektrostatische Effekte bei der Adsorption eines starren Polyelektrolyten,
2000, Diploma thesis

Markus Kollmann
Dynamics and Microstructure of Interacting Brownian Systems: Elektrokinetic Effects, Quasi-two-dimensional Systems and Sphere Caging,
June 2001, PhD thesis

Leiderer Group

Matthias Brunner,
Lichtinduziertes Gefrieren und Schmelzen eines zweidimensionalen Kolloidsystems,
2000, Diploma thesis.

C. Lutz,
Messung von Partikel-Wandpotentialen mit evaneszenter Lichtstreuung,
2000, Diploma thesis.

Stefanie Marx,
Dynamisches Verhalten von Flüssigkeiten auf strukturierten Oberflächen,
1999, Diploma thesis.

Daniel Rudhardt,
Kolloidale Teilchen in der Nähe einer Wand,
1999, PhD thesis.
C. Bechinger,
Optische Experimente mit kolloidalen Suspensionen in eingeschränkter Geometrie,

Martin Ruppenthal,
Erzeugung von Nanostrukturen *über den Sol-Gel-Prozeß,*
1999, Diploma thesis.

Detlef Sontag,
Optische Untersuchungen kolloidaler Systeme in der Nähe von Oberflächen,
1999, Diploma thesis.

Maret Group

Rainer Müller,
Vielfachstreuung von Licht in dicht gepackten Medien,
2000, Diploma thesis.

Nielaba Group

Martin Gerstenmaier,
Modellierung von Wachstumskinetik auf 1dim periodischen Oberflächen,
2000, Staatsexamen

Sebastian Haase,
Quantenflüssigkeiten in eingeschränkter Geometrie
1999, Diploma thesis

Klaus-Peter Heue,
Monte Carlo Simulationen zum Höhenwachstumsstop von Au-Inseln auf WSe$_2$,
2000, Staatsexamen

Dirk Löding,
Adsorbate Layers,
2000, PhD thesis

Martina Schwarz van Doorn,
Adsorbed Layers,
2000, Diploma thesis

Wolfram Strepp,
2dim harte Kugeln in äußeren Potenialen,
1999, Diploma thesis

Scientific and Technical Staff

Group Leaders

Prof Dr. Wolfgang Dieterich

Phone: +49-(0)7531-88-3816
Fax: +49-(0)7531-88-3760
E-mail: wolfgang.dieterich@uni-konstanz.de
WWW: http://www.uni-konstanz.de/FuF/Physik/Dieterich/
Secretary: Renate Beck, phone +49-(0)7531-88-3815

Prof. Dr. Rudolf Klein

phone: +49-(0)7531-88-2955
Fax: +49-(0)7531-88-3157
E-mail: rudolf.klein@uni-konstanz.de
WWW: http://www.uni-konstanz.de/FuF/Physik/Klein/homepage.html
Secretary   Marianne Grieser, phone +49-(0)7531-88-2087

Prof. Dr. Paul Leiderer

phone: +49-(0)7531-88-3793
Fax: +49-(0)7531-88-3091
E-mail: paul.leiderer@uni-konstanz.de
WWW: http://www.uni-konstanz.de/FuF/Physik/Leiderer/homede.html
Secretary   Sabine Widmann-Schmid, phone +49-(0)7531-88-3792

Prof. Dr. Georg Maret

phone: +49-(0)7531-88-4151
Fax: +49-(0)7531-88-3090
E-mail: georg.maret@uni-konstanz.de
WWW: http://hera.physik.uni-konstanz.de/Start.htm
Secretary   Christiane Bustamante, phone +49-(0)7531-88-3864

Prof. Dr. Peter Nielaba

phone: +49-(0)7531-88-4259
Fax: +49-(0)7531-88-4462
E-mail: peter.nielaba@uni-konstanz.de
WWW: http://www.uni-konstanz.de/nielaba/
Secretary   Yolanda Fischer, phone +49-(0)7531-88-4272

Prof. Dr. Günther Schatz

phone: +49-(0)7531-88-3540
Fax: +49-(0)7531-88-3090
E-mail: guenter.schatz@uni-konstanz.de
WWW: http://www.agschatz.physik.uni-konstanz.de/ag/index.thm
Secretary   Christiane Bustamante, phone +49-(0)7531-88-3864

Scientific Staff

Banchio, Adolfo J.	(Kl)	colloid dynamics and rheology	C13
Bechinger, Clemens	(Le)	waveguide imaging, 2D colloid patterning, wetting of patterned surfaces, sol-gel-process, light-induced-phase transitions in colloids, depletion interactions, in colloid-polymer mixtures, total internal reflection microscopy, single-file-diffusion	A5, C16, C17, C2 C9
Brunner, Matthias	(Le)	light-induced-phase transitions in colloids	C2
Bubeck, Ralf	(Le)	dynamics of 2D colloidal systems in hard wall cavities	
Dürr, Oliver	(Di)	polymer electrolyts	B2
Eiden, Stefanie	(Ma)	synthesis and characterization of colloids	E, C19
Eurich, Frank	(Di)	computer simulations as well as application and development of scaling theories for semi-makroscopic models of polymeric systems	B1
Fleck, Christian	(Kl)	DNA near oppositely charged planar membranes	B3
Giebel, Karl-Friedrich	(Le)	waveguide imaging	
Gisler, Thomas	(Ma)	low-frequency protein dynamics	D1
Grünberg, Hans-Hennig.	(Kl)	the eccentric Poisson-Boltzmann cell model, entropic forces, nonlinear screening in concentrated colloidal suspensions, charge renormalisation in concentrated colloidal suspensions, density functional theory in colloidal suspensions: depletion forces	B3, C3 C6, C9, C10
Haller, Gerd	(Ma)	hexatic phase in 2D colloids	C5
Helden, Laurent	(Le)	depletion interactions in colloid-polymer mixtures total internal reflection microscopy	C9
Hoffmann, Jochen	(Ni)	phase transitions in pore condensates'	A2
Hund, Roland	(Ma)	glass transition in 2D colloids	C14
Keim, Peter	(Ma)	2D colloids in confined geometries	C15
Kollmann, Markus	(Kl)	electrokinetic effects; 2D colloids and scaling properties	C7, C11
König, Hans	(Ma)	glass transition in 2D colloids	C14
Lehner, Roman	(Ma)	coherent backscattering	E3
Lenke, Ralf	(Ma)	coherent backscattering; localization of light	E1, E2, E3
Lohrer, Marc	(Ni)	simulations of model fluids in external potentials'	C1
Mangold, Konrad	(Le)	phase behavior of colloids on magnetically patterned surfaces	

Maass, Philipp	(Di)	density functional theory for lattice gases, charge transport in polymer ion conductors, spinodal decomposition in thin films, slow dynamics in glassy systems: subaging and multiple aging regime, soft-ellipsoid model, effective medium approximation for lattice gases with asymmetric hopping rates	B1, C12
Mbamala, Emmanuel	(Kl)	charged colloids near dielectric interfaces	C10
Mosbacher, Mario	(Le)	laser cleaning of silicon surfaces	C18
Pesché, Raphael	(Kl)	2D colloids and scaling properties colloids in confined geometries	C7, C8
Rinn, Bernd	(Di)	computer simulations and analytical studies of various complex systems; Brownian dynamics of colloidal suspensions, hopping processes in disordered media, aging dynamics of glasses	C12
Rudhard, Daniel	(Le)	depletion interactions in colloid-polymer mixtures, total internal reflection microscopy	C16
Runge, Bernd-Uwe	(Le)	laser cleaning, magneto-optical investigations on high Tc superconductors, time resolved magnetooptics	C18
Schäfle, Claudia	(Le)	sol-gel-process, wetting of patterned surfaces	A5,
Strepp, Wolfram	(Ni)	simulations of model colloids in external potentials	C1
Tweer, Ralf	(Ma)	localization of light	E1, E2
Wei, Qi-Huo	(Le)	single-file-diffusion	C17
Weissenborn, Ralf	(Ma)	Brillouin scattering from protein crystals, low-frequency dynamics of proteins	D1
Wille, Axel	(Ma)	elasticity of 2D colloids	C4, C5
Zahn, Klaus	(Ma)	2D glass transition, 2D crystallization	C4, C5 C14, C15
Zhang, Haiyan	(Kl)	colloid dynamics and rheology	C13

Technical Staff

Ballot, Hans

Betz, Wolfgang,

Goldbach, Christoph

Lax, Jutta

Möbius, Walter

Abbreviations:

(Di): Dieterich, (Kl): Klein, (Le): Leiderer, (Ma): Maret, (Ni): Nielaba,